THE UNIVERSITY OF MANITOBA

AN INVESTIGATION OF COAXIAL YAGI LOOP ARRAYS

by

Alireza Shoamanesh

A THESIS

SUBMITTED TO THE FACULTY OF GRADUATE STUDIES

IN PARTIAL FULFILLMENT OF THE REQUIREMENTS FOR THE DEGREE

OF MASTER OF SCIENCE

DEPARTMENT OF ELECTRICAL ENGINEERING

WINNIPEG, MANITOBA

October 1975

"AN INVESTIGATION OF COAXIAL YAGI LOOP ARRAYS"

by

ALIREZA SHOAMANESH

A dissertation submitted to the Faculty of Graduate Studies of the University of Manitoba in partial fulfillment of the requirements of the degree of

MASTER OF SCIENCE

To my parents

ABSTRACT

The electrical characteristics of coaxial circular loop arrays are investigated by a numerical solution of the integral equation for the loop currents. Loop currents are expressed in a Fourier series of the azimuthal coordinate and the resonant property of the loop antenna is utilized to improve the convergence of the series. For arrays with different loop sizes this resonant effect is beneficially used to reduce their electrical length. As a result, with a negligible loss in the accuracy of the computation, the required labour for the investigation of the array characteristics is reduced significantly.

The effect of array parameters on its characteristics such as the input admittance, the directive gain and the radiation pattern are then studied. For a specific wire cross section extensive design data for arrays of three to twelve elements are computed.

ACKNOWLEDGEMENTS

The author wishes to thank Dr. L. Shafai for his continuous interest, helpful advice, cheerful and able guidance in all phases of this work.

I would also like to thank my friends and colleagues for their discussions and suggestions, and in particular, Mr. Rashid Ali Rafek for reading the manuscript, and Mrs. Darlene Lowry for typing it.

The financial assistances provided by the National Research Council of Canada (Grant A-7702) and the Department of Electrical Engineering of the University of Manitoba are greatly appreciated.

Alireza Shoamanesh

TABLE OF CONTENTS

CHAPTER		PAGE
	ABSTRACT	(i)
	ACKNOWLEDGEMENTS	(ii)
	TABLE OF CONTENTS	(iii)
	LIST OF FIGURES	(v)
	LIST OF TABLES	(viii)
	LIST OF MOST USED SYMBOLS	(x)
I	INTRODUCTION	1
II	FORMULATION OF THE PROBLEM	9
	2.1 Introduction	9
	2.2 Formulation of the Problem	9
	2.3 Evaluation of K_{ij}^{n}	14
	2.4 Discussions on K_{ij}^{n}	18
	2.5 Current Distribution and the Admittance.	20
	2.6 The Radiation Field and the Directive Gain	23
III	RESONANCE EFFECTS IN ARRAY OF CIRCULAR LOOP ANTENNA	26
	3.1 Introduction	26
	3.2 Resonance Effects	26
	3.3 Application to Input Admittance	42
	3.4 Computation of Dominant Modes	47
	3.5 Typical Pattern Calculation	50
IV	INVESTIGATIONS OF THE FAR FIELD PATTERN OF THE LOOP ARRAY	57
	4.1 Introduction	57
	4.2 Radiation Pattern of the Loop Arrays .	57
	4.3 Effect of Reflector Spacing	60
	4.4 Effect of the Reflector Size	63
	4.5 Effect of Director Spacings	66

CHAPTER		PAGE
	4.6 Effects of the Director Size	70
	4.7 Effects of the Exciter Size	76
	4.8 Effects of wire cross section	79
	4.9 Summary	82
V	DESIGN DATA FOR SHORT AND MEDIUM LENGTH LOOP YAGI ARRAYS	83
	5.1 Introduction	83
	5.2 Treatment of the Problem	83
	5.3 Optimum Adjustment of the Feeder-Reflector Combination	84
	5.4 Outline of Results	87
VI	CONCLUSIONS	101
	REFERENCES	103
	APPENDIX A Convergence of Equation (2.20)	106
	APPENDIX B Comparison Between Z_{ij}^{n} and Z_{ii}^{n} . . .	115

LIST OF FIGURES

FIGURE		PAGE
2.1	Geometry of the array	10
2.2	Determination of three regions where $\alpha = 4 \sin^2 \frac{\delta}{2} >> (\frac{a_i}{b_i})^2$ and $\delta << 1$	15
3.1	Dominant mode of each array element at $\phi=0°$	30
3.2	Current distributions on the active element	31
3.3	Radiation pattern of a "12-element" loop array	32
3.4	Current distributions on the active element	35
3.5	Radiation pattern of a "12-element" loop array in the H-plane	36
3.6	Dominant mode of each array element at $\phi=0°$	38
3.7	Radiation pattern of a "12-element" array in the H-plane	39
3.8	Dominant mode of each array element at $\phi=0°$	40
3.9	Dominant mode of each array element at $\phi=0°$	41
3.10	A "12-element" loop array divided into two groups	50
3.11	Radiation pattern of a "12-element" loop array in the H-plane	53
3.12	Radiation pattern of a "12-element" loop array in the H-plane	54
3.13	Radiation pattern of a "12-element" loop array in the H-plane	55
3.14	Radiation pattern of a "12-element" loop array in the H-plane	56
4.1	Radiation patterns in the H-plane for different reflector spacings	61

FIGURE		PAGE
4.2	Behaviour of the directive gains, Gr and Gd, and the input admittance for different reflector spacing	62
4.3	Radiation patterns in the H-plane for various reflector sizes	64
4.4	Behaviour of the directive gains, Gr and Gd, and the input admittance for different reflector sizes	65
4.5	Radiation patterns in the H-plane for various director spacings	67
4.6	Radiation patterns in the H-plane for various director spacings	68
4.7	Behaviour of the directive gains, Gr and Gd, and the input admittance for various director spacing	69
4.8	Radiation patterns in the H-plane for different director size	71
4.9	Radiation patterns in the H-plane for different director size	72
4.10	Radiation patterns in the H-plane for different director size	73
4.11	Effects of the director size on the directive gains, Gd and Gr, and the input admittance	74
4.12	Effects of the director size on the directive gains, Gd and Gr, and the input admittance	75
4.13	Radiation patterns in the H-plane for various exciter sizes	77
4.14	Effects of the exciter size on the directive gains and the input admittance .	78
4.15	Radiation patterns in the H-plane for different wire cross section	80
4.16	Effects of wire cross section in the directive gains, Gr and Gd, and the input admittance	81

FIGURE		PAGE
5.1	The conductance and the susceptance of a circular loop of radius b	85
5.2	Directive gain of feeder-reflector combination in the positive z direction as a function of reflector size for various reflector spacing	86
5.3	Maximum directive gain of feeder-reflector combination in the positive z direction as a function of reflector spacing	86
A.1	Examples of computed values of a_n^m	110
A.2	Examples of computed values of a_n^m	111
A.3	Approximation $\sum_{m=0}^{M} a_n^m$ of $\mathrm{Re}\,(K_{ij}^n)/kb_i$ and its error $a_n^{M+1}/(1-r)$	112
A.4	Examples of computed values of a_n^m	113
A.5	Approximation $\sum_{m=0}^{M} a_n^m$ of $\mathrm{Re}(K_{ij}^n)/kb_i$ and its error $a_n^{M+1}/(1-r)$	114
B.1	Comparison between the imaginary parts of generalized self and mutual impedance . . .	117
B.2	Comparison between the imaginary parts of generalized self and mutual impedance . . .	118

LIST OF TABLES

TABLE		PAGE
2.1	Approximate equations for K'^{n}_{ii}	16
2.2	Approximate equations for K^{n}_{ii}	17
3.1	The current modes on each loop of a "12-element" loop array	29
3.2	The current modes on each loop of a "12-element" loop array	34
3.3	Comparison of the exact and approximate results for y^{n}_{22}	44
3.4	Comparison of the exact and approximate values of the input admittance	46
5.1	Computed characteristics of "three-element" circular loop Yagi arrays	91
5.2	Computed characteristics of "four-element" circular loop Yagi arrays	92
5.3	Computed characteristics of "five-element" circular loop Yagi arrays	93
5.4	Computed characteristics of "six-element" circular loop Yagi arrays	94
5.5	Computed characteristics of "seven-element" circular loop Yagi arrays	95
5.6	Computed characteristics of "eight-element" circular loop Yagi arrays	96
5.7	Computed characteristics of "nine-element" circular loop Yagi arrays	97
5.8	Computed characteristics of "ten-element" circular loop Yagi arrays	98
5.9	Computed characteristics of "eleven-element" circular loop Yagi arrays	99

TABLE		PAGE
5.10	Computed characteristics of "twelve-element" circular loop Yagi arrays	100
A.1	Required values of M for satisfactory convergence	109
B.1	Required values of m_o after which Z_{ij}^{n} can be assumed diagonal	116

LIST OF MOST USED SYMBOLS

a_i	radius of wire cross section of the ith-element
b_i	radius of the ith-lement in a circular loop array
C_{gi}	gap capacitance
d_D	director spacing
d_{ij}	the separation distance between the ith and the jth element
d_r	reflector spacing
E_θ	θ component of the electric field
E_ϕ	ϕ component of the electric field
E_{2n}	Weber Lommel function of order 2n
Gd	directive gain in the positive z direction
Gr	directive gain in the negative z direction
H_o^2	zero-order Hankel function of the second kind
h_{n+2m}^2	second kind spherical Hankel function of order n+2m
J_{2n}	Bessel function of the first kind of order 2n
$I_i(\phi_i)$	total current
I_j^n	coefficient of the nth current mode
k	wave number in free space
K_{ij}^n	nth coefficient of Fourier series
R_{ij}	distance between two current components normalized by radius b_i
$U_i(\theta_i)$	a function equal to unity at the driving point and zero elsewhere
V_i	driving voltage of the ith element
$W_{ij}(\phi_i-\phi_j')$	kernel of integral

n	
Z_{ij}	generalized self and mutual impedance
y^n_{ij}	generalized self and mutual admittance
Y_2	input admittance of loop Yagi array
γ	Euler's constant
$\delta\phi_i$	gap width of the driving point of the ith-element
ϵ_o	permittivity of free space
η_o	intrinsic impedance of free space
η_{n+2m}	(n+2m)th order spherical Bessel function of the 2nd kind
μ_o	permeability of free space
λ	wave length in free space
Ω_i	thickness parameter of the ith-element
ω	angular frequency

CHAPTER I

INTRODUCTION

A circular loop antenna, like a dipole, is one of the most common structures and has been the subject of many theoretical studies. Historically, small loop antennas were used as direction finders and flux detectors. As a radiator, the radiation pattern of a small loop antenna shows a figure of eight shape in the vertical plane involving the loop axis. As its size increases in terms of wavelength, the radiation in the axial direction increases and becomes maximum when the circumference is about one wavelength long [1]-[2]. As a result, a highly directive beam in the axial direction may be obtained by an array of coaxial loops of proper dimension.

A coaxial loop array with only one active element is the most common configuration. Its operating principle is similar to that of a Yagi-Uda array, but for a 2-element array a gain difference of about 1.8 dB in favor of the loop array is reported [3]. Unfortunately, published data for loop arrays of more than 2 elements is scarce. It is however reported that the radiation characteristics of loop arrays above the ground plane are less affected by the electrical properties of the soil, when compared with those of dipole arrays [4]. In addition, the use of parasitic loop arrays in place of dipoles has resulted in the elimination of corona problems at high altitudes [3]. These beneficial properties of loop arrays justify further investigation of their characteristics.

There are no difficulties in evaluating the radiation characteristics of a loop which is small with respect to the wavelength of operation. Here a uniform current distribution is assumed, and expressions for the radiated field are easily formulated [5]. For a larger loop, a more realistic current distribution must be found. G. Glinski has assumed a hyperbolic cosine form for the current distribution, similar to that of a lossy parallel-wire transmission line, in order to explain the experimental results for the horizontal radiation pattern of a comparatively large loop. To simplify his analysis, he has retained only the first few terms of an infinite series of the field expressions. This approximation, however, restricts his formula to loops in which the circumference is less than one-half a wavelength [6].

Several other methods have also been applied in the past to the analysis of a thin loop antenna in free space. One of the methods is the electromotive force method, or simply emf, for the determination of antenna impedance, where a current distribution corresponding to that of a wire of zero thickness is assumed. In general, the current distribution on an extremely thin wire antenna can be assumed to approximate a sine wave form very closely. Because of this the self impedance, determined by applying the emf method to an assumed sine wave current distribution, is generally a good practical approximation. Thus, a calculation of the antenna impedance by the emf, gives results, which are quite close to the actual values, except in the region around anti-resonance [7].

Another method which involves a more precise and practical theory, requires the computation of the current distribution from which the impedance is then determined. This technique requires the solution of integral equations by various approximation methods, of which the successive approximation method [1]-[2] and the series expansion method [8]-[11] are representative.

The first general analysis of a circular loop as a transmitting antenna appears to have been carried out by Hallen [8]. He analyzed circular loop antennas driven by an idealized delta function generator and obtained a solution, again in the form of a Fourier series, for the current and impedance. However, owing to the occurance of a singularity or a very large value in the Fourier coefficient, when the index n is close to a certain large number determined by the loop's geometry, Hallen limited its application to loop antennas small compared to the wavelength. He explained that this nonconvergent series might be the result of his assumption of the one-dimensional flow of the current. Moreover, the individual terms were complicated and their evaluation and summation involved a somewhat difficult numerical task.

After Hallen's theory, Storer avoided the contribution from the large term by first replacing the Fourier series by a corresponding integral and then evaluating the integral using the Cauchy principle value. He provided extensive tables and graphs of the impedance, admittance and current distribution

for loops up to a wavelength in circumference and a number of different wire sizes [9]. Storer also examined the validity of the constant current distribution on a small loop and was led to the conclusion that loops larger than $kb = 0.2$ ($k = \frac{2\pi}{\lambda}$) can not be considered small.

T.T. Wu re-examined the problem of evaluating the Fourier series. He pointed out that assuming that the current flows along the center of the conductor, as with Hallen and Storer it does not converge everywhere on the antenna [10]. He explained that the satisfactory values obtained under this assumption were due to a false approximation. He examined the surface current distribution on a perfectly conducting loop and verified that the obtained Fourier series for $I(\phi)$ converges everywhere except at the driving point ($\phi=0$).

Later, King et al. [12] computed the input admittance of a circular loop by taking a partial summation of the infinite series obtained by Wu. They suggested that a Fourier series solution with 20 terms is satisfactory for determining the admittance of thin ($\Omega = 2 \ell n \frac{2\pi b}{a} \geq 10$) and small ($kb \leq 2.5$) loops in air and dissipative media. Here k, a, and b are the free space propagation constant and the wire and loop radii, respectively.

Inagaki et al. by assuming a finite gap at the driving-point gave a theoretical basis for determining the required number of terms in current and admittance computations [11]. They obtained an expression for the driving-point admittance in which the gap capacitance is a lumped representation of the

effect of the gap width. According to their analysis, the driving-point admittance can be treated apart from the gap capacitance, independent of the gap width. It thus is calculated by a partial summation of the Fourier series truncated at a term whose order is equal to the ratio of the loop radius to conductor radius.

On the other hand, Iizuka et al. [13] have analyzed two identical parallel loop antennas. They have decomposed the voltage and current into symmetric and antisymmetric components As a result, the simultaneous integral equations for the distribution of current along the loops have been converted into a single integral equation similar to that for an isolated circular loop antenna which has already been studied. This method, however, is not applicable to antennas with loops of different circumference.

More recently the properties of an array of coaxial circular loop antennas with arbitrary circumferences have been analyzed by means of Fourier series expansions, with emphasis on the existance of finite gaps at the driving-points [14]. The expressions for the current distribution on each loop and the input admittance involve matrix inversion, where the dimension of the matrix is related to the array size. Thus, in investigations of loop arrays the required computer time and storage increase with the array size and for very large arrays become excessive.

This thesis considers coaxial loop arrays and utilizes the resonant property of loops to develop an efficient method for investigation of their characteristics. The current distri-

bution on each loop is expressed by Fourier series around the resonant mode and the Fourier coefficients are found numerically from the integral equation satisfied by the currents. It is shown that for resonant loops a single mode adequately describes the current distribution and a rapid calculation of the antenna parameters is generally feasible. For loops of arbitrary size, other modes are however significant, but a selection of a few modes adjacent to the nearest resonant modes usually provides an accurate representation. Such an approximation further simplifies the problem, if the array consists of loops of different sizes. Here, the resonant modes of loops are different and a given mode may not have a significant excitation in certain loops. As a result, the non-resonant loops can usually be neglected, which effectively reduces the electrical length of the array for such modes. This phenomenon further reduces the computation time and is used whenever possible. Chapter III is devoted to the investigation of these properties.

Chapter IV considers the effects of array parameters on the input admittance, the radiation field and the directivity of the loop Yagi array. It will be seen that the effects of altering the reflector spacing and size are negligible in the forward direction whereas the input impedance of the array and its directive gain Gr in the negative z direction are very much dependent on these alterations. As a result, the reflector size or spacing may be used to vary the back lobe level and the impedance of the array. The driven loop dimensions and the wire cross section have negligible effect on the forward

radiation, but again have considerable effect on the array's input impedance.

It is also shown in Chapter IV that there are two principle ways by which the far field pattern of a Yagi loop array may be controlled. One is to vary the director spacing while holding the element circumference and reflector spacing constant. The second is to vary the director size while holding all other parameters fixed. Either one of these two ways will have a considerable effect on the far-field patterns. Numerical results show that when the exciter size is about a wave length, the director sizes must be less than or equal to the wave length, otherwise the far field patterns will not be useful.

The importance of loop Yagi arrays has already been discussed in [3] and [15]. Unfortunately, there exists very little information on design data for these type of arrays. The prime intention of Chapter V is to present numerical data for rapid design of uniform loop Yagi arrays in which the combination of the exciter and reflector is optimum for the directive gain in the forward direction. The data are for arrays containing between 3 to 12 elements when the director size, kb, changes from 1 to 0.7 with $\Delta(kb) = 0.1$, and the director spacing, d_D, alters from 0.1λ to 0.3λ with $\Delta(d_D) = 0.05\lambda$. From these tables it is seen that for the director circumference $kb = 0.9$ the directive gain Gd has the largest value for any director spacing as long as the array contains more than two directors. The maximum value of directive gain Gd is found

to be 15.2 db, which is for the particular array of 10 directors at a spacing of 0.3λ.

CHAPTER II

FORMULATION OF THE PROBLEM

2.1 Introduction

An array of circular loops composed of N elements with arbitrary circumferences, arranged parallel in a row is analyzed for the case of a finite gap at the driving-point. Integral equations for the current distributions are obtained by expressing the electric field, through the use of Helmholtz integrals, in terms of currents and equating the total electric field to zero along the wire surface. A solution for the integral equations is sought with the aid of Fourier-series expansions of the kernels and the currents. Then the integral equations are reduced to a set of linear simultaneous equations for the Fourier coefficients of the electric currents of the same order. A solution of this set gives the unknown coefficients which are then used to evaluate the required antenna characteristics. In particular, it is shown that the self admittance may be obtained as a sum of two parts: a finite series truncated at a number determined by the ratio of the circular loop to the wire cross section radii and a gap capacitance. The mutal admittance, on the other hand, can be obtained from a finite series only.

2.2 Formulation of the Problem

Consider an array consisting of N circular loops of arbitrary circumferences and arranged parallel to each other with their centers on the z axis, figure (2.1). The radius

of the ith loop, the radius of the conductive wire, and the driving-point voltage are denoted by b_i, a_i, and V_i, respectively.

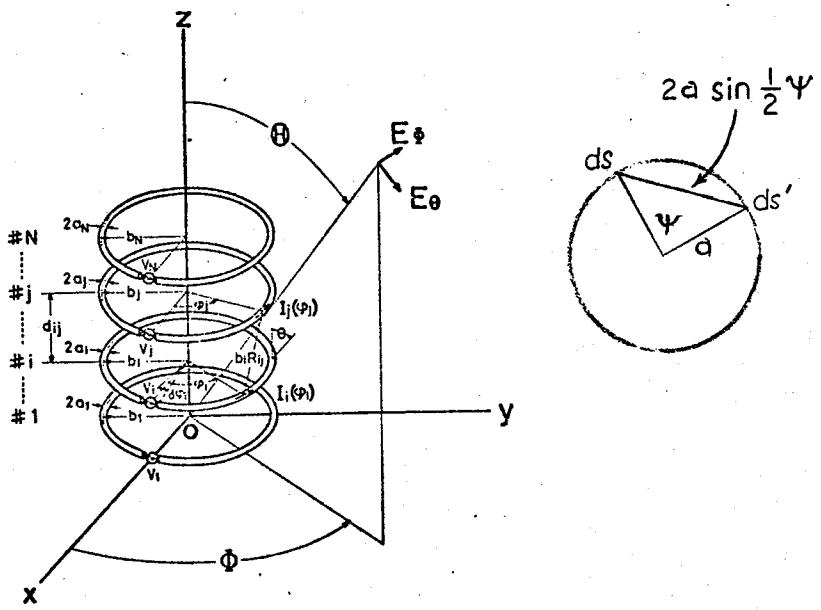

Figure 2.1 Geometry of the array.

It is assumed that

$$\frac{b_i}{a_i} >> 1 \qquad \text{and} \qquad \frac{a_i}{\lambda} << 1 \tag{2.1}$$

where λ is the wave length of the signal in free space.

The array is immersed in an infinite isotropic homogeneous medium, where its complex propagation constant is

$k = \beta - j\alpha$. If the medium is air $\alpha = 0$ and $\beta = \omega\sqrt{\varepsilon_o \mu_o} = 2\pi/\lambda = k$, where ε_o and μ_o are the permittivity and the permeability of the air, respectively. This thesis considers the latter case only, when the array is located in the air.

It is assumed that the driving-point gap width $b_i\ \delta\phi_i$ is finite and that the current $I_i(\phi_i)$ on the ith element flows uniformly in the ψ direction along the conductor surface. Following the procedure in [8]-[10] for a single loop, the integral equation satisfying the boundary conditions of the electric field on the surfaces of N circular loops may be shown to be [14]

$$-\frac{V_i}{b_i \delta\phi_i} U_i(\phi_i) = j\frac{\eta_o}{4\pi b_i} \sum_{j=1}^{N} \int_o^{2\pi} [k\, b_j \cos(\phi_i - \phi_j') + \frac{1}{kb_i} \frac{\partial^2}{\partial \phi_i^2}] W_{ij}(\phi_i - \phi_j')\, I_j(\phi_j') d\phi_j' \qquad (2.2)$$

where $i = 1, 2, 3, \ldots, N$ and

$$W_{ij}(\phi) = \begin{cases} \frac{1}{2\pi} \int_o^{2\pi} \frac{\exp[-jkb_i R_{ii}(\phi,\psi)]}{R_{ii}(\phi,\psi)}\, d\psi, & i=j \qquad (2.3) \\ \frac{\exp[-jkb_i R_{ij}(\phi)]}{R_{ij}(\phi)}, & i\neq j \qquad (2.4) \end{cases}$$

where $I_i(\phi_i)$ is the current on the ith loop, $k = \frac{2\pi}{\lambda}$ is the propagation constant, and $\eta_o = \sqrt{\frac{\mu}{\varepsilon}} = 120\Omega$ is the characteristic impedance of free space. $U_i(\phi_i)$ is equal to 1 within the driving-point gap and is zero elsewhere. The distance R_{ij} between two currents, normalized by the loop radius b_i and for $i = j$ is

$$R_{ii}(\phi,\psi) = [4 \sin^2 \frac{\phi}{2} + 4(\frac{a_i}{b_i})^2 \sin^2 \frac{\psi}{2}]^{\frac{1}{2}} \qquad (2.5)$$

and when $i \neq j$ and assuming $d_{ij} >> a_i$, it is

$$R_{ij}(\phi) = [4(\frac{b_j}{b_i})^2 \sin^2 \frac{\phi}{2} + (\frac{d_{ij}}{b_i})^2 + (\frac{b_j}{b_i} - 1)^2]^{\frac{1}{2}}$$

$$= [1 + (\frac{b_j}{b_i})^2 + (\frac{d_{ij}}{b_i})^2 - 2(\frac{b_j}{b_i}) \cos \phi]^{\frac{1}{2}} \qquad (2.6)$$

The contribution of the magnetic current existing at the driving point is omitted in the right hand side of equation (2.2) but will later be introduced as an adjustment for the gap capacitance.

In order to solve the above simultaneous integral equations the current $I_j(\phi_i)$ and the kernel $W_{ij}(\phi)$ are expanded into Fourier series

$$I_j(\phi_j) = \sum_{n=o}^{\infty} I_j^n \cos n \phi_j \qquad (j= 1, 2, \ldots, N) \qquad (2.7)$$

$$W_{ij}(\phi) = \sum_{n=-\infty}^{\infty} K_{ij}^n e^{-jn\phi} \qquad (i, j=1, 2, \ldots, N) \qquad (2.8)$$

where

$$K_{ij}^{n} = K_{ij}^{-n} = \frac{1}{2\pi}\int_{o}^{2\pi} K_{ij}^{n}(\psi)\, d\psi \qquad (2.9)$$

where for $i = j$

$$K_{ii}^{n}(\psi) = K_{ii}^{-n}(\psi) = \frac{1}{2\pi}\int_{o}^{2\pi} \frac{e^{-jkb_i R_{ii}(\phi,\psi)}}{R_{ii}(\phi,\psi)} \cdot e^{jn\phi} d\phi \qquad (2.10)$$

and for $i \neq j$

$$K_{ij}^{n} = K_{ij}^{-n} = \frac{1}{2\pi}\int_{o}^{2\pi} \frac{e^{-jkb_i R_{ij}(\phi)}}{R_{ij}(\phi)} e^{jn\phi}\, d\phi \qquad (2.11)$$

An introduction of equations (2.7) and (2.8) into the right hand side of equation (2.2), after some manipulation gives [14]

$$\beta_i^n = \frac{\sin n\left(\frac{\delta\phi_i}{2}\right)}{n\,\frac{\delta\phi_i}{2}} V_i = \sum_{j=1}^{N} Z_{ij}^{n} I_j^{n} \qquad (2.12)$$

$$(i = 1, 2, \ldots, N, \quad n \geq o)$$

where

$$Z_{ij}^{n} = \begin{cases} j\pi\eta_o kb_i K_{ij}^{1}, & n = o \\ \frac{j\pi\eta_o}{2}\left(kb_j \frac{K_{ij}^{n+1} + K_{ij}^{n-1}}{2} - \frac{n^2}{kb_i} K_{ij}^{n}\right), & n \geq 1 \end{cases} \qquad (2.13)$$

Equation (2.12) in the matrix form is

$$(Z_{ij}^{n})\,(I_j^{n}) = (\beta_i^{n}), \qquad n > o \qquad (2.14)$$

These simultaneous equations contain a group of Fourier coefficients of the current I_j^n $(j = 1, 2, \ldots, N)$ for the same order n only. The diagonal and off diagonal elements of the matrix Z_{ij}^n represents the generalized self and mutual impedances of the nth order mode of the loop current, respectively. Z_{ii}^n and Z_{ij}^n correspond to cases where the observation point of the electric field is on the same or different current elements. To calculate Z_{ij}^n and Z_{ii}^n the values of K_{ij}^n and K_{ii}^n should be known, which are given in [11] and [14], and are summarized in the following sections.

2.3 Evaluation of K_{ii}^n

$R_{ii}(\phi,\psi)$ in equation (2.10) is defined by (2.5). The term $2\, a_i/b_i \sin\frac{\psi}{2}$ in equation (2.5) corresponds to the distributed surface current. To simplify the evaluation of K_{ii}^n, the Storer's kernel [9] will be used which corresponds to the assumption of a central filamentary current. Therefore, (2.10) will be changed to

$$K_{ii}'^n = \frac{1}{2\pi}\int_0^{2\pi} \frac{e^{-jkb_i r_s}}{r_s}\, e^{jn\phi}\, d\phi \qquad (2.15)$$

where $\frac{e^{-jkb_i r_s}}{r_s}$ is Storer's kernel and

$$r_s = \sqrt{4\sin^2\frac{\phi}{2} + \left(\frac{a_i}{b_i}\right)^2} \qquad (2.16)$$

Later, after replacing a_i by $2a_i \sin\frac{\psi}{2}$ the integration with respect to ψ will be carried out.

To evaluate (2.15), Inagaki et al. [9] divided the range of integration into three regions, where in each region the value of r_s was expressed by a suitable approximation. Figure (2.2) shows the two terms in the function r_s, equation (2.16), in order to compare their magnitudes. In each region, K'^{n}_{ii} can be expressed by a suitable approximation and each term of the integral can be calculated to yield approximate results for K'^{n}_{ii} as listed in Table (2.1)

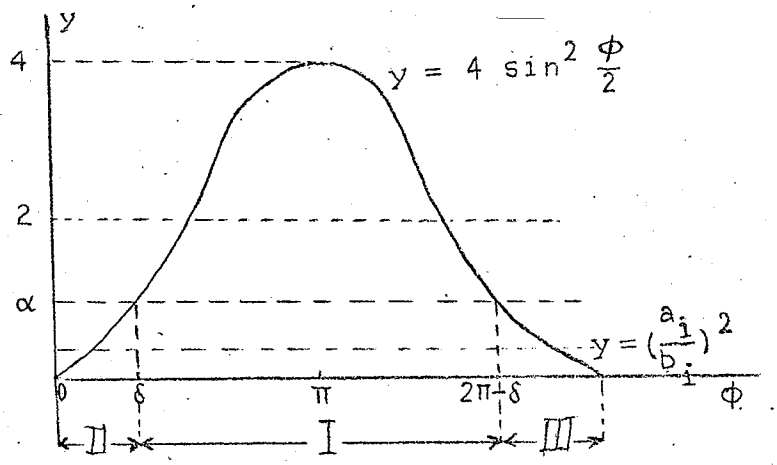

Figure 2.2 Determination of three regions where

$$\alpha = 4\sin^2\frac{\delta}{2} >> \left(\frac{a_i}{b_i}\right)^2 \quad \text{and} \quad \delta >> 1 .$$

TABLE 2.1 Approximate Equations for K'^{n}_{ii}

$n < kb_i$	$-j\frac{1}{2}H_o^2[\frac{a_i}{b_i}\sqrt{(kb_i)^2-n^2}] + \frac{1}{2\pi}\ln 16[(kb_i)^2-n^2]+j\frac{1}{2} + P_n$
$n = kb_i$	$-j\frac{1}{2}H_o^2(\frac{a_i}{b_i}n) + \frac{1}{\pi}\ln 4n + j\frac{1}{2} + P_n$
$n > kb_i$	$\frac{1}{\pi}K_o[\frac{a_i}{b_i}\sqrt{n^2-(kb_i)^2} + \frac{1}{2\pi}\ln 16[n^2-(kb_i)^2] + P_n$
$P_n = \frac{1}{2}\int_o^{2kb_i}[E_{2n}(x) - j J_{2n}(x)]dx - \frac{2}{\pi}\sum_{m=o}^{n-1}\frac{1}{2m+1} + \frac{\gamma}{\pi}$	

where

H_o^2 is the zero-order Hankel function of the second kind

K_o is the modified Bessel function of the second kind of order zero

E_{2n} is the Weber Lommel function of order $2n$

J_{2n} is the Bessel function of the first kind of order $2n$

γ is the Euler's constant (= 0.57721...) .

Replacing a_i in Table (2.1) with the variable $2a_i \sin\frac{\psi}{2}$, the integration with respect to ψ can be carried out. Since only the first terms in Table (2.1) contain the constant a_i, K'^{n}_{ii} can readily be derived with the help of the relation

$$\int_0^{\frac{\pi}{2}} K\,[2x \cos u]du = \frac{\pi}{2} I_o(X) \cdot K_o(X) \qquad (2.17)$$

where I_o is the modified Bessel function of the first kind. The results are given in Table (2.2).

Table 2.2 Approximate Equations for K_{ii}^{n}

$n < kb_i$	$-\frac{j}{2} J_o\left[\frac{a_i}{b_i}\sqrt{(kb_i)^2-n^2}\right] \cdot H_o\left[\frac{a_i}{b_i}\sqrt{(kb_i)^2-n^2}\right] + \frac{1}{2\pi} \ell n\ 16\ [(kb_i)^2-n^2] + \frac{j}{2} + P_n$
$n = kb_i$	$-\frac{j}{2} J_o\left(\frac{a_i}{b_i} n\right) \cdot H_o\left(\frac{a_i}{b_i} n\right) + \frac{1}{\pi} \ell n\ 4n + \frac{j}{2} + P_n$
$n > kb_i$	$\frac{1}{\pi} I_o\left[\frac{a_i}{b_i}\sqrt{n^2-(kb_i)^2}\right] \cdot K_o\left[\frac{a_i}{b_i}\sqrt{n^2-(kb_i)^2}\right] + \frac{1}{2\pi} \ell n\ 16\ [n^2-(kb_i)^2] + P_n$
$P_n = \frac{1}{2}\int_o^{2kb_i} [E_{2n}(x) - j\,J_{2n}(x)]dx - \frac{2}{\pi}\sum_{m=o}^{n-1} \frac{1}{2m+1} + \frac{\gamma}{\pi}$	

The integral appearing in Table (2.2) may be expressed in the following series,

$$\frac{1}{2}\int_o^{2kb_i} [E_{2n}(x) - j\,J_{2n}(x)]dx = \frac{1}{2\pi} \sum_{m=o}^{\infty} \frac{(kb_i)^{2(m+1)}}{(m+1)(n+m+\frac{1}{2})(n-m-\frac{1}{2}) \cdots} \frac{(kb_i)^{2(m+1)}}{(n+\frac{1}{2})(n-\frac{1}{2})} - j \sum_{m=o}^{\infty} J_{2n+2m+1}(2kb_i)$$

When n is very large $(n > n_i \cong \frac{b_i}{a_i})$ and noting that $I_o(x)\, K_o(x) \cong \frac{1}{2x}$ for $x \geq 1$, the asymptotic value of K_{ii}^n is,

$$K_{ii}^n \cong \frac{1}{2\pi} \frac{b_i}{a_i} \cdot \frac{1}{n} \qquad \text{for} \quad n > n_i \cong \frac{b_i}{a_i} \tag{2.18}$$

Thus, the asymptotic value of Z_{ii}^n is,

$$Z_{ii}^n = -j \frac{\eta_o}{4ka_i} \cdot n \qquad n > n_i \tag{2.19}$$

2.4 Discussions on K_{ij}^n

The coefficient K_{ij}^n which is related to the generalized mutal impedance Z_{ij}^n $(i \neq j)$ given by equation (2.11) can be represented in polynomial form in the same manner as that obtained by Greene [16] for the case n=1. Thus [17]

$$K_{ij}^n = -jkb_i \sum_{m=o}^{\infty} \frac{(\frac{y}{2z})^{n+2m}}{m!\,(n+m)!}\, h_{n+2m}^2(z) \tag{2.20}$$

$(i, j = 1, 2, \ldots, N; \quad n = 0, 1, \ldots)$

where

$$y = kb_i\, k\, b_j \tag{2.21}$$

$$z = [(kb_i)^2 + (kb_j)^2 + (kd_{ij})^2]^{\frac{1}{2}} \tag{2.22}$$

and $h_{n+2m}^2(z)$ is the second kind spherical Hankel function of order $(n + 2m)$. As the order of the spherical Hankel function

increases, its real part decreases and its imaginary part increases. Therefore, the convergence of (2.20) is determined by its real parts. Let a_n^m denote the real part of each term which constitute a series of K_{ij}^n/kb_i, then we have

$$a_n^m = - \frac{(\frac{y}{2z})^{n+2m}}{m!(n+m)!} \eta_{n+2m}(z) \qquad (2.23)$$

where, $\eta_{n+2m}(z)$ is the $(n + 2m)$th order spherical Bessel function of the 2nd kind. The ratio of the two adjacent terms a_n^{m+1} and a_n^m approaches a limit as m becomes infinite. This limit is given by

$$\frac{a_n^{m+1}}{a_n^m} \longrightarrow r = (\frac{2y}{z^2})^2 \quad , \qquad m \to \infty \qquad (2.24)$$

where, from relations (2.21) and (2.22) it is obvious that for practical arrays $(d_{ij} \neq o)$, r is always less than one. Thus, equation (2.20) converges very rapidly when r is small and can be approximated by a summation of a few terms (Appendix A).

Furthermore, another ratio can be obtained as follows

$$\frac{a_{n+1}^m}{a_n^m} \longrightarrow \begin{cases} r' = \frac{y}{z^2} & n \to \infty \ , \ m \text{ constant} \\ r'' = \frac{2y}{z^2} & m \to \infty \ , \ n \text{ constant} \end{cases} \qquad (2.25)$$

Because r' and r'' are smaller than one, a_n^m decreases monotonically with large n. Then one may consider the following inequality

$$r' \, a_n^m < a_{n+1}^m < r'' \, a_n^m \qquad , \qquad (m \geq 0) \tag{2.26}$$

summing up each term of this inequality, the following relation can be obtained

$$r' < \frac{\mathrm{Re}\,(K_{ij}^{n+1})}{\mathrm{Re}\,(K_{ij}^{n})} < r'' \tag{2.27}$$

Thus K_{ij}^n decreases monotonically for large n according to the above relationship. By considering (2.27) together with (2.13), it is concluded that the nondiagonal element Z_{ij}^n of the matrix decreases rapidly when n is greater than a certain value m_o determined by the magnitude of b_i, b_j and the spacing of the array d_{ij}. Then, the matrix (Z_{ij}^n) approaches a diagonal one. For example, if d_{ij} is more than 0.1λ and $kb_i \cong kb_j = 1$, for $n > 10$ the ratio of Z_{ii}^n to Z_{ij}^n is greater than 100 and the matrix can be approximated by a diagonal matrix (Appendix B).

2.5 Current Distribution and the Admittance

Assuming that (y_{ij}^n) represents the inverse of the matrix (Z_{ij}^n) in equation (2.14), the current $I_i(\phi_i)$ on the ith element then is given by

$$I_i(\phi_i) = \sum_{n=o}^{\infty} \left(\sum_{j=1}^{N} y_{ij}^n \beta_j^n \right) \cos n\phi_i \tag{2.28}$$

According to the preceding discussions, (y_{ij}^n) for n larger than m_o is a diagonal matrix. Thus, equation (2.28) may be reduced to

$$I_i(\phi_i) = \sum_{n=o}^{m_o} \left(\sum_{j=1}^{N} y_{ij}^{n} \beta_j^{n} \right) \cos n\phi_i + \sum_{n=m_o+1}^{\infty} \frac{\beta_i^{n}}{z_{ii}^{n}} \cos n\phi_i \tag{2.29}$$

For values of n for which the approximation (2.19) is valid, we get

$$\sum_{n=n_i+1}^{\infty} \frac{\beta_i^{n}}{z_{ii}^{n}} \cos n\phi_i = -j \frac{4ka_iV_i}{\eta_o \delta\phi_i} \int_{\phi_i-\delta\phi_i/2}^{\phi_i+\delta\phi_i/2} \ln\left(2 \sin \frac{|t|}{2}\right) dt -$$

$$- j \frac{4ka_iV_i}{\eta_o} \cdot \sum_{n=1}^{n_i} \frac{\sin\left(n \frac{\delta\phi_i}{2}\right)}{n \frac{\delta\phi_i}{2}} \cdot \frac{\cos n\phi_i}{n} \tag{2.30}$$

where $n_i \geq m_o$. For the case $0 \leq |\phi_i| \ll 1$, the integral in (2.30) can be approximated as [14]

$$- j \frac{4ka_iV_i}{\eta_o \delta\phi_i} \int \simeq$$

$$- j \frac{4ka_iV_i}{\eta_o} \left\{ \frac{\phi_i + \frac{\delta\phi_i}{2}}{\delta\phi_i} \cdot \ln\left(\phi_i + \frac{\delta\phi_i}{2}\right) - \frac{\phi_i - \frac{\delta\phi_i}{2}}{\delta\phi_i} \ln\left|\phi_i - \frac{\delta\phi_i}{2}\right| - 1 \right\} \tag{2.31}$$

When $\phi_i = \frac{\delta\phi_i}{2}$, equation (2.29) represents the driving-point current. Substituting equation (2.30) in (2.29) the results for the input current may be shown to be

$$I_i = \sum_{n=o}^{m_o} \sum_{j=1}^{N} y_{ij}^{n} \beta_j^{n} \cos \frac{n\delta\phi_i}{2} + \sum_{n=m_o+1}^{n_i} \frac{\beta_i^{n}}{z_{ii}^{n}} \cos \frac{n\delta\phi_i}{2} +$$

$$+ j4\omega\varepsilon_o a_i V_i \cdot \ell n \left(\frac{a_i e}{2\beta b_i \delta\phi_i}\right) + j \frac{4ka_i V_i}{\eta_o} \sum_{n=1}^{n_i} \frac{1}{n} \cdot \left(1 - \frac{\sin n\delta\phi_i}{n\delta\phi_i}\right) \tag{2.32}$$

where $\ell n 2\beta = \gamma$ and $\gamma = 0.5772$ is Euler's constant and use has been made of the relation

$$\sum_{n=1}^{n_i} \frac{1}{n} \cong \gamma + \ell n\, n_i$$

The fourth term in (2.32) is negligible in comparison to the sum of the first and the second terms and can be neglected. Using the relation $\sin \frac{n\delta\phi_i}{n\delta\phi_i} \cong 1$ for $n \leq n_i$, (2.32) can be written as

$$I\left(\frac{\delta\phi_i}{2}\right) = \sum_{n=o}^{m_o} \sum_{j=1}^{N} Y_{ij}^{n} V_j + \sum_{n=m_o+1}^{n_i} \frac{1}{n} \frac{V_i}{Z_{ii}} + j4\omega\varepsilon_o a_i V_i \ell n \frac{a_i e}{2\beta b_i \delta\phi_i} \tag{2.33}$$

where $b_i \delta\phi_i$ represents the gap width and hence the third term relates to the gap capacitance. Because in derivation of (2.33) the magnetic current has been neglected the gap capacitance is twice as large [18]-[19], that is

$$C_{gi} = 2\, \varepsilon_o\, a_i\, \ell n \frac{a_i e}{2\beta b_i \delta\phi_i} \tag{2.34}$$

and therefore

$$I_i\left(\frac{\delta\phi_i}{2}\right) = \sum_{n=o}^{m_o} \sum_{j=1}^{N} y_{ij}^{n} V_j + \left(\sum_{n=m_o+1}^{n_i} \frac{1}{z_{ii}^{n}} + j\omega C_{gi} \right) V_i \qquad (2.35)$$

An ordinary antenna whose gap width $b_i \delta\phi_i$ is almost equal to the diameter of the conductor has very little capacitance C_{gi}. Nevertheless the admittance matrix Y_{ij} of the array is given by the following equations:

$$Y_{ij} \begin{cases} \sum_{n=o}^{m_o} y_{ii}^{n} + \sum_{n=m_o+1}^{n_i} \frac{1}{z_{ii}^{n}} + j\omega C_{gi} , & i = j \qquad (2.36) \\ \sum_{n=o}^{m_o} y_{ij} , & i \neq j \qquad (2.37) \end{cases}$$

where $(i, j = 1, 2, \ldots, N)$.

The contribution of the magnetic current was omitted in equation (2.2), since the effect of the gap capacitance is limited to the vicinity of the driving-point [14]. The current distribution on an antenna element is not significantly affected by this omission, and hence can be expressed by

$$I_i(\phi_i) = \sum_{n=o}^{m_o} \sum_{j=1}^{N} y_{ij}^{n} V_j \cos n\phi_i + V_i \sum_{n=m_o+1}^{n_i} \frac{1}{z_{ii}^{n}} \cos n\phi_i$$

2.6 The Radiation Field and the Directive Gain

The radiation field of an N element parallel loop antenna array is the vector sum of the fields maintained by the

currents in the individual elements. In terms of spherical coordinates r, θ, ϕ, that have their origin at the center of the first loop in Figure (2.1), the radiation field can be expressed by:

$$E_\theta = -j \frac{\eta_o}{4} \frac{\exp(-jkr)}{r} \cos\theta \sum_{i=1}^{N} kb_i \exp(jkd_{i1} \cos\theta)$$

$$\cdot \sum_{n=1}^{\infty} j^n I_i^n \{J_{n-1}(x_i) + J_{n+1}(x_i)\} \sin n\phi \qquad (2.39)$$

$$E_\phi = -j \frac{\eta_o}{4} \frac{\exp(-jkr)}{r} \sum_{i=1}^{N} kb_i \exp(jkd_{i1} \cos\theta)$$

$$\cdot \sum_{n=o}^{\infty} j^n I_i^n \{J_{n-1}(x_i) - J_{n+1}(x_i)\} \cos n\phi \qquad (2.40)$$

where $x_i = kb_i \sin\theta$, r is the distance between the antenna and the observing point, $J_n(n)$ is the Bessel function of first kind of order n, and d_{i1} represents the spacing between the ith and the first elements.

Using equations (2.39) and (2.40) and the definition of the directive gain, the directive gain with respect to the z axis direction is given by

$$G_z = \frac{\pi\eta_o}{4} \frac{\left| \sum_{i=1}^{N} kb_i \exp(\pm jkd_{i1}) \cdot I_i^1 \right|^2}{\sum_{i=1}^{N} R_e(y_i) |V_i|^2} \qquad (2.41)$$

where the plus sign is for the positive direction of the z axis ($\theta = 0$) and the minus sign is for the negative direction ($\theta = \pi$).

So far it has been shown that the input admittance, the current distribution, the radiation field and the directive gain of an array of circular loop antennas can be found from equations (2.36) through (2.41). Their computation, however consumes considerable computer time when the array is made of many loops. In addition, the computer storage increases with the number of array elements and their spacings. In the next chapter, a technique is investigated, that overcomes these problems and enables the rapid calculation of the array characteristics for Yagi-Uda arrays of significant practical importance.

CHAPTER III

RESONANCE EFFECTS IN ARRAY OF CIRCULAR LOOP ANTENNAS

3.1 Introduction

The combination of a single driven loop and a closely coupled parasitic element which may function either as a reflector or as a director, as was discussed by Ito et al. [14], strongly suggests that an array of such elements would have interesting properties. An array of this kind is referred to as a Yagi array, although the name Yagi-Uda array is more appropriate since this type of array was originally described by S. Uda in Japanese at the Tohoku Imperial University in Japan.

A common Yagi antenna consists of a number of rods parallel to each other along a straight line. Only one of the elements is excited, and all others are parasitic. The elements in the direction of the increased gain are called directors and the one in the opposite direction is called the reflector. In our case all elements are replaced by circular loops.

3.2 Resonance Effects

It was shown in Chapter II that the equation for calculating the input current on each element is

$$I_i = \sum_{n=o}^{m_o} \left(\sum_{j=1}^{N} y_{ij}^{n} V_j \right) + \left(\sum_{n=m_o+1}^{n_i} \frac{1}{Z_{ii}^{n}} + j\omega C_{gi} \right) V_i \qquad (3.1)$$

where all parameters are defined as before. In the case of the Yagi-Uda array, the second element is excited and the

others are parasitics. Therefore (3.1) will be changed to

$$I_i = \begin{cases} \sum_{n=o}^{m_o} {}^{n}y_{22}\, V_2 + \sum_{n=m_o+1}^{n_i} \frac{1}{{}^{n}z_{22}} + j\omega C_{g2} , & i=2 \\ \sum_{n=o}^{m_o} {}^{n}y_{i2}\, V_2 , & i\neq 2 \end{cases} \tag{3.2}$$

The input admittance of a Yagi array is the total current at the driving point of the excited loop divided by the source voltage

$$Y_2 = \sum_{n=o}^{m_o} {}^{n}y_{22} + \left(\sum_{n=m_o+1}^{n_i} \frac{1}{{}^{n}z_{22}} + j\omega C_{g2} \right) \tag{3.3}$$

The major problem in the evaluation of Y_2 is the dimension of the matrices $({}^{n}z_{ij})$.

It can be seen that the dimension of the impedance matrices increase with the number of array elements, and the value of m_o increases with ⇒ slow rate of convergence (Appendix B). Thus the required computer storage and the computational time naturally increase with the number and size of the loops and their spacings. This introduces difficulties in the investigation of large arrays. On the other hand, circular loops are basically resonant elements and their induced currents are, mostly due to resonant modes. As a result, it may be possible to obtain satisfactory results by expanding the currents

around the resonant modes.

To investigate this, a 12-element coaxial array of equal size loops with $kb=1$ and equally spaced with $\frac{d}{\lambda} = 0.3$ is considered, where d is the separation distance of two adjacent elements. In the computation, the radius a of the wire cross section is the same in both the driven and parasitic elements, and a is related to b by $\Omega = 2\ell n\ (\frac{2\pi b}{a}) = 11$, that is, $\frac{b}{a} = 38.94$. Loop circumferences were chosen to be one wave length, since loops of this size are resonant and are of particular interest. For resonant loops one of the coefficients of the Fourier expansion becomes relatively large and an accurate result can be obtained by retaining this dominant mode only. Resonance occurs near $kb = m$, where m is an integer [20].

Table (3.1) shows the current modes on each array element at $\phi=0$. Note that the dominant mode on each loop is as expected. Other modes are relatively small, especially on the parasitic elements and die out very rapidly. In figure (3.1) the amplitude of the dominant modes and the total current computed up to 10 terms at $\phi= 0$ are shown. Except for the excited element, the total currents were too close to the dominant mode current to be distinguished in the figure. Figure (3.2) compares the magnitude of the total current on the active element with its dominant first mode. The difference between the results is almost constant along the loop and too large to be neglected. The computed H-plane radiation field using the first 10 terms of equation (2.40) is compared in Figure (3.3) with that obtained

Table 3.1 The current modes on each loop of a "12-element" loop array

kb = 1 , $d/\lambda = 0.3$

mode number n	element number i	$\lvert I_i^n \rvert$	phase of I_i^n (degrees)
0	1	0.4804×10^{-4}	+36.2
1		0.8170×10^{-2}	+12.3
2		0.6825×10^{-5}	-51.9
3		0.2947×10^{-6}	-80.1
4		0.3329×10^{-7}	-89.1
0	2	0.6291×10^{-3}	-84.7
1		0.1113×10^{-1}	-63.5
2		0.5584×10^{-3}	+89.2
3		0.2425×10^{-3}	+90.0
4		0.1453×10^{-3}	+90.0
0	3	0.4890×10^{-4}	+36.7
1		0.1306×10^{-1}	+98.3
2		0.6794×10^{-5}	-51.8
3		0.2946×10^{-6}	-80.1
4		0.3329×10^{-7}	-89.1
0	4	0.1272×10^{-4}	-60.0
1		0.9567×10^{-2}	-84.1
2		0.2542×10^{-5}	-99.0
3		0.2664×10^{-7}	-59.0
4		0.3930×10^{-9}	-57.9
0	5	0.5962×10^{-5}	-163.6
1		0.6202×10^{-2}	+100.0
2		0.1322×10^{-5}	+172.7
3		0.9925×10^{-8}	-126.5
4		0.9380×10^{-10}	- 81.7
0	6	0.3487×10^{-5}	+ 91.2
1		0.3858×10^{-2}	- 76.9
2		0.7928×10^{-6}	+ 75.3
3		0.4567×10^{-8}	+144.1
4		0.3407×10^{-10}	-157.6

kb = 1 , $d/\lambda = 0.3$

mode element n	element number i	$\lvert I_i^n \rvert$	phase of I_i^n (degrees)
0	7	0.2293×10^{-5}	- 14.6
1		0.2113×10^{-2}	+100.1
2		0.5228×10^{-6}	- 25.9
3		0.2434×10^{-8}	+ 47.0
4		0.1485×10^{-10}	+112.1
0	8	0.1624×10^{-5}	-121.1
1		0.1576×10^{-2}	- 85.9
2		0.3681×10^{-6}	-129.4
3		0.1438×10^{-8}	- 53.6
4		0.7408×10^{-11}	+ 15.7
0	9	0.1212×10^{-5}	+132.0
1		0.9753×10^{-3}	+ 95.6
2		0.2725×10^{-6}	+125.8
3		0.9170×10^{-9}	-156.5
4		0.4076×10^{-11}	- 84.1
0	10	0.9369×10^{-6}	+ 25.1
1		0.6207×10^{-3}	- 73.0
2		0.2098×10^{-6}	+ 20.1
3		0.6193×10^{-9}	+ 99.3
4		0.2419×10^{-11}	+174.0
0	11	0.7561×10^{-6}	- 82.1
1		0.3070×10^{-3}	+124.6
2		0.1657×10^{-6}	- 85.8
3		0.4375×10^{-9}	- 5.7
4		0.1523×10^{-11}	+ 70.7
0	12	0.5816×10^{-6}	+169.7
1		0.9798×10^{-4}	- 31.4
2		0.1349×10^{-6}	+167.1
3		0.3201×10^{-9}	-111.4
4		0.1005×10^{-11}	- 33.5

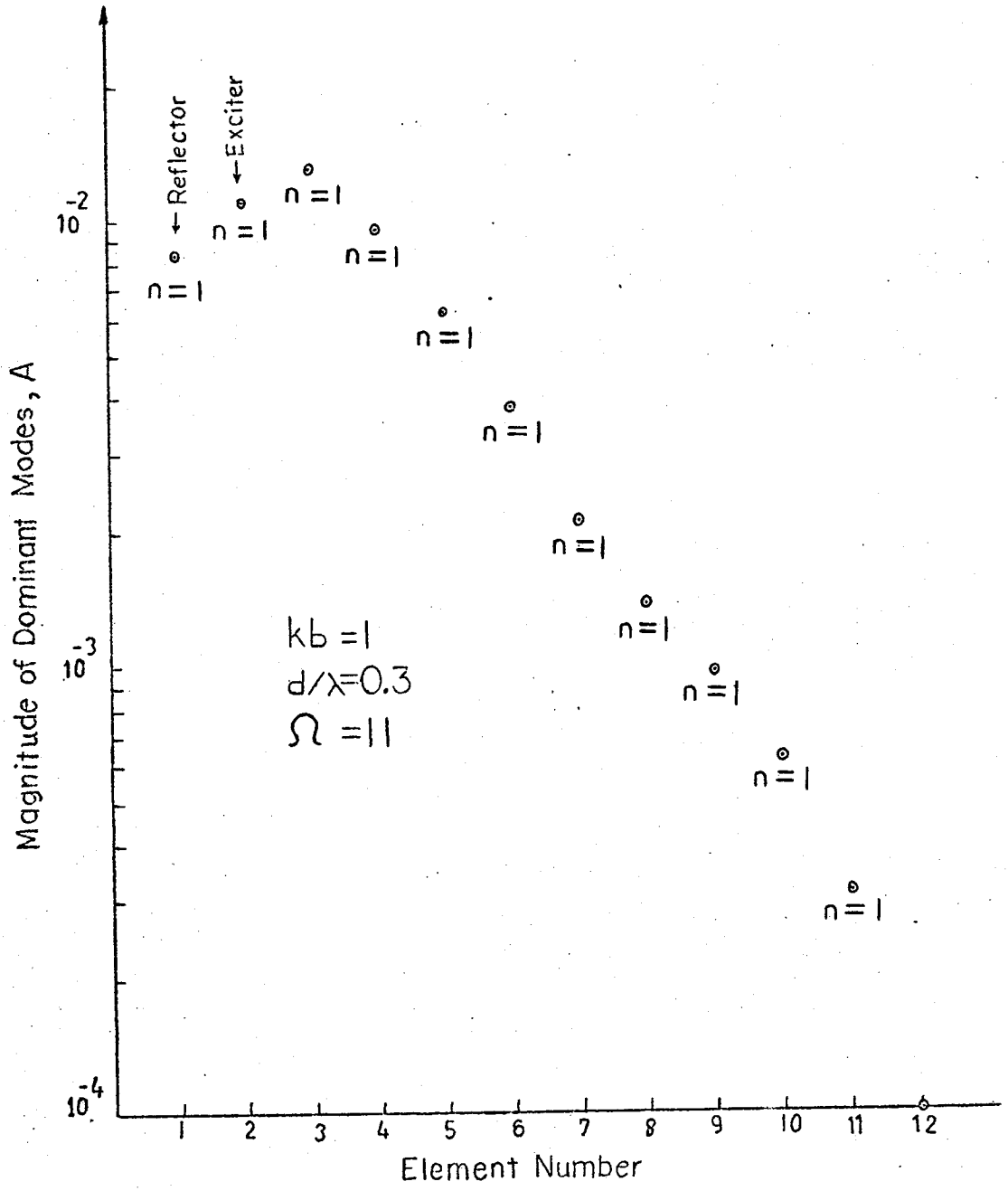

FIG. 3.1 Dominant mode of each array element at $\phi = 0°$

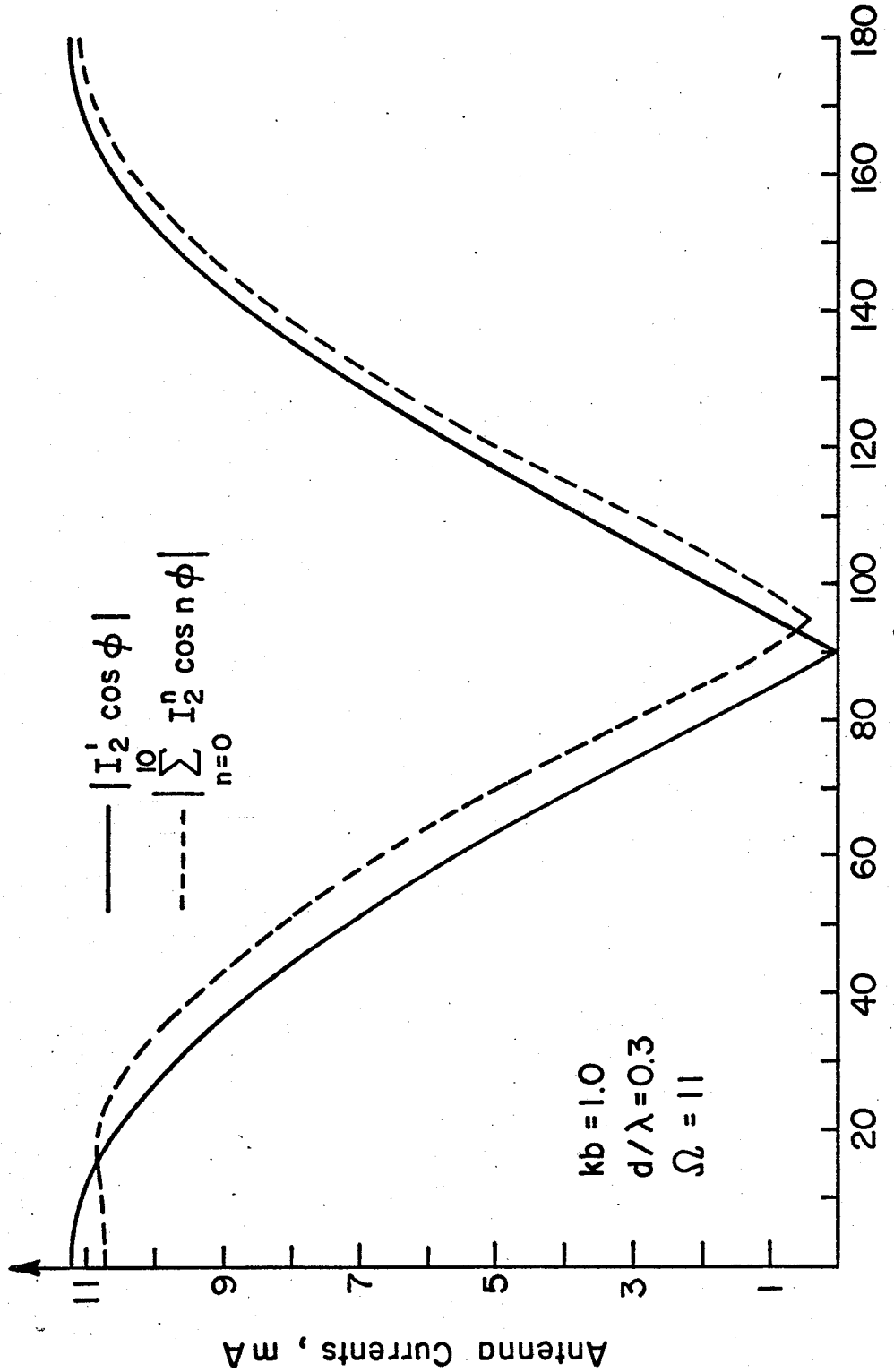

Fig. 3.2 Current distributions on the active element

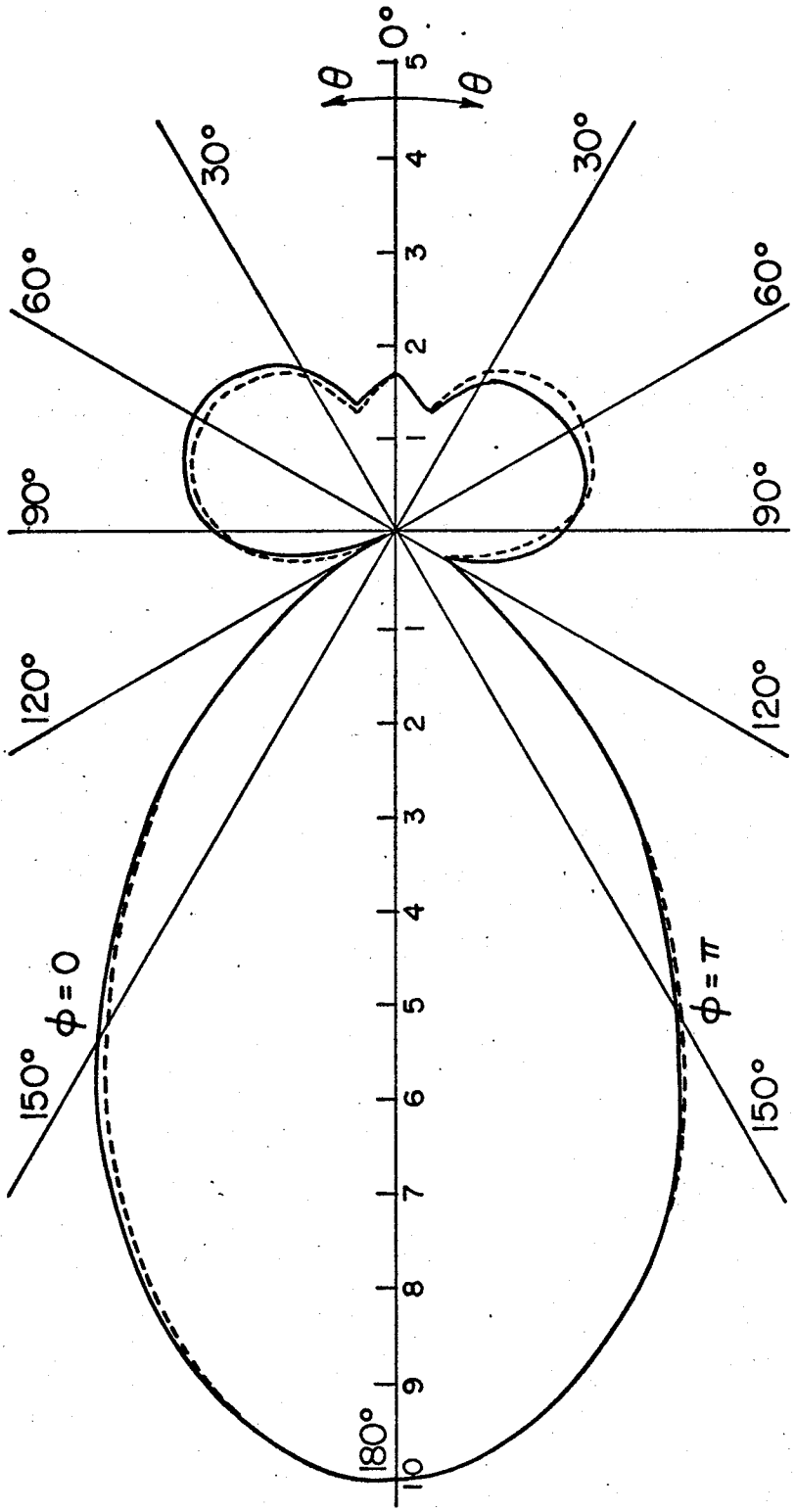

Fig. 3.3 Radiation pattern of a "Twelve-element" loop array

using the dominant mode (n=1). As illustrated in the figure, the two field patterns are in good agreement with each other. Therefore, it can be said that the n=1 mode contributes the principle part of the field for this particular circumference of the array elements.

For further examination another 12-element array of equal size and equispaced loops was chosen where kb=1.5, $d/\lambda=0.3$, and $\Omega=2\ell n\ 2\pi b/a=11$ as before. The circumferences of the loops were chosen to be 1.5λ, since these loops are off resonance and provide a worst case analysis for the above technique. The computed magnitude of the current modes up to the tenth mode on each loop, at $\phi=0$, are shown in Table (3.2). It is easy to see that although the n=1 mode has the largest magnitude other modes for n=0 and 2 are not that small, relative to the first mode, and thus can not be ignored, especially on the exciter. As an example, Table (3.2) gives the ratio of the magnitude of the current for n=1 and 2 at the center of the array (the sixth element) as almost 10, but the same ratio obtained from Table (3.1) is more than 1000. Thus here, one should not expect to get an accurate pattern by using only the n=1 mode in the computation. Figure (3.4) shows the magnitude of the current distributions on the active loop for the total of the first 10 modes, sum of the n=0, 1, and 2 modes, sum of the n=0, and 1 modes and the n=1 mode alone, along the loop. From this figure it is clear that retaining the n=0, 1 and 2 modes should be adequate for accurate field calculations. The exact radiation field of

Table 3.2. The current modes on each loop of "12-element" loop array

kb = 1.5, d/λ = 0.3				kb = 1.5, d/λ = 0.3			
mode number n	element number i	$\|I_i^n\|$	phase of I_i^n (degrees)	mode number	element number	$\|I_i^n\|$	phase of I_i^n (degrees)
0	1	0.6788×10^{-4}	+ 35.1	0	7	0.3486×10^{-5}	- 20.2
1		0.1299×10^{-2}	- 30.1	1		0.1697×10^{-3}	+176.8
2		0.1308×10^{-3}	- 61.5	2		0.2015×10^{-4}	- 50.8
3		0.3626×10^{-5}	- 68.3	3		0.8242×10^{-7}	+ 39.1
4		0.5441×10^{-6}	- 87.2	4		0.9367×10^{-9}	+105.2
0	2	0.3887×10^{-3}	- 77.3	0	8	0.2518×10^{-5}	-127.2
1		0.3012×10^{-2}	- 47.3	1		0.1395×10^{-3}	+145.8
2		0.1346×10^{-2}	+ 84.3	2		0.1520×10^{-4}	-151.6
3		0.4219×10^{-3}	+ 89.7	3		0.4916×10^{-7}	- 60.1
4		0.2341×10^{-3}	+ 90.0	4		0.4757×10^{-9}	+ 9.7
0	3	0.7063×10^{-4}	+ 35.7	0	9	0.1911×10^{-5}	+125.8
1		0.1742×10^{-2}	- 35.1	1		0.1048×10^{-3}	+ 93.0
2		0.1256×10^{-3}	- 59.9	2		0.1183×10^{-4}	+107.2
3		0.3620×10^{-5}	- 68.3	3		0.3153×10^{-7}	-161.9
4		0.5440×10^{-6}	- 87.2	4		0.2640×10^{-9}	- 89.4
0	4	0.1795×10^{-4}	- 60.9	0	10	0.1496×10^{-5}	+ 19.2
1		0.1173×10^{-2}	- 81.4	1		0.5595×10^{-4}	+ 32.5
2		0.6233×10^{-4}	-126.8	2		0.9457×10^{-5}	+ 3.4
3		0.7325×10^{-6}	- 67.2	3		0.2137×10^{-7}	+ 94.6
4		0.1798×10^{-7}	- 52.2	4		0.1577×10^{-9}	+169.3
0	5	0.8603×10^{-5}	-167.9	0	11	0.1230×10^{-5}	- 88.4
1		0.6503×10^{-3}	-127.3	1		0.8845×10^{-5}	- 55.6
2		0.3972×10^{-4}	+143.1	2		0.7543×10^{-5}	- 98.4
3		0.3077×10^{-6}	-137.7	3		0.1512×10^{-7}	- 9.8
4		0.5417×10^{-8}	- 89.1	4		0.9983×10^{-10}	+ 66.4
0	6	0.5214×10^{-5}	+ 85.4	0	12	0.8886×10^{-6}	+163.8
1		0.3072×10^{-3}	-164.1	1		0.1147×10^{-4}	+106.5
2		0.2757×10^{-4}	+ 47.2	2		0.6360×10^{-5}	+152.8
3		0.1501×10^{-6}	+134.5	3		0.1107×10^{-7}	-115.4
4		0.2086×10^{-8}	-165.4	4		0.6610×10^{-10}	- 37.4

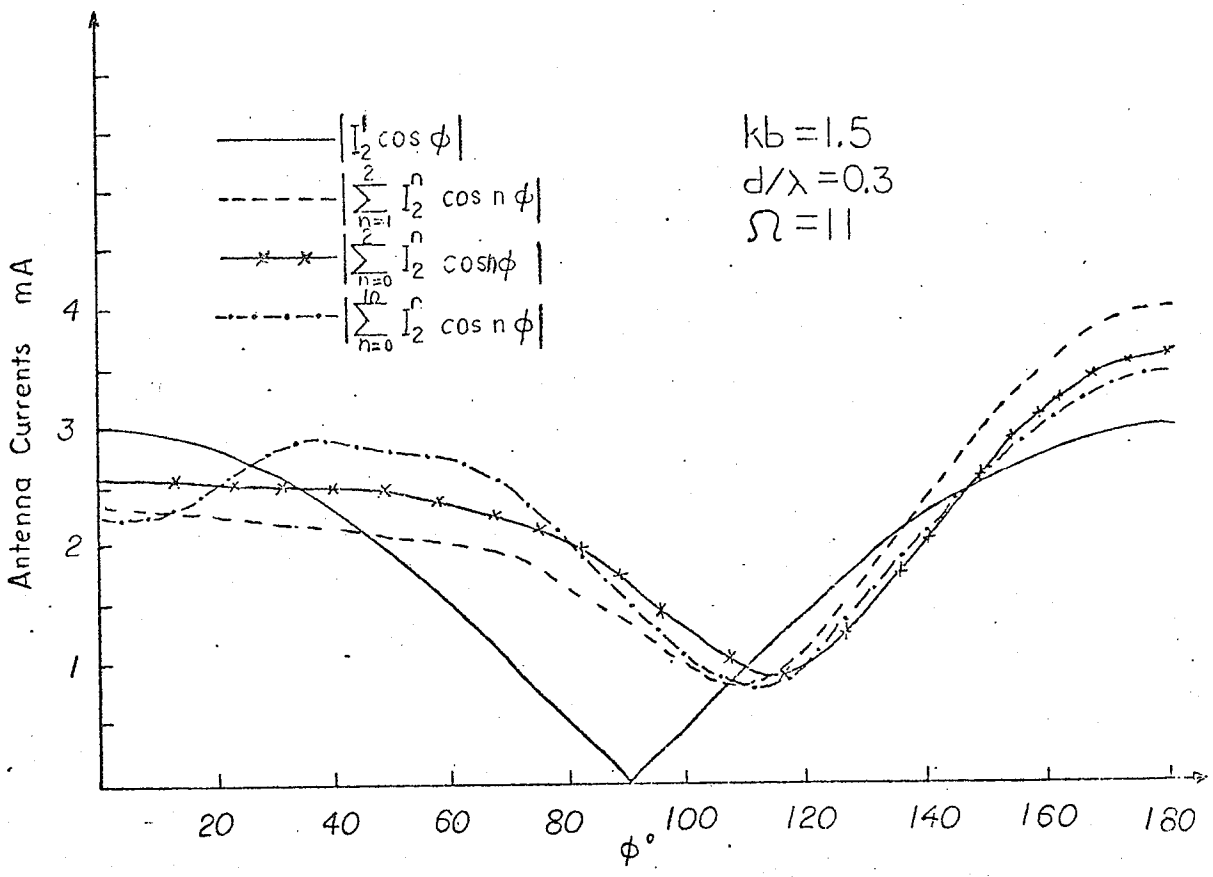

Fig.3.4 Current distributions on the active element

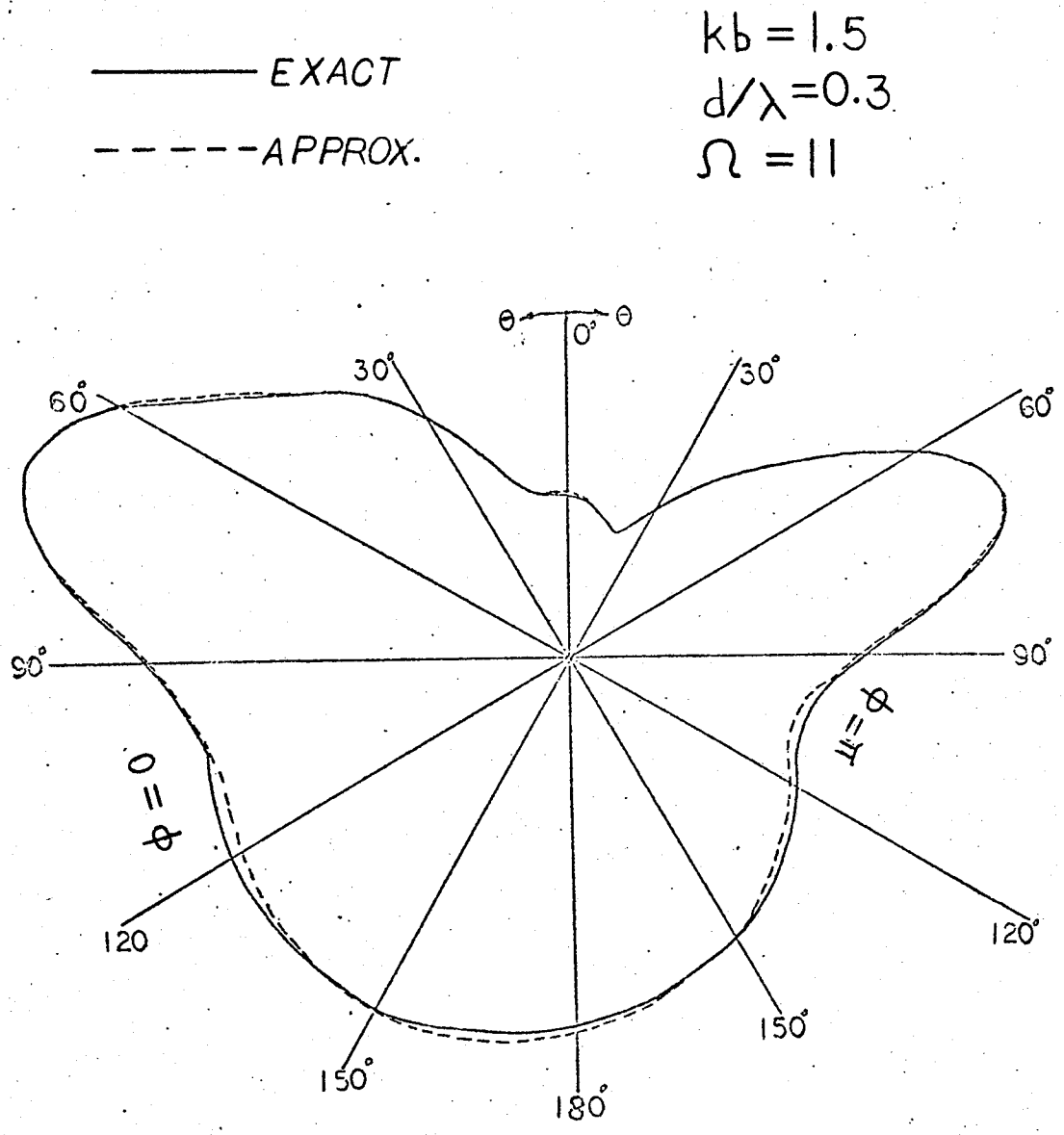

Figure 3.5 Radiation patterns of a "12-element" loop array in the H-plane.

this antenna in the H-plane and computed field pattern using only the n=0, 1, and 2 modes is given in Figure (3.5). Their good agreement is evident.

For further investigations, an array of unequal loops was considered. In this array the circumference of the elements was varied from $kb_1 = 4$ to $kb_{12} = 0.7$ with $\Delta(kb) = 0.3$ and $d/\lambda = 0.3$. The large difference between the circumference of these loops was chosen to provide different dominant modes for different array elements. The magnitudes of the current dominant modes on each loop computed at $\phi=0$ are shown in Figure (3.6). It is interesting to note that the order of dominant modes decreases with the element size. That is, for a particular mode in current expansions the effective size of the array is much shorter than its actual physical size and neglecting the remaining part of the array will have negligible effect on the computed results. The matrix elements and consequently the required storage and computational time. From Figure (3.6) it is clear that modes up to at least n=4 need to be included in the computation of the radiation field of this antenna. Figure (3.7) shows the exact computed field pattern along with the pattern found by using four current modes. Again, the agreement is acceptable.

Next, the same array was studied but it was excited at the opposite end ($kb_1 = 0.7$, $kb_2 = 1$, ..., $kb_{11} = 3.7$, $kb_{12} = 4$). The magnitude of dominant modes at $\phi=0$ are shown in Figure (3.8). It is interesting to see that the dominant mode for all elements is the n=1 mode, in spite of the element size. This means that when the active loop is

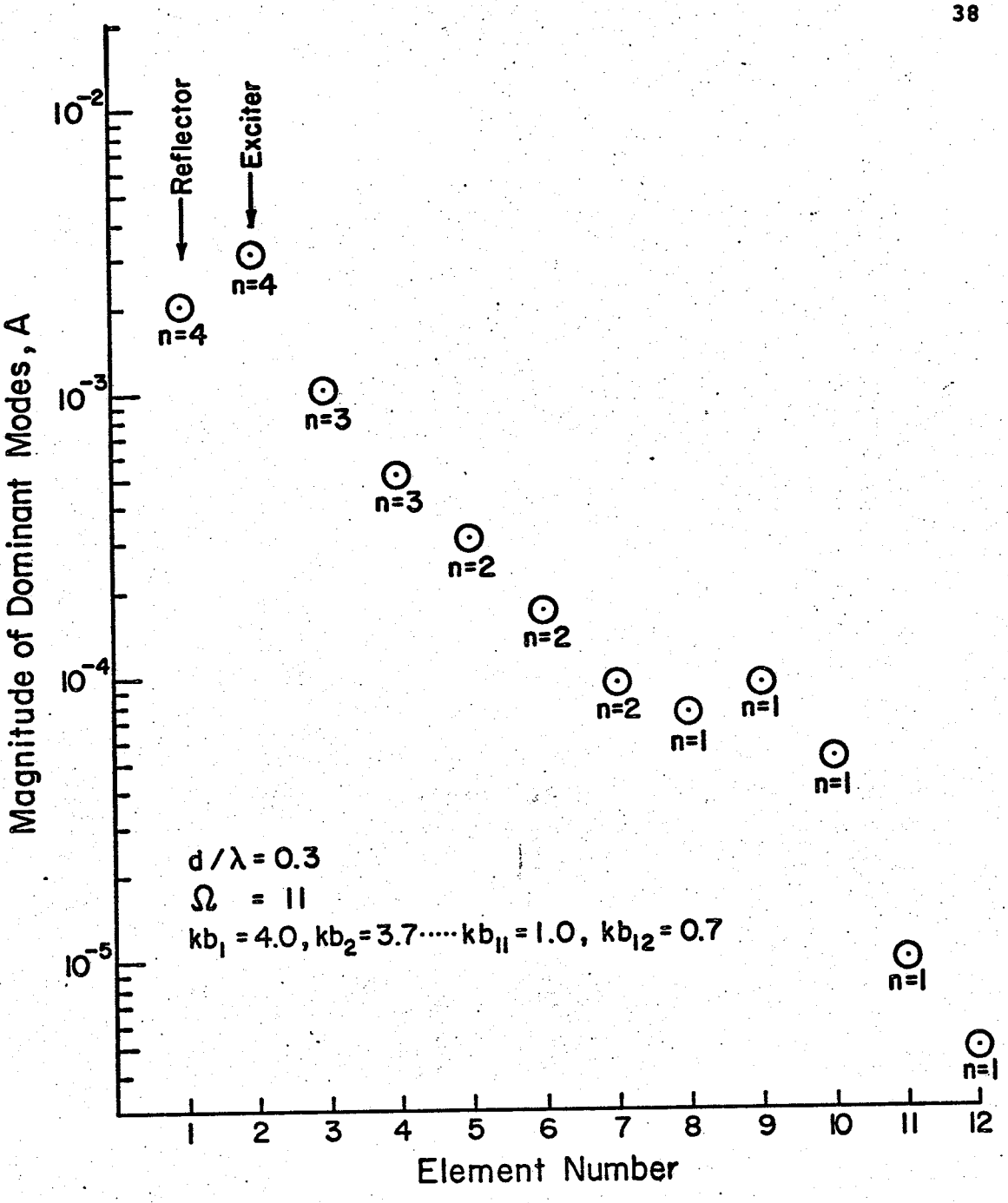

FIG.36 Dominant mode of each array element at $\phi = 0°$

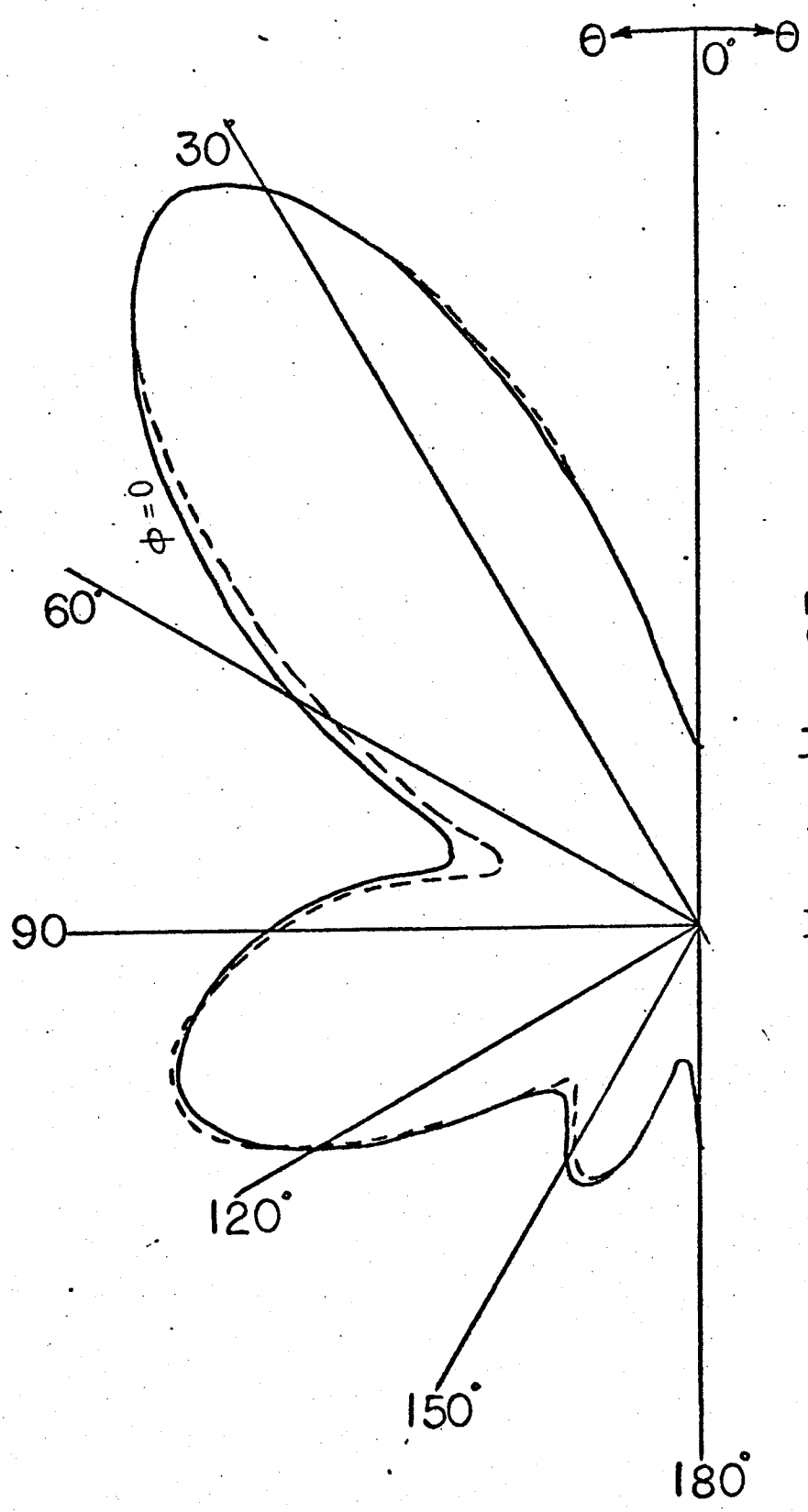

Figure 3.7 Radiation pattern of a "12 element" array in the H-plane.

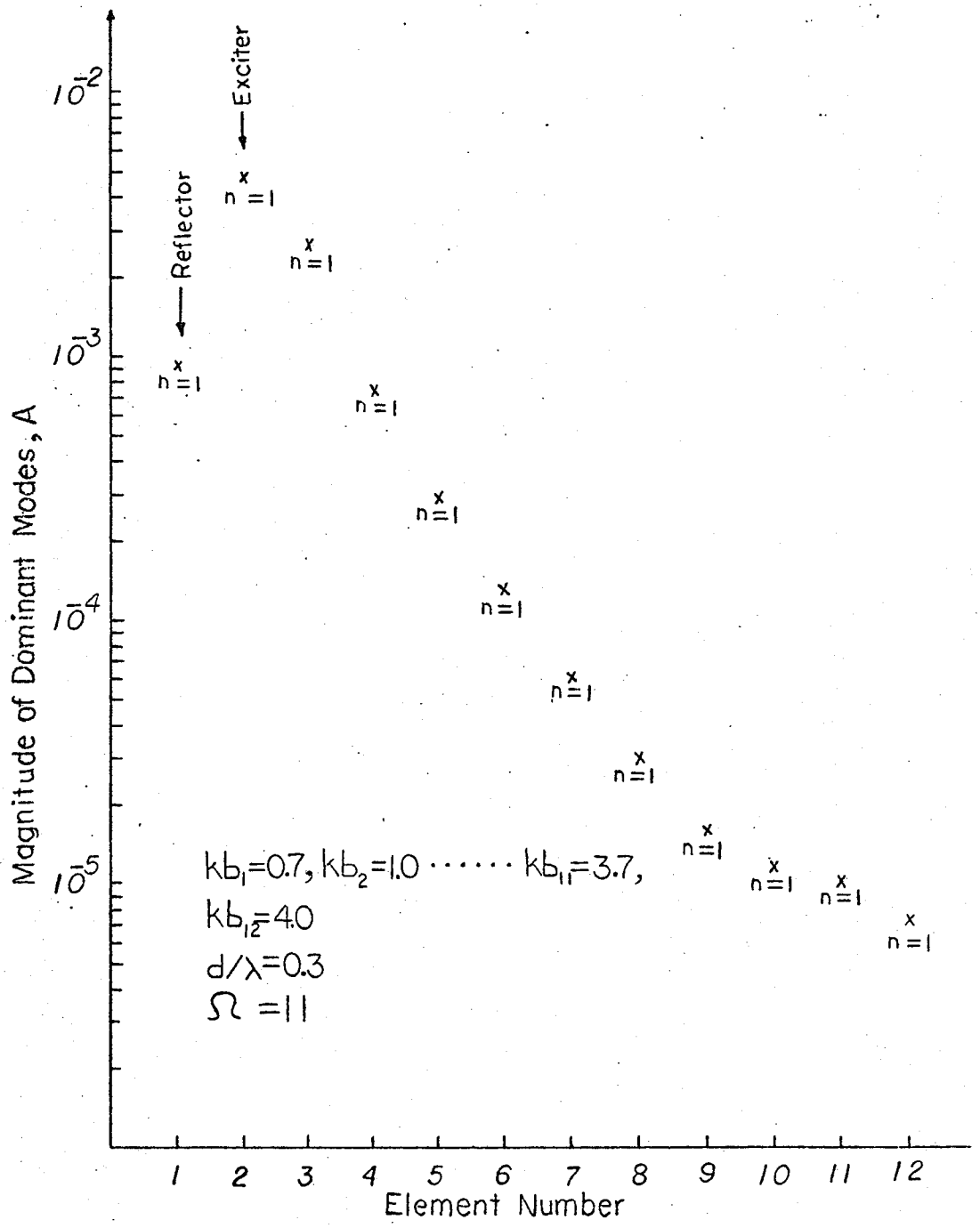

Fig.3.8 Dominant mode of each array element at $\phi=0°$

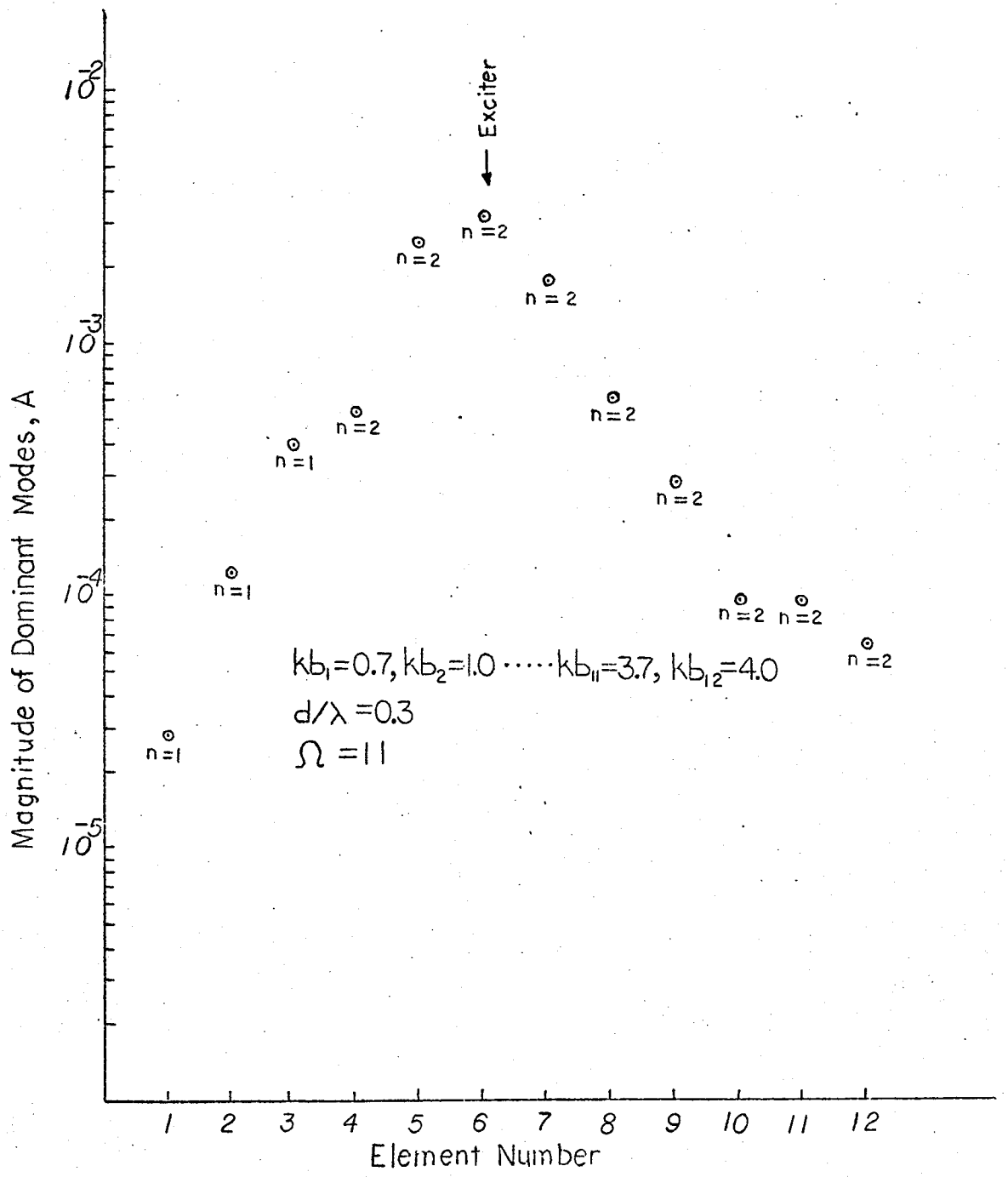

Fig.3.9 Dominant mode of each array element at $\phi=0°$

smaller than the directors, the dominant mode along the array is the same as the dominant mode of the excited loop, no matter how big the directors are. To investigate this further, the same array was excited at $kb_6 = 2.5$. The magnitude of dominant modes at $\phi=0$ are given in Figure (3.9). Note that again loops greater than kb_6 have the same dominant mode as kb_6.

The following may clarify the behaviour of the currents in the array. It is known that the currents appearing in the parasitic elements are induced by the radiation from a near by driven antenna. When the loops are equal, i.e., $kb=1$, the dominant mode for the active loop is at $n=1$ and can propagate along the array as the dominant mode. But in the case of unequal loops ($kb_1=4$, $kb_2=3.7$, ..., $kb_{11}=1$, $kb_{12}=0.7$) the dominant mode for the excited one is at $n=4$ and is described by $I_2^4 \cos 4\phi$. This mode can not be supported on smaller loops and has smaller magnitude. Lower modes are more suitable and appear stronger. Now, the same array is excited at $kb=1$ loops. The dominant mode for this loop is at $n=1$ and $I_2^1 \cos\phi$ represents its distribution around the loop. This mode can be supported on all elements and will be propagated along the array.

3.3 Application to the Input Admittance

Input or terminal admittance of the antenna is of primary concern for the communication engineer interested in the overall design of a radio communication system. The terminal admittance of a Yagi-Uda array is given by equation

(3.3). Difficulty arises from the value of m_o, apart from the number of loops in the array which is related to the dimension of the impedance matrix. Here, the difficulty is more severe, since one cannot find an accurate value for Y_2 by considering only the dominant mode and neglecting the others. However, it is still possible to focus on the dominant mode (or modes), which can propagate along the array much stronger than the others. Referring to Tables (3.1) and (3.2), the current modes (except the dominant one) after a few directors adjacent to driven element become very small and do not contribute appreciably to the input admittance. Therefore, their effectmaybe neglected on the rest of the array. This fact suggests the truncation of the array for these modes. For further clarification, rewrite equation (3.3) in the following form

$$Y_2 = Y + Y' + Y'' \tag{3.5}$$

where

$$Y = \sum_{N}^{N} y_{22} \tag{3.6}$$

$$Y' = \sum_{n}^{m_o} y_{22} \qquad (n \neq N) \tag{3.7}$$

$$Y'' = \sum_{n=m_o+1}^{n_i} \frac{1}{z_{22}^{n}} + j\omega C_{g2} \tag{3.8}$$

and N is the dominant mode number (or numbers). Equation (3.6) should be computed for the whole array and (3.7) may

be computed for an array containing only few directors (usually two). To compute Y_2 the value of m_o should be determined and is shown in Appendix B for different sizes and spacings of loops.

Now the exact values of the input admittance for the above arrays and those obtained by the above technique will be compared.

Case 1

Loops are equal (kb=1) and the spacings between two adjacent ones is $d=0.3\lambda$. As it was shown in Table (3.1) the n=1 mode is dominant and others are relatively small. Thus, N in equation (3.6) is 1, and for other modes (3.7), which represents an array of only two directors (kb_3 and kb_4) may be used. Table (3.3) compares the computed y_{22}^n using all directors in the computation, and taking only the first two. The last line of this table shows the approximate results as computed by the above procedure. Their excellent agreement is obvious.

Table 3.3 Comparison of the exact and approximate results for y_{22}^n

n	y_{22}^n taking the whole array into account		y_{22}^n truncating the array after the second director	
0	0.580173×10^{-4}	$-j0.626517 \times 10^{-3}$	0.580172×10^{-4}	$-j0.626315 \times 10^{-3}$
2	0.708141×10^{-5}	$+j0.558406 \times 10^{-3}$	0.708189×10^{-5}	$+j0.558408 \times 10^{-3}$
3	0.697450×10^{-7}	$+j0.242559 \times 10^{-3}$	0.697448×10^{-7}	$+j0.242559 \times 10^{-3}$
4	0.516293×10^{-9}	$+j0.145315 \times 10^{-3}$	0.516293×10^{-9}	$+j0.145315 \times 10^{-3}$
5	$-0.641727 \times 10^{-10}$	$+j0.100117 \times 10^{-3}$	0.641727×10^{-10}	$+j0.100117 \times 10^{-3}$
6	$-0.555189 \times 10^{-10}$	$+j0.747491 \times 10^{-4}$	0.555189×10^{-10}	$+j0.747491 \times 10^{-3}$
7	$-0.472830 \times 10^{-10}$	$+j0.588312 \times 10^{-4}$	0.472830×10^{-10}	$+j0.588312 \times 10^{-4}$
8	$-0.415294 \times 10^{-10}$	$+j0.480671 \times 10^{-4}$	0.415294×10^{-10}	$+j0.480671 \times 10^{-4}$
Input admittance of array (exact value)			Input admittance of array (approximation)	
	0.5025439×10^{-2}	$- j0.891805 \times 10^{-2}$	0.5025412×10^{-2}	$-j0.891804 \times 10^{-2}$

Case 2

$$kb_1 = kb_2 = \ldots, kb_{12} = 1.5 \quad , \frac{d}{\lambda} = 0.3 \quad , \Omega = 2\ell n \frac{2\pi b}{a} = 11$$

From Table (3.2), equations (3.6) - (3.8) will become

$$Y = \sum_{n=0}^{2} {}^{N}y_{22} \tag{3.6}'$$

$$Y' = \sum_{n=3}^{m_o} {}^{n}y_{22} \tag{3.7}'$$

$$Y'' = \sum_{n=m_o+1}^{n_i} \frac{1}{{}^{n}z_{22}} + j\omega C_{g2} \tag{3.8}'$$

Case 3

$$kb_1 = 4,\ kb_2 = 3.7,\ kb_3 = 3.4,\ \ldots,\ kb_{11} = 1$$

and $kb_{12} = 0.7$, $d/\lambda = 0.3$ and $\Omega = 2\ell n\ 2\pi b/a$.

From Figure (3.8), equations (3.6) - (3.8) can be written as

$$Y = \sum_{N=1}^{4} {}^{N}y_{22} \tag{3.6}''$$

$$Y' = y_{22}^{o} + \sum_{n=5}^{m_o} {}^{n}y_{22} \tag{3.7}''$$

$$Y'' = \sum_{n=m_o+1}^{n_i} \frac{1}{{}^{n}z_{22}} + j\omega C_{g2} \tag{3.8}''$$

The exact computed admittance and the approximated one for cases 2 and 3 are given as follows.

Table 3.4 Comparison of the exact and approximate values of the input admittance.

	INPUT ADMITTANCE USING:	
	Ito et al. formula	The approximation technique
Case 2	$0.226065 \times 10^{-2} + j0.512048 \times 10^{-3}$	$0.226065 \times 10^{-2} + j0.512049 \times 10^{-3}$
Case 3	$0.259196 \times 10^{-2} + j0.4721224 \times 10^{-2}$	$0.259196 \times 10^{-2} + j0.4721222 \times 10^{-3}$

Again, the excellent agreement between the two values is obvious.

Therefore, one concludes that when the array is composed of equal loops of kb=1 (resonance length), N is one in equation (3.6). That is, taking the inverse of the impedance matrix only for the n=1 mode is enough, which reduces the required computer storage and time significantly.

If loops are about or equal to 1.5λ (anteresonance length) using N=0, 1, and 2, i.e., using equations (3.6)', (3.7)' and (3.8)' will give accurate results for the input admittance. But, if the loops are unequal, then it is advisable to choose N from the lowest possible dominant mode in the array to the highest one, as it was seen in case 3. However, in a practical array the difference between the circumferences of adjacent loops is very small. Thus, it is adequate to take the whole array into account not more than a few times.

The above discussion is also walid for the pattern computation and the infinite series in equations (2.39) and (2.40) could be replaced by a finite one with a small loss in the accuracy of the results.

3.4 Computation of Dominant Modes

So far, it was shown that to obtain the radiation field and the input admittance of a large array, only the dominant mode (or modes) must be computed by considering the whole array. Therefore, the computer running time and the required memory are reduced considerably. However, if

the array is very large, computing the dominant mode (or modes) will itself be costly. Recalling that in a Yagi array only one of the elements; which is usually near one of the ends, is excited, the others being parasitic, one may expect that the induced currents on the elements far from the exciter are small compared to those of the exciter and elements adjacent to it. Therefore, these currents should not affect significantly the loop currents at the other end of the array and may be neglected. To investigate such an approximation equations (2.12)-(2.14) of Chapter II are rewritten, thus:

$$(Z_{ij}^{n})\ (I_j^{n}) = (\beta_i^{n})$$

where

$$\beta_i^{n} = \sin \frac{n\frac{\delta\phi_i}{2}}{n\frac{\delta\phi_i}{2}}\ V_i$$

Assuming that

$$\sin \frac{n\frac{\delta\phi_i}{2}}{n\frac{\delta\phi_i}{2}} \simeq 1 \qquad \text{for } n\frac{\delta\phi_i}{2} \ll 1$$

and only the second loop is excited, then

$$Z_{11}^{n}\ I_1^{n} + Z_{12}^{n}\ I_2^{n} + \ldots, \quad Z_{1,N}^{n}\ I_N^{n} = 0$$

$$Z_{21}^{n}\ I_1^{n} + Z_{22}^{n}\ I_2^{n} + \ldots, \quad Z_{2,N}^{n}\ I_N^{n} = V_2$$

(3.9).....

$$
\begin{aligned}
&Z^{n}_{31} I^{n}_{1} + Z^{n}_{32} I^{n}_{2} + \cdots \quad Z^{n}_{3,N} I^{n}_{N} = 0 \\
&\vdots \qquad\qquad\qquad\qquad\qquad\qquad\qquad\qquad \vdots \\
&Z^{n}_{N,1} I^{n}_{1} + Z^{n}_{N,2} I^{n}_{2} + \cdots \quad Z^{n}_{N,N} I^{n}_{N} = 0
\end{aligned}
\tag{3.9}
$$

where N is the number of loops.

Assume now that the currents on the last m loops are very small relative to the others so that replacing them by zero would not affect the currents on the other loops. Therefore, the problem of an array with N loops becomes equivalent to that of having $M = N - m$ loops. Hence

$$
\begin{aligned}
&Z^{n}_{11} I^{n}_{1} + Z^{n}_{12} I^{n}_{2} + \cdots, \quad Z^{n}_{1,M} I^{n}_{M} = 0 \\
&Z^{n}_{21} I^{n}_{1} + Z^{n}_{22} I^{n}_{2} + \cdots, \quad Z^{n}_{2,M} I^{n}_{M} = V_2 \\
&Z^{n}_{31} I^{n}_{1} + Z^{n}_{32} I^{n}_{2} + \cdots, \quad Z^{n}_{3,M} I^{n}_{M} = 0 \\
&\vdots \qquad\qquad\qquad\qquad\qquad\qquad\qquad\qquad \vdots \\
&Z^{n}_{M,1} I^{n}_{1} + Z^{n}_{M,2} I^{n}_{2} + \cdots, \quad Z^{n}_{M,M} I^{n}_{M} = 0
\end{aligned}
\tag{3.10}
$$

The above set of equations may be solved for I^{n}_{1}, I^{n}_{2}, ..., I^{n}_{M}. The calculated currents on truncated elements will differ from those on original array elements, especially on the mth element and those adjacent to it. However, with a good approximation, it is possible to have the current close to their exact values. Now, if the currents on the first m' loops are accurate, substituting these currents in the set of equations (3.9), will yield a new set of equations with

N - m' unknowns. If the array had a large number of elements one may assume that the currents on the last elements are still very small relative to the (m'+1)th element and retruncate the array for further approximation and calculation of the currents. The process may be continued until all the currents are calculated.

3.5 Typical Pattern Calculation

Based on the previously discussed concepts, a computer program was written to calculate the radiation pattern of an array of 12 equispaced and equisized loops with kb = 1 and a separation distance d = 0.3λ. The array was divided into two groups

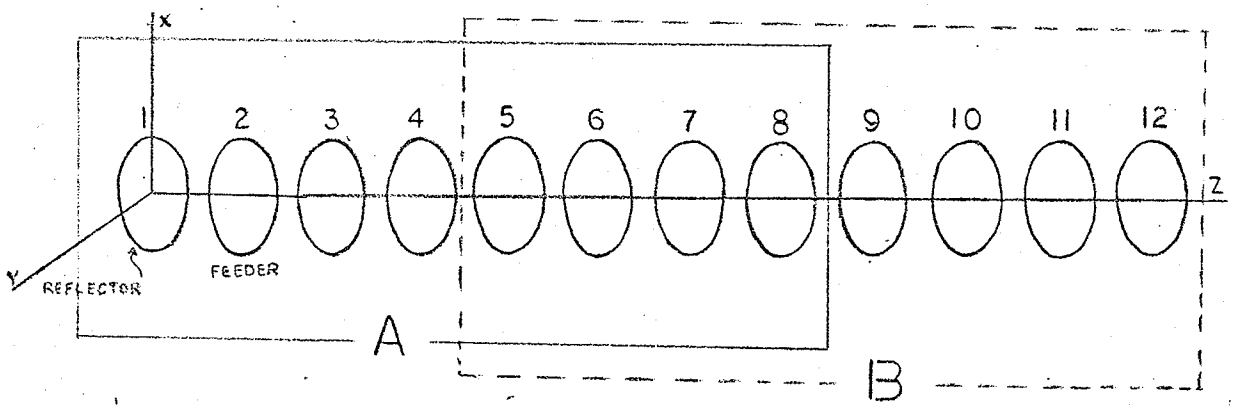

Figure 3.10 A "12-element" loop array divided into two groups.

A, and B, such that each had eight loop and had a common part as shown in Figure 3.10. The dominant mode of group A was calculated by neglecting the remaining portion of the array. It was then assumed that the computed currents on half of the elements in A were accurate. These currents were substituted into the original matrix equation for the whole

array and the new set of equations was solved for the currents on the loops in group B. The far fields were computed with and without the truncation and are given in Figure 3.11.

To examine the accuracy of the truncation method, many arrays with different sizes and spacing were chosen and some of the computed patterns are shown in Figures 3.12 - 3.14.

From the results it was found that for this method to yield accurate results, some restrictions have to be placed on the director spacings for different director sizes:

i. for director sizes close to one wave length, i.e., resonant length, the director spacing must be at least about 0.3λ ($d_D \geq 0.3\lambda$),

ii. for director sizes about $kb \approx 0.9$ one must have $d_D \geq 0.2\lambda$,

iii. when director circumferences are 0.7 to 0.8 wave lengths then one should have $d_D \geq 0.1\lambda$,

These restrictions arise from the fact that this method is based on the negligibility of the currents on the directors far from the driven element. When director circumference is about 0.7λ or 0.8λ the amplitudes of the currents in all of the parasitic elements except those close to the driven loop are quite small relative to those on the driven elements and loops close to it. Therefore, neglecting them is a good approximation if the groups are not too small. On the other hand, as director circumference approaches the resonant

length the amplitudes of the currents increase greatly and oscillate in magnitude from element to element which indicates the existence of a standing wave on the array. To use the method discussed in this section, the above mentioned restriction on the director size and spacing about resonance should be imposed.

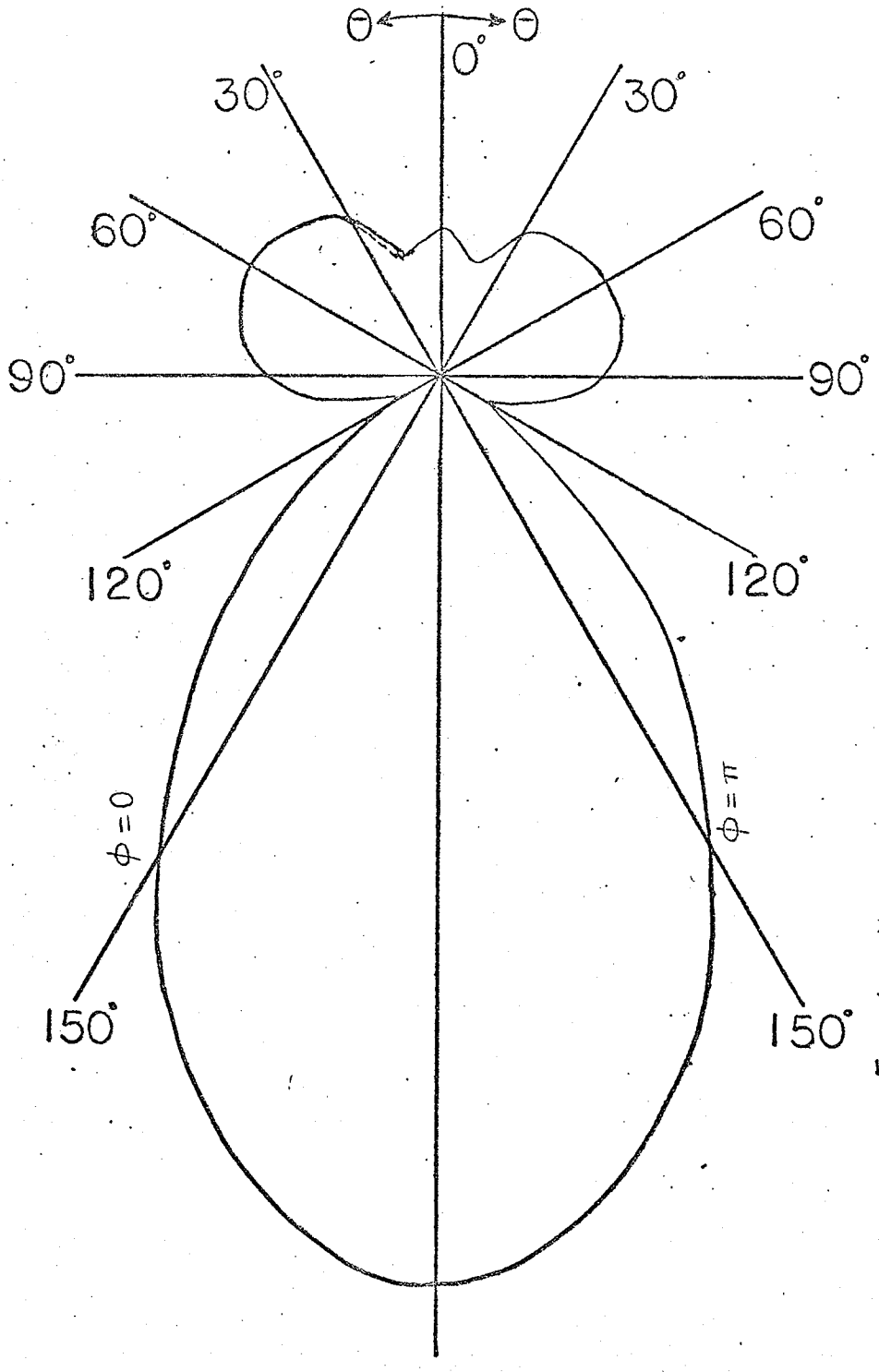

Fig. 3.11 Radiation pattern of a "Twelve-element" loop array

Excellent agreement can be seen

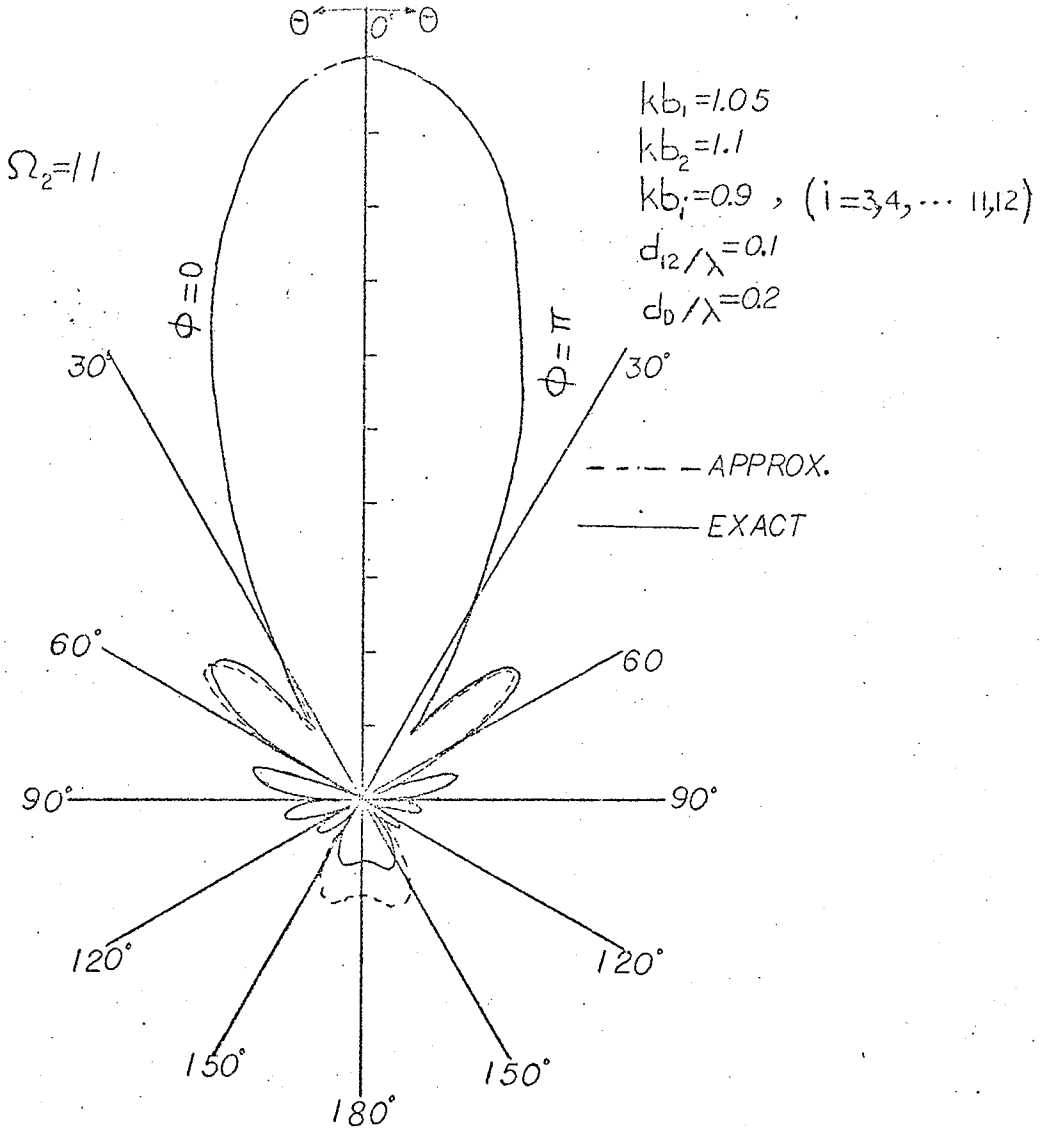

Figure 3.12 Radiation pattern of a "12-element" loop array in the H-plane.

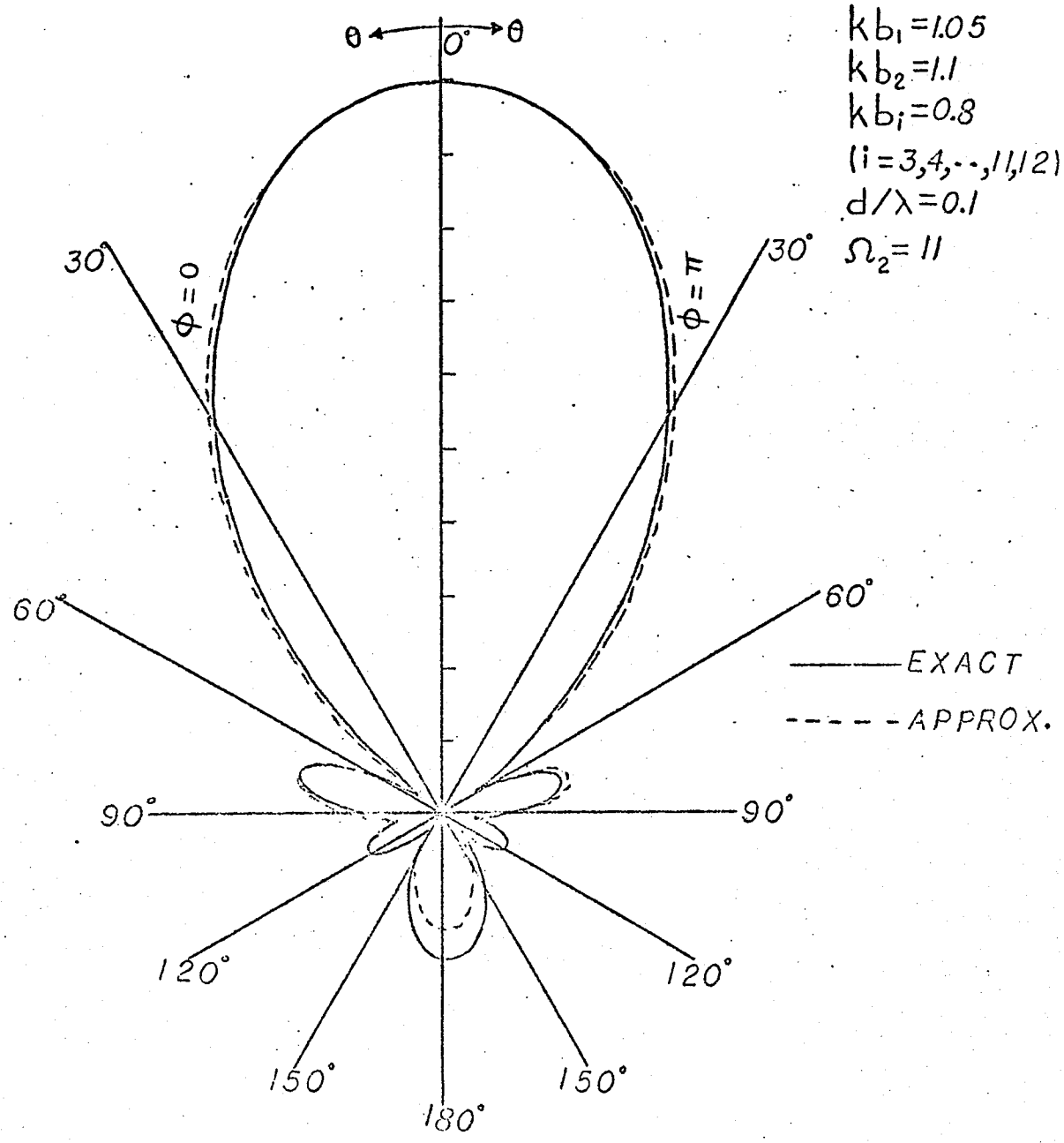

Figure 3.13 Radiation pattern of a "12-element" loop array in the H-plane.

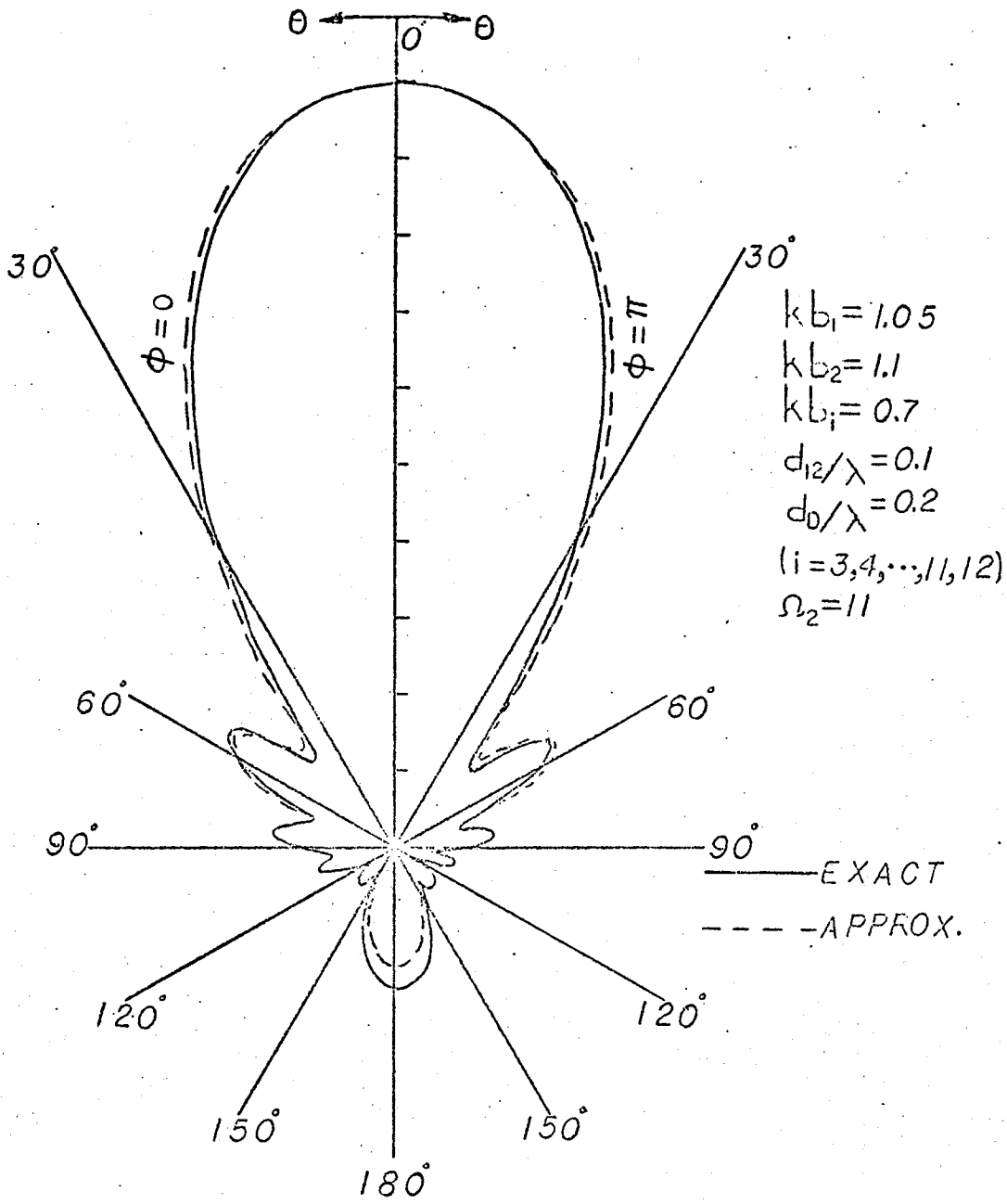

Figure 3.14 Radiation pattern of a "12-element" loop array in the H-plane.

CHAPTER IV

INVESTIGATION OF THE FAR FIELD PATTERN OF THE LOOP ARRAYS

4.1 Introduction

The radiation pattern of an antenna is generally its basic requirement, since it determines the spatial distribution of the radiated energy. A complete radiation pattern gives the radiation for all angels of ϕ and θ and requires a three-dimensional representation. In practice, however, its cross sections in planes of interest are usually adequate. Cross sections in which the radiation patterns are most frequently given are the horizontal ($\theta = 90°$) and vertical (ϕ = constant) planes. The terms E-plane pattern and H-plane pattern are also in common use. The E and H planes are respectively the planes passing through the antenna axis in the direction of maximum $\vec{E}$ and $\vec{H}$ vectors [21]. All radiation patterns depicted here show the relative field strength in various directions, referred to unity in the direction of maximum radiation.

4.2 Radiation Pattern of the Loop Arrays

The problem of determining the radiation field of a Yagi-Uda array has been of great importance and has received considerable attention. By a proper choice of the antenna parameters (loop's size, spacing, wire cross section, and array's length) it is practically possible to obtain a large

gain in the array direction. As a result, a yagi-Uda array is an end fire antenna. An end fire aerial is one in which the direction of maximum radiation is parallel, or nearly parallel, to the major dimension of the aerial and its radiation pattern is usually symmetric about the direction and thus has equal beamwidths in its two principal planes. Because an end fire array is of major interest, it is sufficient to consider the far field pattern only in the y-z plane (E-plane) or x-z plane (H plane).

It has been shown by Zucker [22] and others that long periodic structures theoretically support a propagating plane wave along their axis. The existance of the traveling wave on such a structure has been confirmed by recent experimentation [19]-[20]. The commonly used Yagi-Uda array can be regarded as a section of this periodic structure with proper terminating ends. The application of the traveling wave idea to the Yagi antenna is a relatively new concept. R.A. Smith [23] suggested that the physical action of the directors in the Yagi array is to reduce the phase velocity of the wave traveling along the axis of the Yagi. This is equivalent to saying that the wave radiated by the driven element travels through a region of refractive index greater than unity.

Since a Yagi-Uda array supports a traveling wave, only one element of the array needs excitation and currents on the parasitic elements have progressive phase shifts resulting in a very directional field pattern. The amount of phase shift and distribution of the current on each element determine the

field pattern and the gain of the antenna. To obtain a desired radiation field the correct dimensions of the parameters must be chosen.

Ehrenspeck and Poehler [24] have shown by experiment that common Yagi antennas can be considered as two parts: the combination of feeder-reflector and the row of director elements. From their experiment it can be concluded that the reflector contributes negligible radiation in the forward direction. If this is the case, changing the reflector length and spacing should not have significant effect on the forward radiation pattern. This will be studied here numerically for the arrays with loop elements. Also, the effect of director size and spacing, wire cross section, and exciter size on the radiation pattern will be studied. The size of the active loop is kept constant ($= 1.1\lambda$) together with the wire cross section, which is the same for all loops ($\Omega_2 = 2 \ell n \, 2\pi \frac{b_2}{a}$ or $\frac{b_2}{a} = 38.94$, where b_2 is the radius of the active loop) while studying all different cases except the cases for which the effects of the excited loop size and wire cross sections were to be investigated. Using the above relation and circumference of loops in wave length, a similar relation for other loops can be found as

$$\frac{b_i}{a} = \frac{kb_i}{1.1} \cdot \frac{b_2}{a} \tag{4.1}$$

where the index i represents the ith element in the array. In the following the effects of array parameters on the radiation pattern will be discussed separately.

4.3 Effects of the Reflector Spacing

An array of twelve elements; equispaced loops; is chosen where the directors are equal loops with $kb_i = 1$ ($i = 2, 3, \ldots, 12$) and the reflector size is equal to 1.05 wave lengths. The separation distance between two adjacent loops is 0.1λ. The computed radiation pattern of this array in the H-plane is given in figure (4.1). Then, the reflector spacing was increased from 0.1λ to 0.125λ and 0.15λ with the other parameters of the array being held constant. A comparison of the radiation pattern of these three cases in figure (4.1) reveals that they are almost the same in the front direction, but there is a change in the back lobe levels. The variations of the computed input admittance and directive gains with the reflector spacing are illustrated in figure (4.2). This figure shows that the imaginary part of the input admittance of the array and Gd, the directive gain in the positive z direction ($\theta = 0$), are independent of the reflector spacing (Gd for $\frac{d_{12}}{\lambda} = 0.1$ is about 0.3 dB greater than Gd for $\frac{d_{12}}{\lambda} = 0.22$). However, the real part of the input admittance which is proportional to the radiation power, and Gr, the directive gain in the negative z direction, are very much dependent on that. Therefore, we can say that altering the reflector spacing is a good method for controlling the input impedance of the array and changing the level of the back lobe without providing a significant change in the foward radiation.

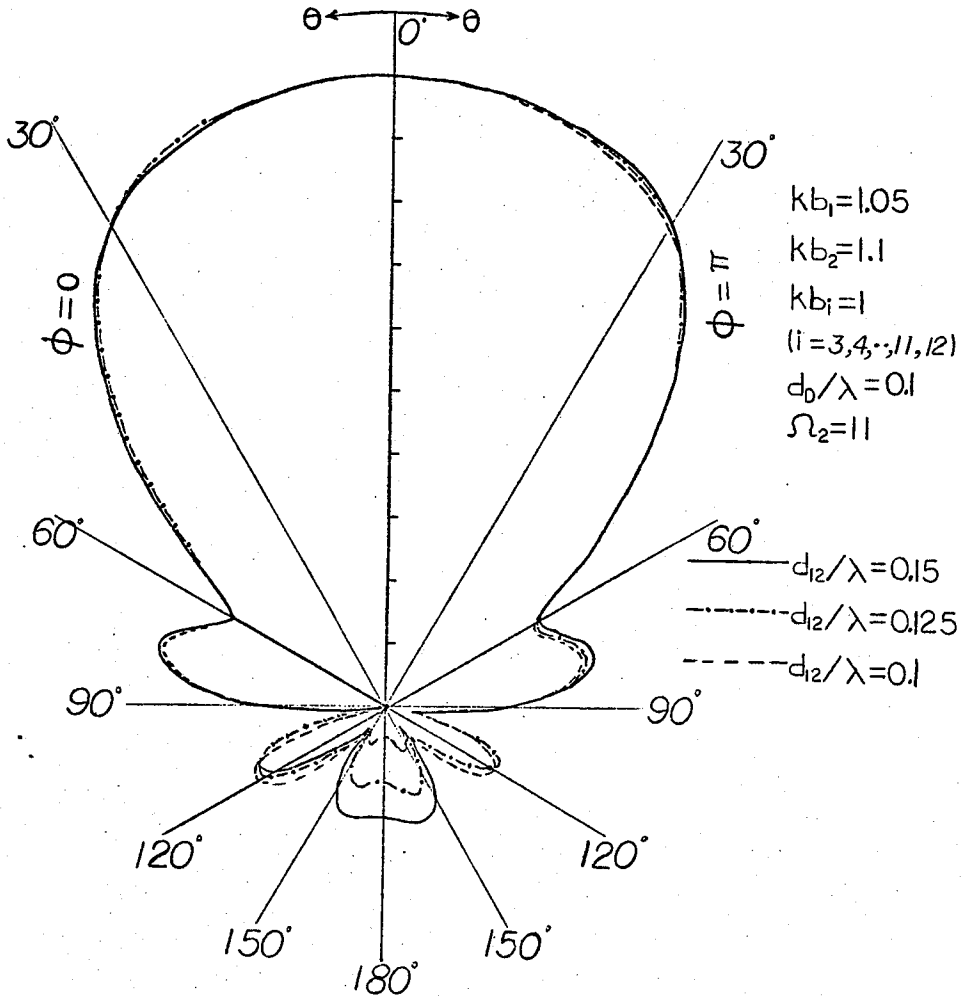

Figure 4.1 Radiation patterns in the H-plane for different reflector spacings.

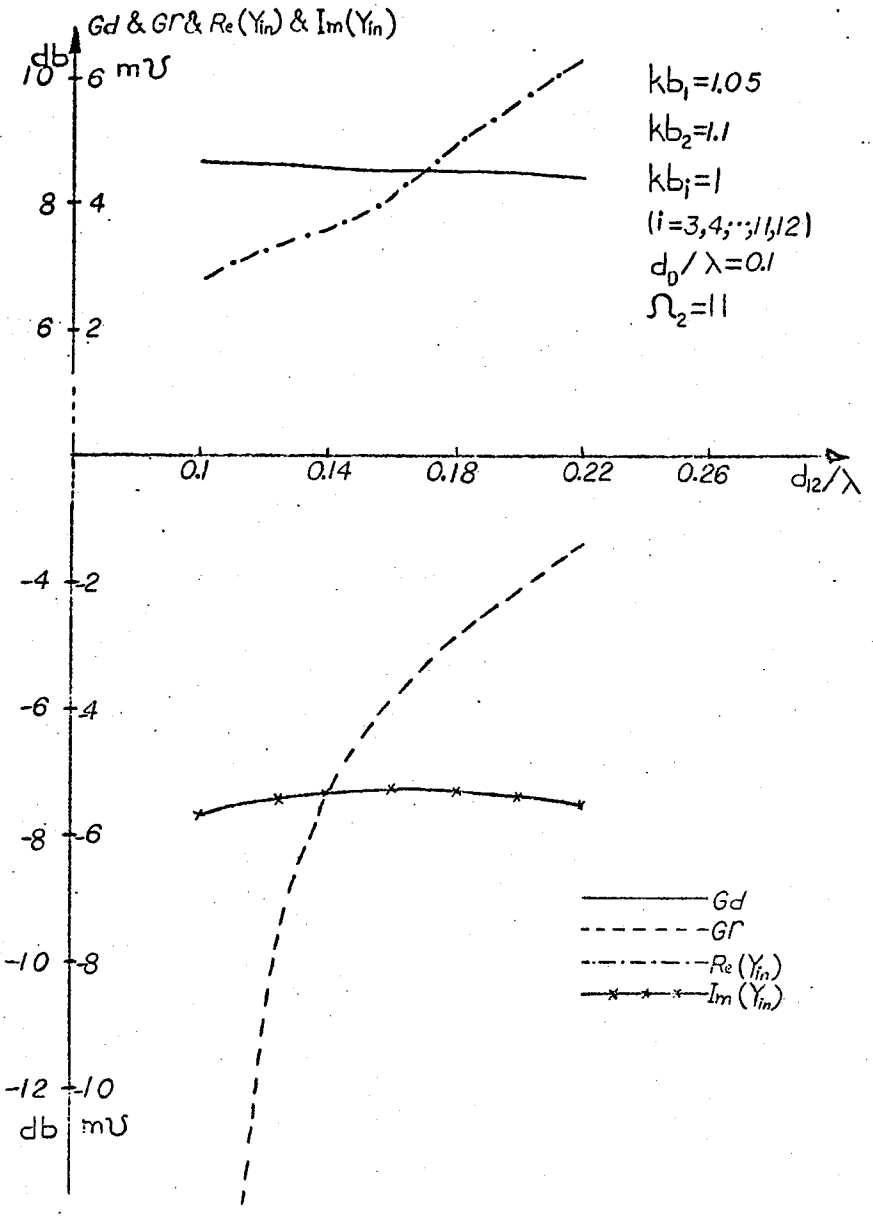

Figure 4.2 Behaviour of the directive gains, Gr and Gd, and the input admittance for different reflector spacing .

4.4 Effect of the Reflector Size

The same array as used in section 4.3 was taken, where the separation distance of adjacent loops was 0.1λ and the reflector size was 1.05 wave lengths, and the reflector size was increased to 1.2 wavelengths in four steps with $\Delta(kb_1) = 0.05$, where all other parameters were held constant. The computed far field in the H-plane for each case is given in figure (4.3) In this figure the forward radiation is the same (variation in the beamwidth is less than 2% in each step) and the side lobe levels are almost equal, but the back radiation is effected significantly by altering the size of the reflector. The variation of the computed directive gain and the input admittance with the reflector size are shown in figure (4.4). An examination of this figure shows that the input admittance and the directive gain in the negative z direction are very sensitive to the size of the reflector. Therefore, altering the reflector size could be also a good method for controlling the input impedance of the array and changing the back lobe level.

The computer print-out of the reflector current for this and those of previous sections has shown that when the directive gain in the back direction decreases, the magnitude of the reflector current at $\phi = 0$ increases. This result is in contrast to that reported for rod Yagi arrays by Theile [25] where the back radiation decreases as the reflector current decreases.

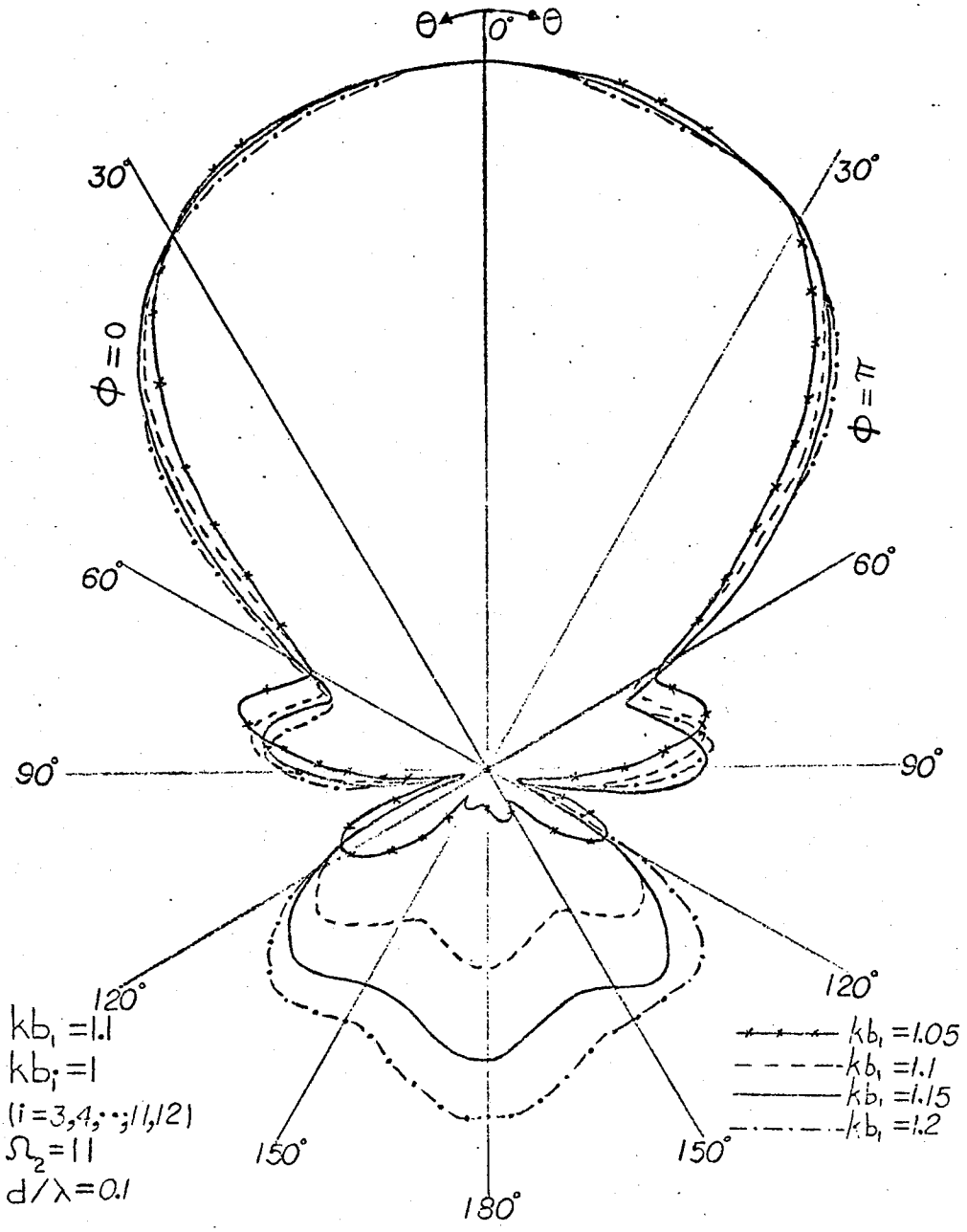

Figure 4.3 Radiation patterns in the H-plane for various director sizes.

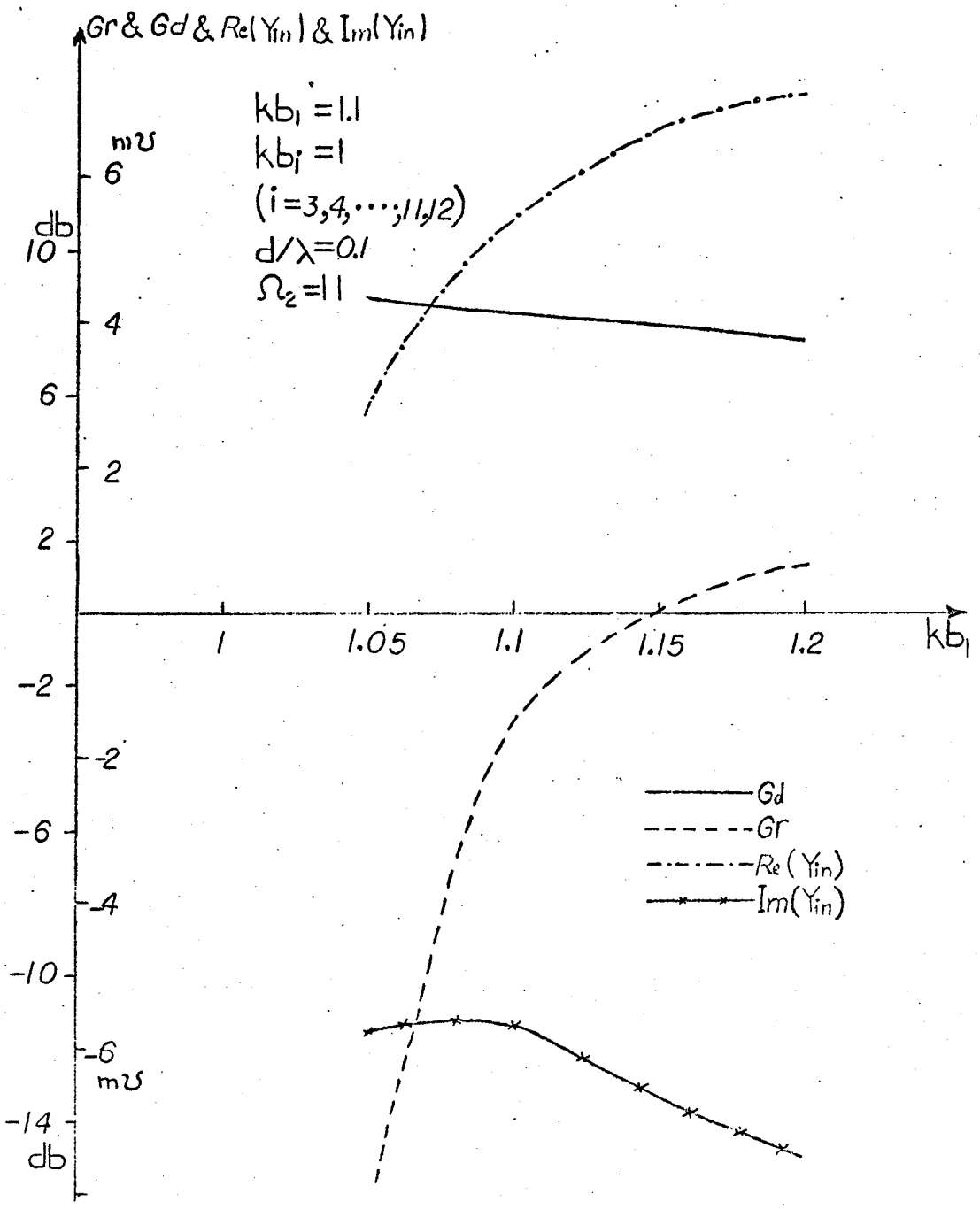

Figure 4.4 Behaviour of the directive gains, Gr and Gd, and the input admittance for different reflector sizes.

4.5 Effect of Director Spacings

So far, it has been shown that the reflector size or spacing did not significantly affect the forward radiation of the loop Yagi array. Since the current distribution on directors determines the far field pattern, and because these current distributions depend on the size and spacings of the directors, one should therefore expect that they have a significant effect on the forward radiation. To examine the effect of directors on the radiation in the forward direction the following cases were considered.

A twelve-element array was chosen with $kb_i = 1$ ($i = 3, 4, \ldots, 12$) and $kb_1 = 1.05$, with the reflector spacing of 0.1λ. The directors were equispaced and their spacing was changed from $d_D = 0.1\lambda$ to 0.3λ in unequal steps. The computed far field patterns in the H-plane are given in figures (4.5) and (4.6). Figure (4.5) shows that increasing d_D from 0.1λ to 0.120λ and then to 0.15λ has decreased the beamwidth by about 20% and 38% respectively, but the side and the back lobe levels have increased. Figure (4.6) depicts the patterns for $d_D = 0.2$, 0.25 and 0.3 wave length. An examination of these patterns reveals that although for $d_D = 0.2\lambda$ the beamwidth has decreased to 40°, the level of side lobes has increases. For $d_D = 0.25\lambda$ the first side lobe has joined the main lobe and maximum radiation is at $\theta = 25°$ and we have almost a unique radiated power in about 60° in front direction. For $d_D = 0.3\lambda$ the radiation pattern is completely deteriorated and maximum radiation is at $\theta=180°$. The variation of Gd, Gr and the

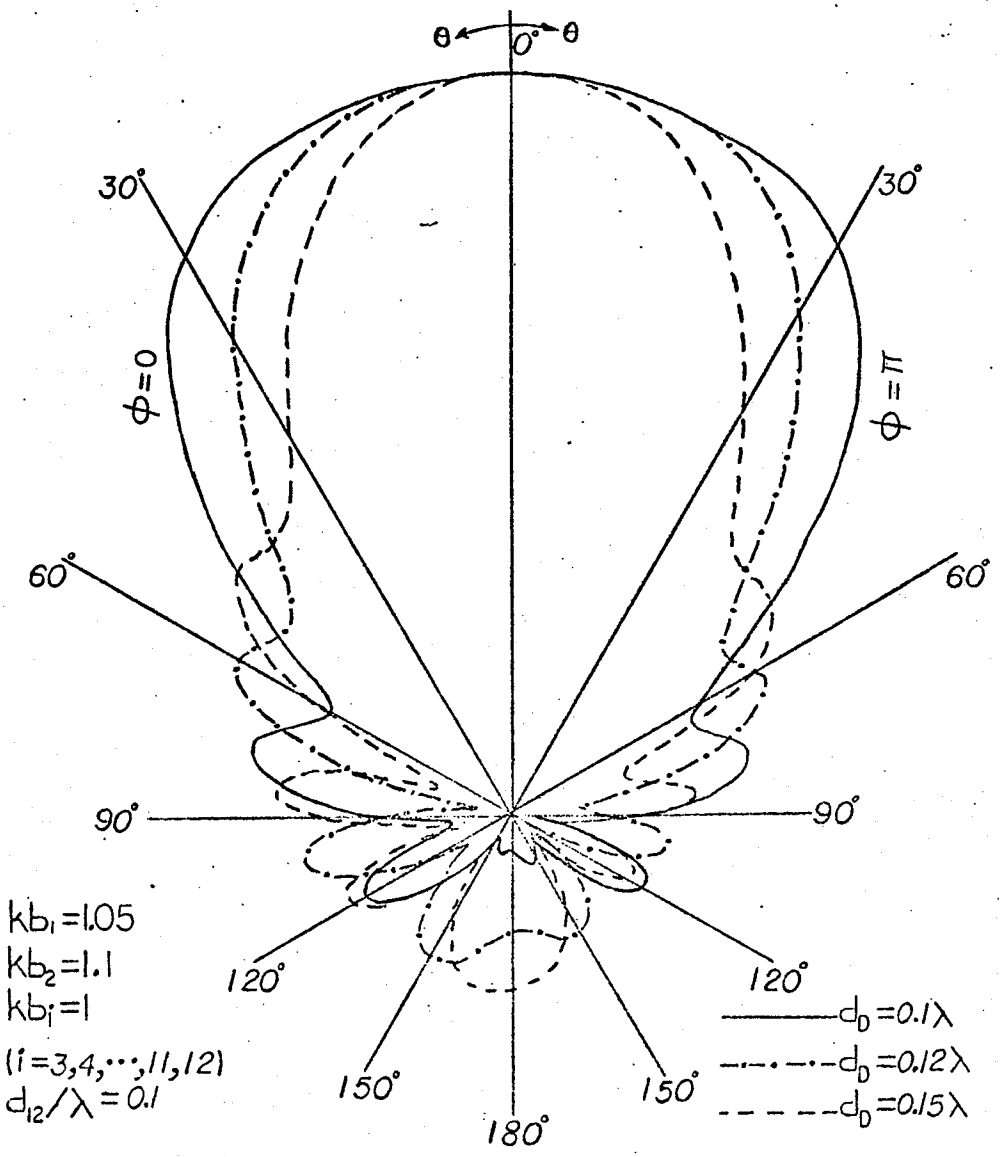

Figure 4.5 Radiation patterns in the H-plane for various director spacings.

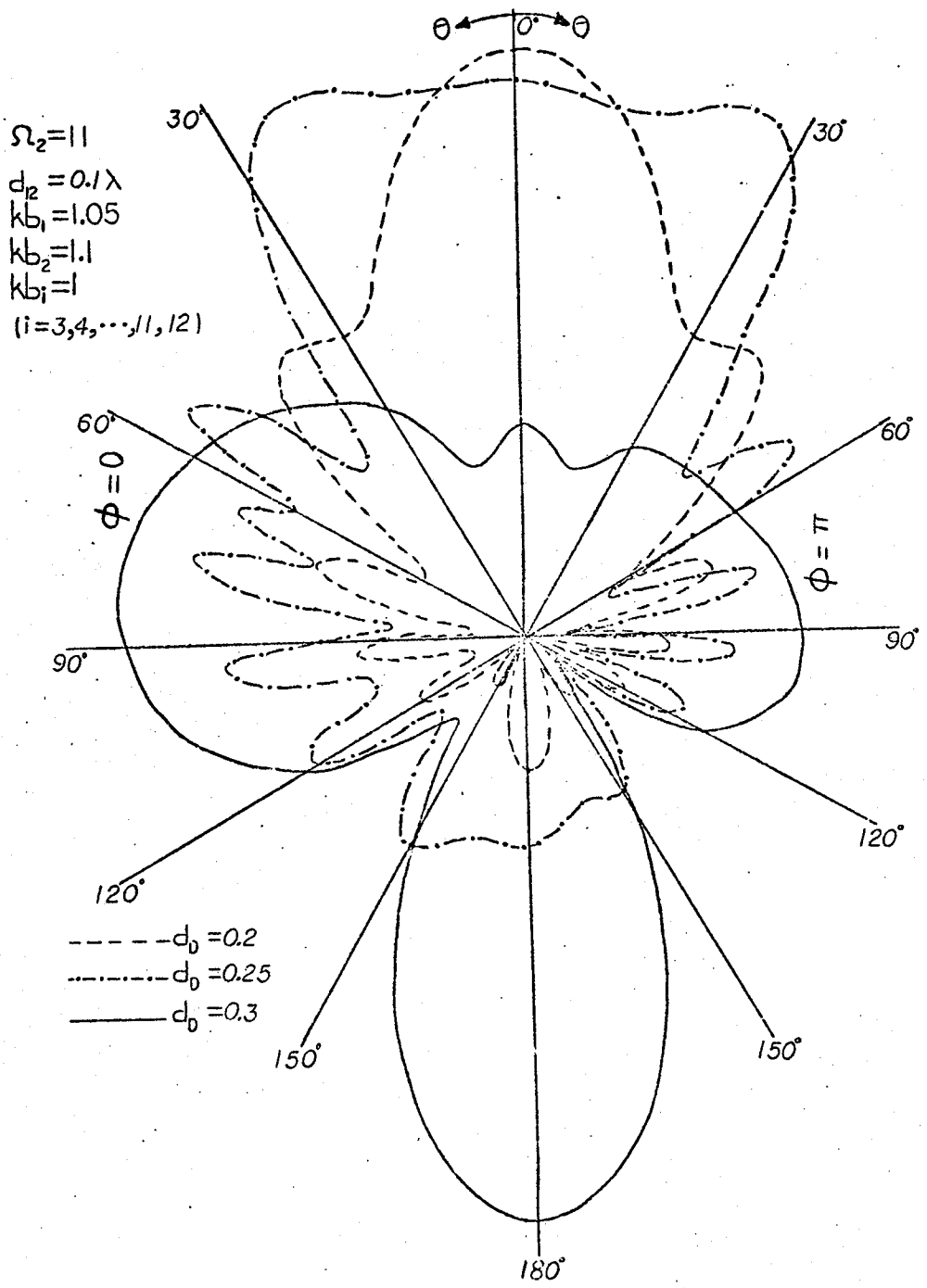

Figure 4.6 Radiation patterns in the H-plane for various director spacings.

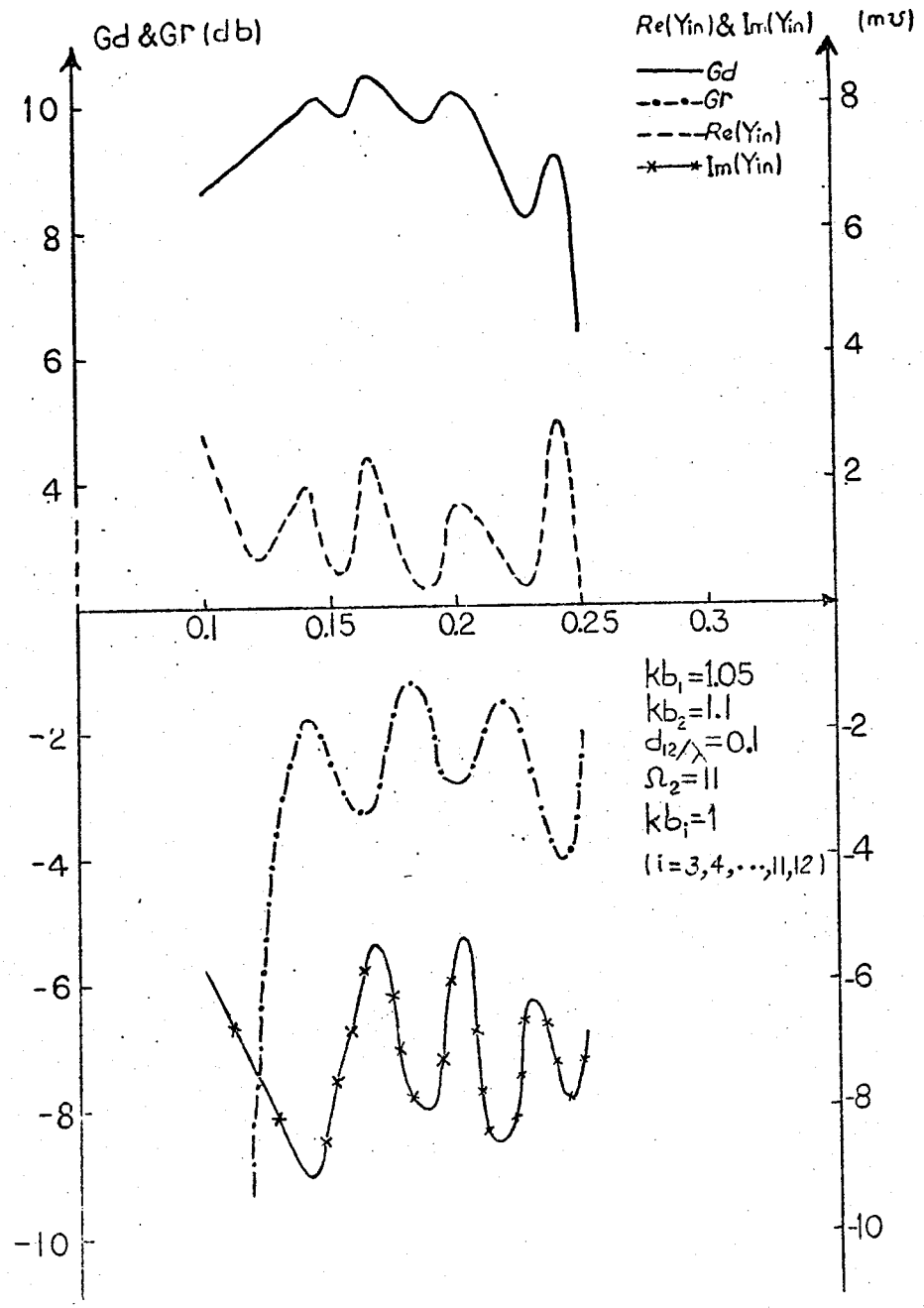

Figure 4.7 Behaviour of the directive gains, Gr and Gd, and the input admittance for various director spacings.

input admittance versus the director spacing are shown in figure (4.7), where for $d_D > 0.2\lambda$ Gd decreases rapidly.

4.6 Effects of the Director Size

Again a twelve-element equispaced loop array was chosen, but this time for $kb_1 = 1.05$ and $d_r = dD = 0.1\lambda$ the length of the directors were varied from $kb_i = 0.7$ to $kb_i = 1.15$ ($i = 3, 4, \ldots, 12$) in unequal steps. The computed radiation patterns in the H-plane are given in figures (4.8) to (4.10). We note that with increasing director lengths from 0.7 to 0.9 the beamwidth decreases. However, for $kb_i = 1$ it has the widest beamwidth, and for $kb_i > 1$ the patterns deteriorate. The computed input admittances and the directive gains are given in figure (4.11). This figure shows that for $kb_i > 1$ the real part of the input admittance drops to a value of almost zero and represents a negligible radiated power. Infact, the maximum radiation field for $kb_i = 1.02$ was found to be about forty times less than the maximum radiation field of $kb_i = 0.9$.

For further examination the distance between adjacent loops was increased to 0.2λ and the director lengths were varied from 0.7 to 2.1 in 20 unequal steps. The computed Gd, Gr and the input admittance are shown in figure (4.12). Here, although the radiation resistance for $kb_i > 1.45$ is large enough, Gd always has a negative db value, as long as $kb_i > 1$. Thus, one concludes that for the selected array far field pattern, can only be useful if the director sizes are equal to or less than one wave length.

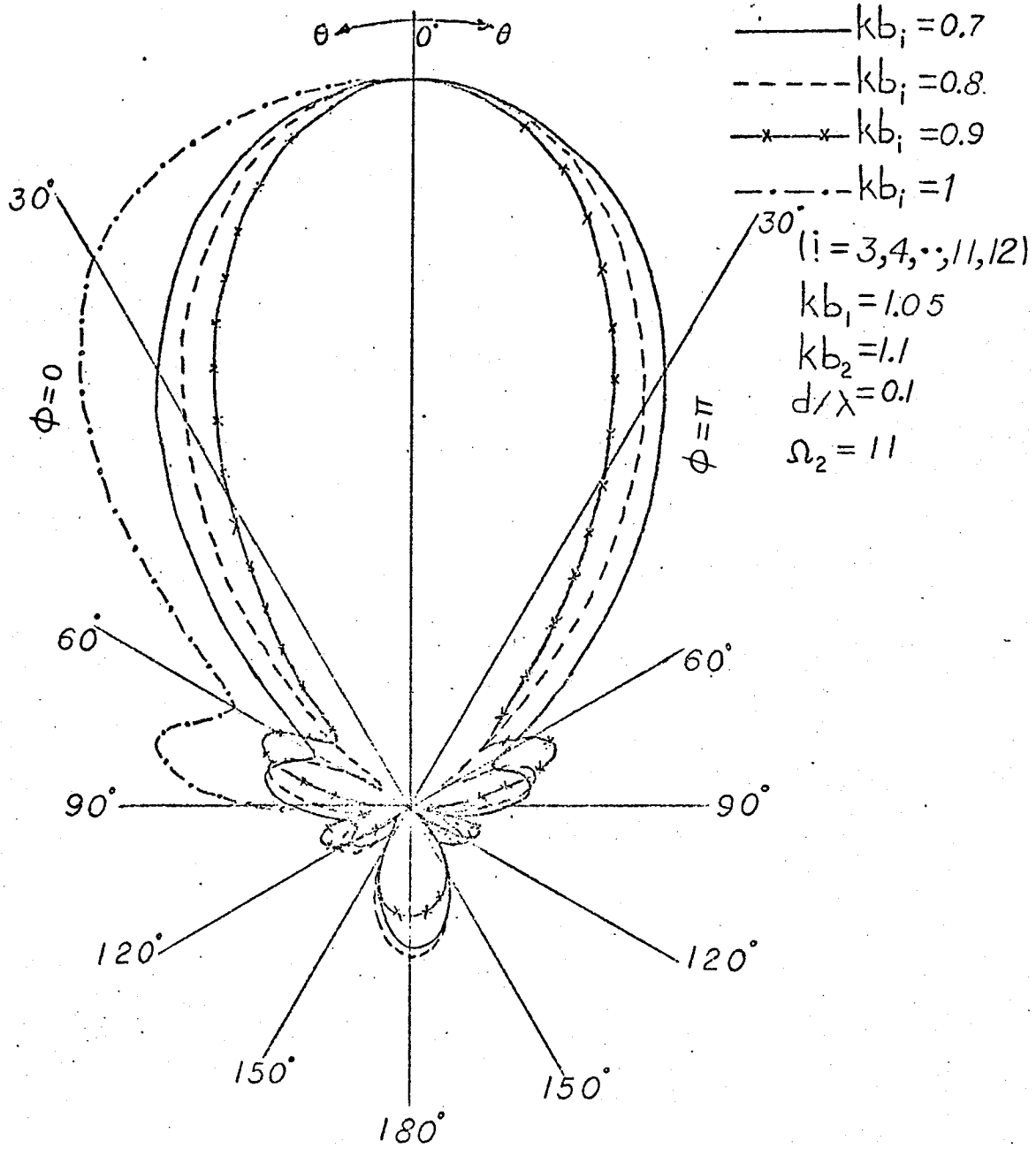

Figure 4.8 Radiation patterns in the H-plane for different director size.

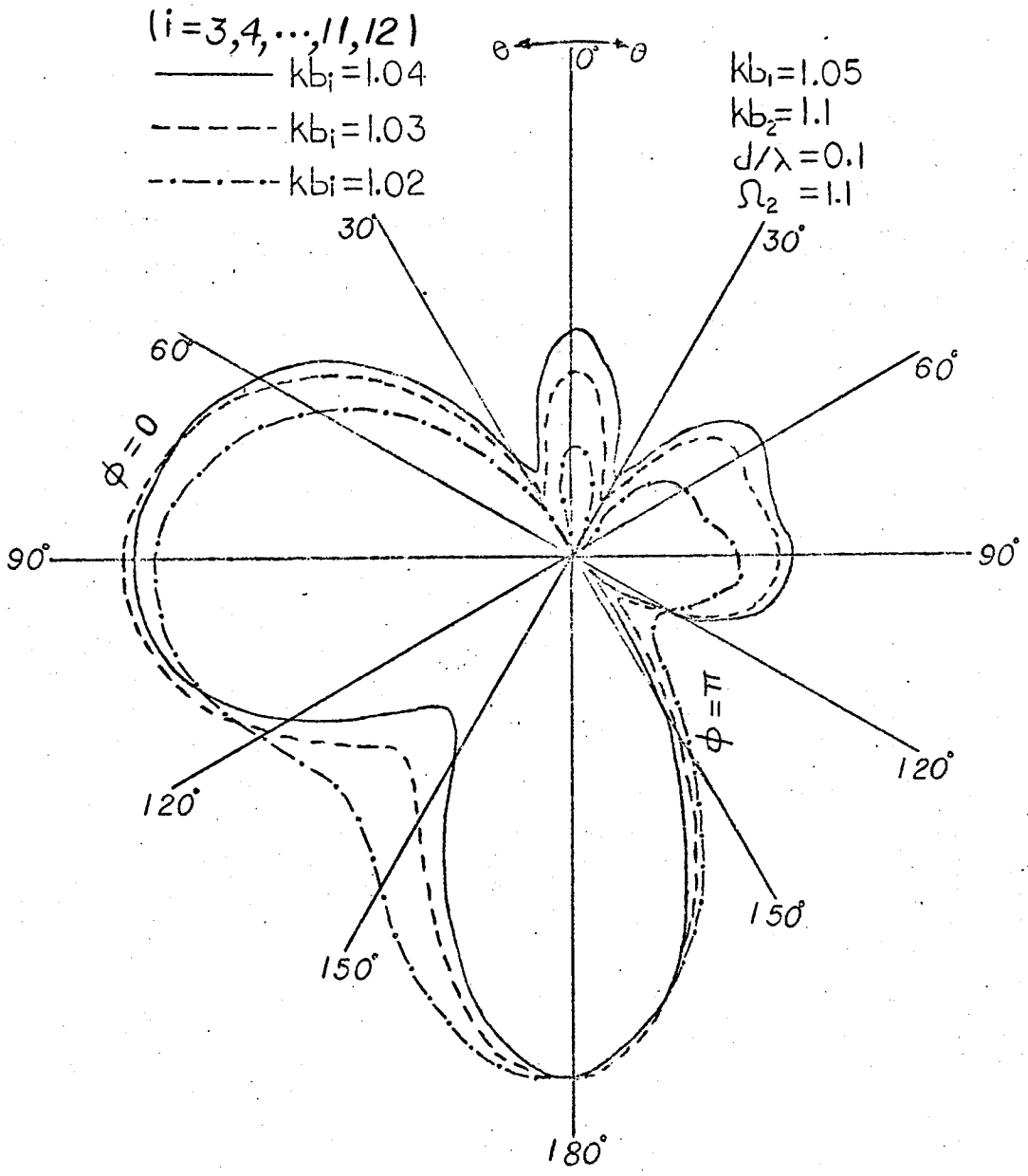

Figure 4.9 Radiation patterns in the H-plane for different director size.

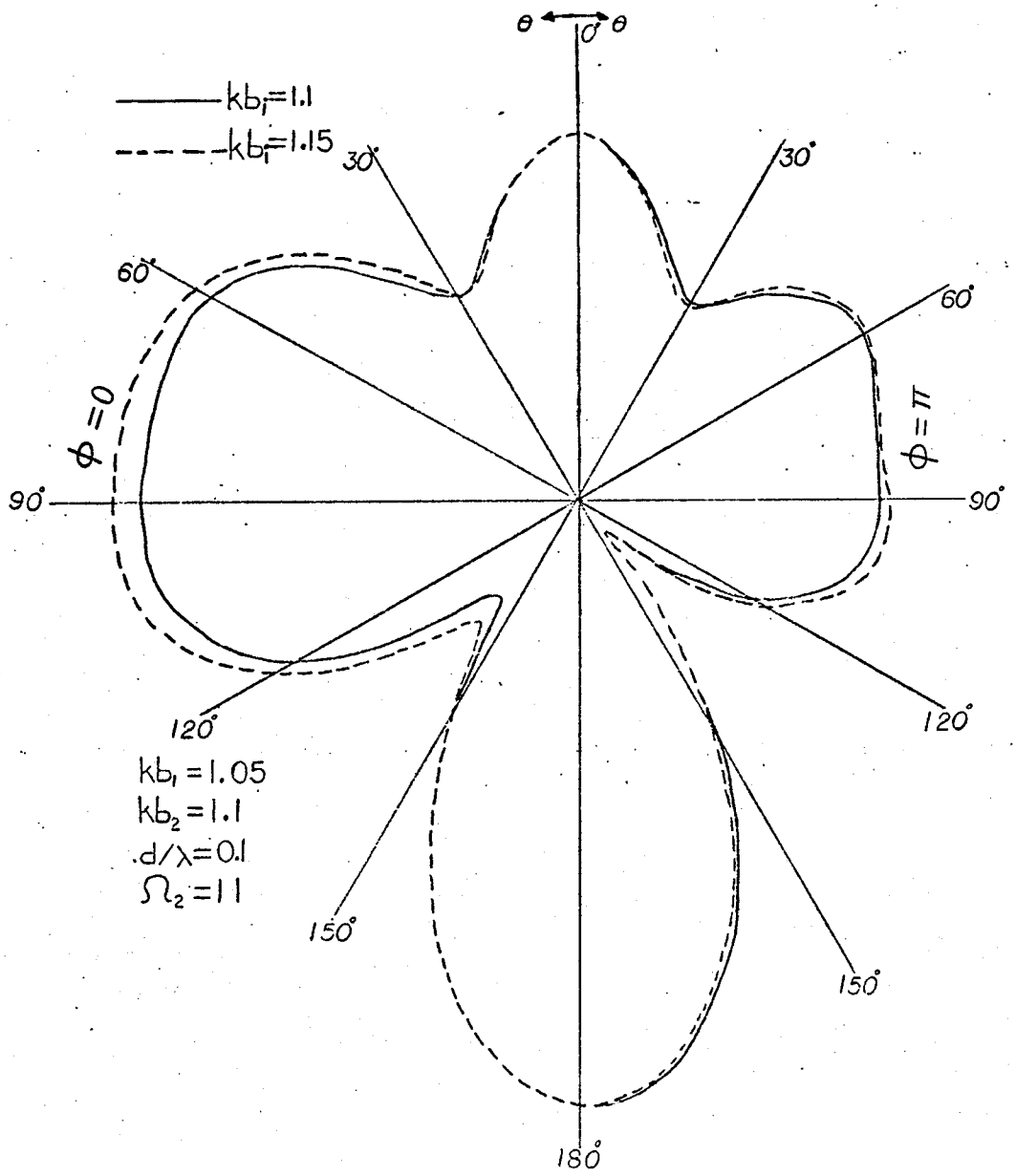

Figure 4.10 Radiation patterns in the H-plane for different director size.

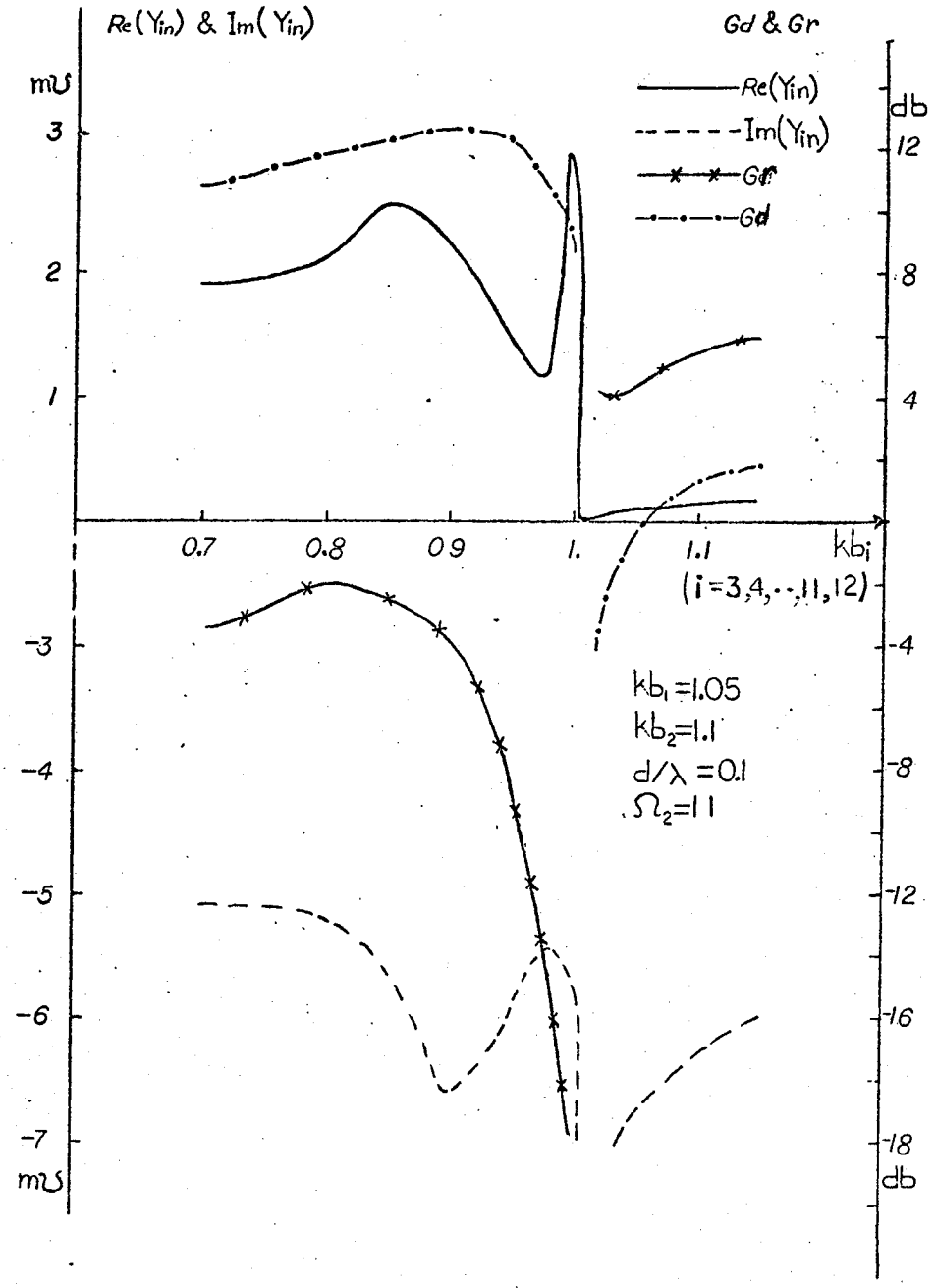

Figure 4.11 Effects of the director size on the directive gains, Gd and Gr, and the input admittance.

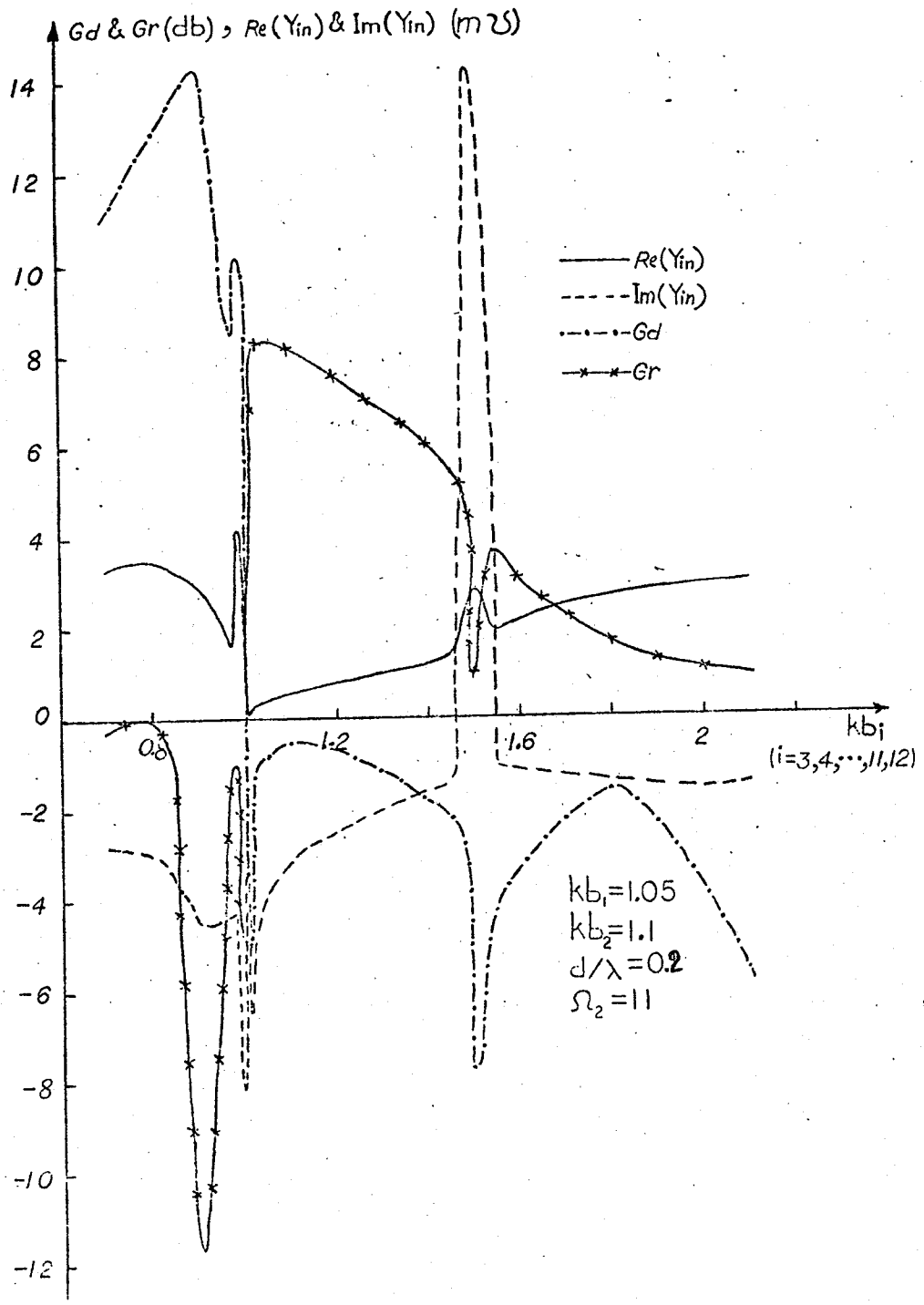

Figure 4.12 Effects of the director size on the directive gains, Gd and Gr, and the input admittance.

4.7 Effects of the Exciter Size

A twelve-element array was chosen with element spacing equal to 0.1λ, $kb_1 = 1.05$ and for directors $kb_i = 1$ ($i = 3, 4, \ldots, 11, 12$). The excitor length was altered from $kb_2 = 1.05$ to $kb_2 = 1.4$ in unequal steps. The computed radiation patterns in the H-plane for cases $kb_2 = 1.1$, 1.2, and 1.3 are given in figure (4.13). It is seen that the main lobes are quite similar to each other except for an approximate decrease of 4% in the beamwidth for each step. But the levels of the side and back lobes have increased. The variation of Gd, Gr and input admittance with exciter length is shown in figure (4.14). Note that the variation of Gd with kb_2 is negligible whereas Gr is highly dependent on it. The real and the imaginary part of the input admittance vary with the exciter length, the real part decreasing with the length and increasing as the length decreases. For $kb_2 > 1.25$ the real part decreases very slowly. When $kb_2 \simeq 1.35$ the imaginary part of the input admittance is zero and we have purely resistive input impedance. At this point the directive gain in the positive z direction is just about 0.4 dB less than when $kb_2 = 1.1$. Therefore, altering the size of the driven element will have a negligible effect on the front radiation but it changes the input admittance of the array and may be used to control the input impedance. The independence of the radiation field in the forward direction of the exciter can be explained using the traveling wave approach. The Yagi-Uda array consists of two distinct parts, a launching device and

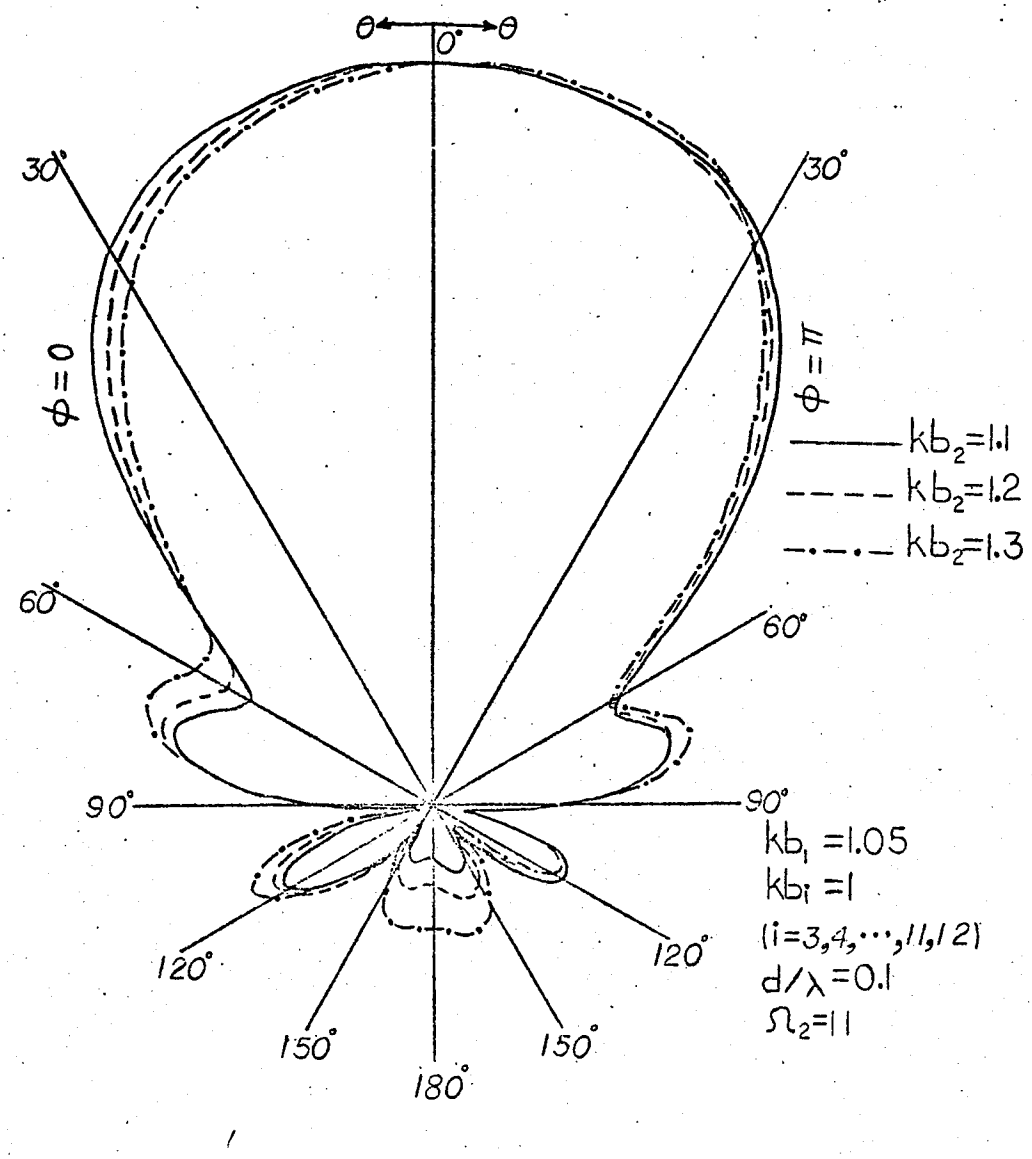

Figure 4.13 Radiation patterns in the H-plane for various exciter sizes.

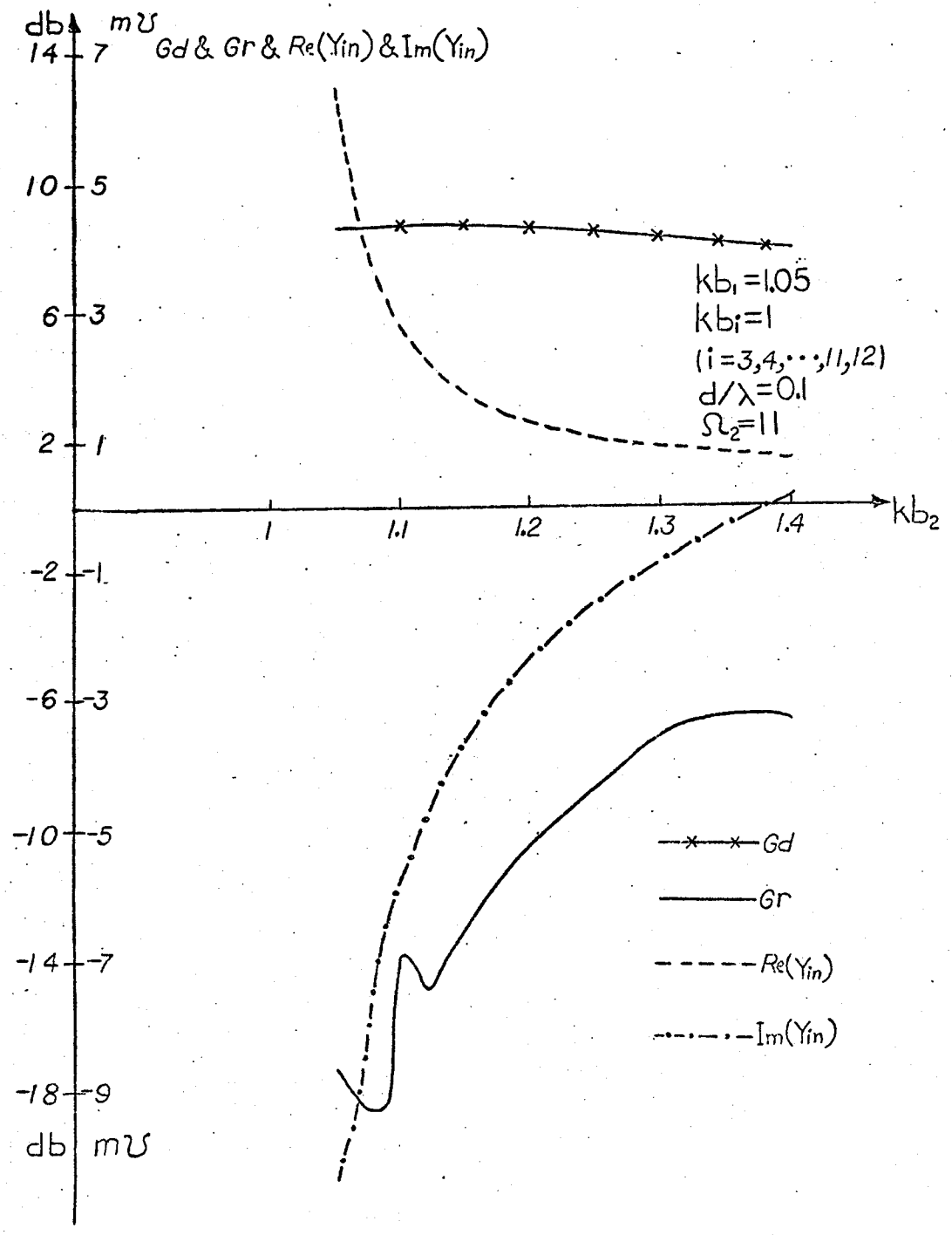

Figure 4.14 Effects of the exciter size on the directive gains and the input admittance.

a reactive surface which supports a traveling wave, these enjoying much the same independence as, say, the feed horn and reflector in a microwave optical system. It is therefore not surprising that the launching device should have an impedance behaviour which is substantially independent of the radiation characteristics of the aerial.

4.8 Effect of the Wire Cross Section

So far we have studied the effects of major array parameters on the far field and the input admittance of the array except the effect of the wire cross section. To complete this chapter, a twelve-element equispaced loop array was chosen with $d/\lambda = 0.1$, $kb_1 = 1.05$, $kb_2 = 1.1$ and for directors $kb = 1$. The wire cross section of the driving element is related to its radius by $\Omega_2 = 9 = \ell n\, 2\pi \frac{b_2}{a}$. By using equation (4.1) the value of Ω_i can be found for any other elements in the array. Ω_2 was increased from 9 to 11 in steps of 0.5. The computed far field patterns for $\Omega_2 = 9$, 10, and 11 in the H-plane are illustrated in figure (4.15) and the independence of the forward radiation pattern from the wire cross section is evident. But there is a decrease in the back lobe level with increasing Ω_2 (decreasing the wire cross section a). Figure (4.16) depicts the variation of Gr, Gd, $Re\,(Y_{in})$ and $I_m(Y_{in})$ with Ω_2. From figures (4.15) and (4.16) it is clear that the input admittance is quite dependent on the wire cross section whereas the radiation field in the forward direction is not. The effect of the diameter on the input impedance will be clear if we notice that it has been

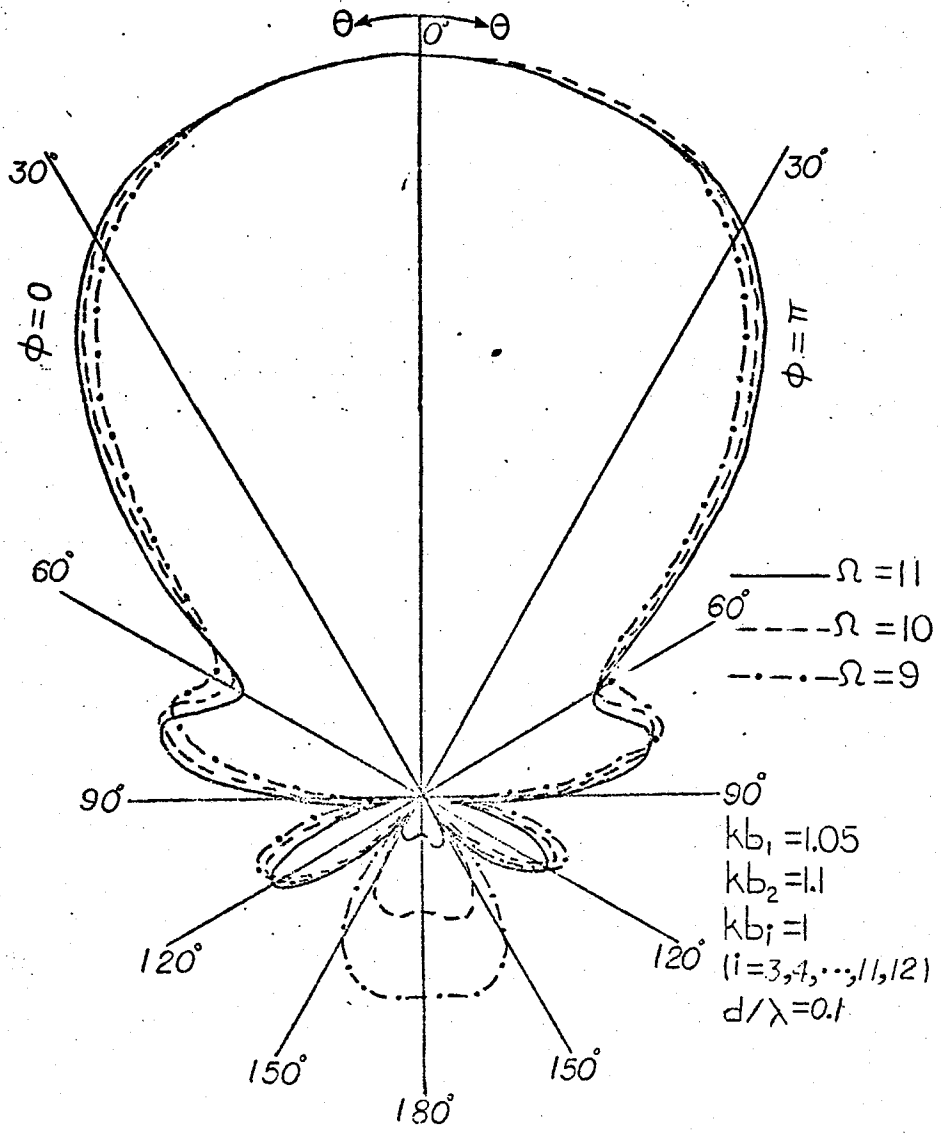

Figure 4.15 Radiation patterns in the H-plane for different wire cross sections.

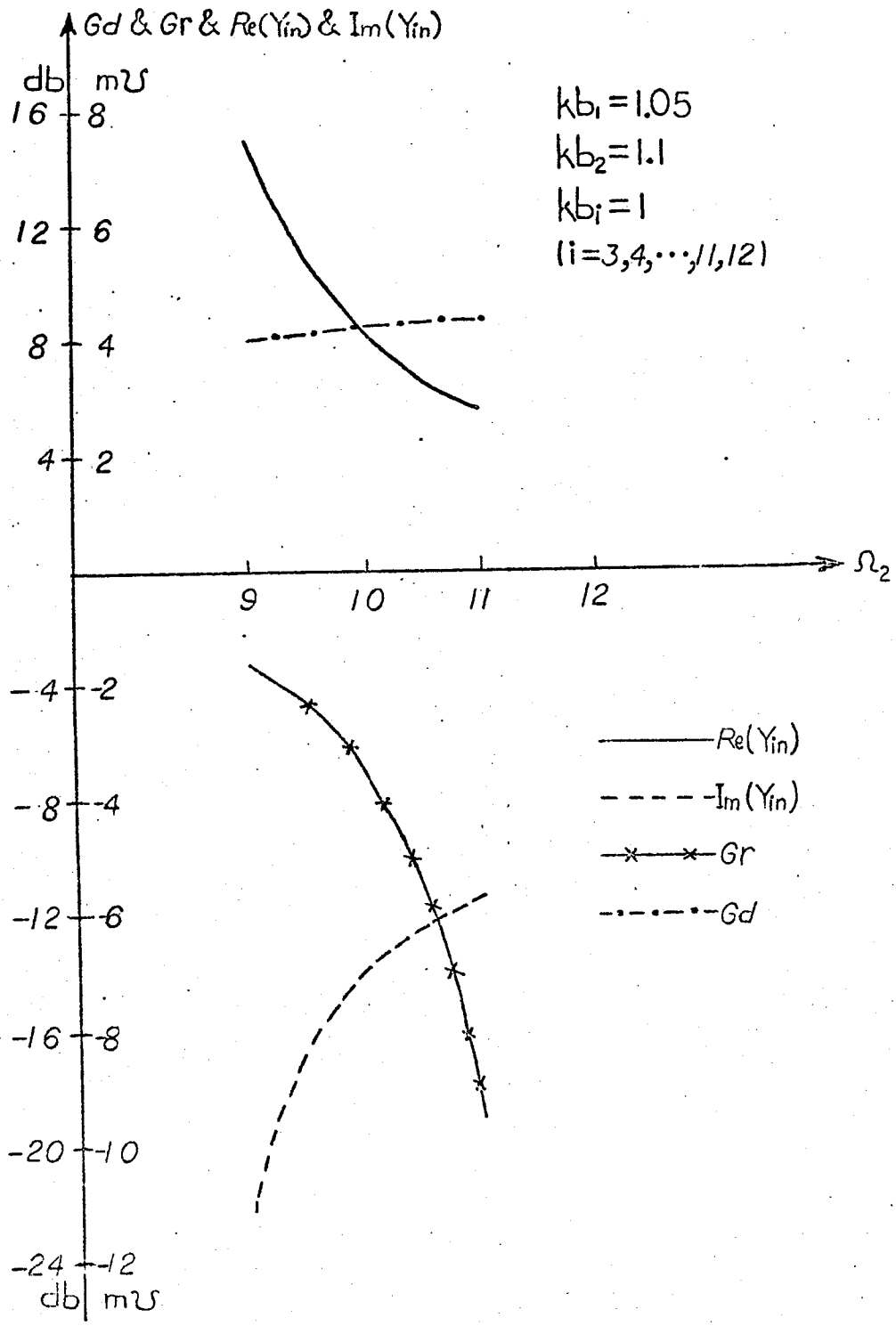

Figure 4.16 Effects of wire cross section on the directive gains, Gr and Gd, and the input admittance.

included only in the calculation of the self impedance and therefore can affect only the principle diagonal of the impedance matrix.

4.9 Summary

From the results of this chapter one concludes that: there are basically two principal ways for controlling the forward far-field pattern of a Yagi loop array. One is to vary the director spacing while holding the element size and reflector spacing constant. The other is to vary the director size while holding all other parameters fixed. Either one of these methods will have a considerable effect on the far field patterns. However, to obtain a useful far field pattern the director sizes should be less than or equal to one wave length when the exciter and reflector sizes are about 1.1λ and 1.05λ respectively.

On the other hand, the usual effects of altering the reflector size or spacing are most effective in changing the back lobe level and the input impedance of the array. Changing the size of the driven loop has a negligible effect on the pattern, but changes the input impedance of the array. This latter property may effectively be used in achieving a purely resistive input impedance. Finally, there is only an insignificant dependence of the directive gain Gd and the forward radiation on the wire cross section. The input impedance, on the other hand, is quite dependent on it.

CHAPTER V

DESIGN DATA FOR SHORT AND MEDIUM LENGTH LOOP YAGI ARRAYS

5.1 Introduction

The importance of the loop Yagi array has already been discussed in [3] and [15]. Unfortunately, very little information on design data for this type of array is available. There are, however, two exceptions: one is reference [14] which gives the computed input admittance and radiation characteristics for an array of two loops, one of which is parasitic. The other one is a paper published by L.C. Shen and G.W. Raffoul [15], who have studied an infinite array of equispaced and equal loops. In their paper, equal phase delay from director to director and equal amplitude for currents on the directors were assumed. They have then applied these assumption to finite arrays. However, calculations made in this thesis indicated that the phase progression and current amplitudes along the array are nonuniform, results which are not illogical when one considers the complexity of finite arrays.

In this chapter numerical data for the rapid design of loop Yagi arrays is presented - the combination of the feeder and reflector is optimum for the directive gain in the forward direction.

5.2 Treatment of the Problem

Many parameters are involved in designing Yagi arrays. These parameters are: the size and spacing of the reflector, the size and spacing of directors, exciter size, and wire cross

section. Optimization of their combination for a desired antenna design represents a formidable engineering problem. To simplify the problem, the numerical data is restricted to loop Yagi arrays with a unique wire cross section, a single reflector, and equispaced directors of equal sizes. For further reduction of parameters, the experimental approach of Ehrenspeck and Poehler [24] is followed numerically, for adjusting the combination of exciter and reflector which gives optimum directive gain in the forward direction. Then, different number of directors are chosen and the directive gain, beamwidth and some other important characteristics of the array are computed. To generalize the results, the reflector spacing d_r, the director spacing d_D, and the circumference of loops are all expressed in terms of λ ($\frac{d_r}{\lambda}$, $\frac{d_D}{\lambda}$, $\frac{2\pi b_i}{\lambda} = kb_i$), the free space wavelength.

5.3 Optimum Adjustment of the Feeder-Reflector Combination

To obtain optimum design criteria for the reflector size and spacing, the directive gain in the forward direction of the combination feeder-reflector was computed from equation (2.41). The size of the driven loop was adjusted for pure resistive input impedance, which, from figure (5.1) occurs for $kb \simeq 1.1$. These curves were obtained from reference [11], using the following equation

$$y = \sum_{n=0}^{n_o} \frac{1}{z^n} + j\omega C_g \qquad (5.1)$$

where z^n is given by equation (2.13) and $n_o \simeq \frac{b}{a}$.

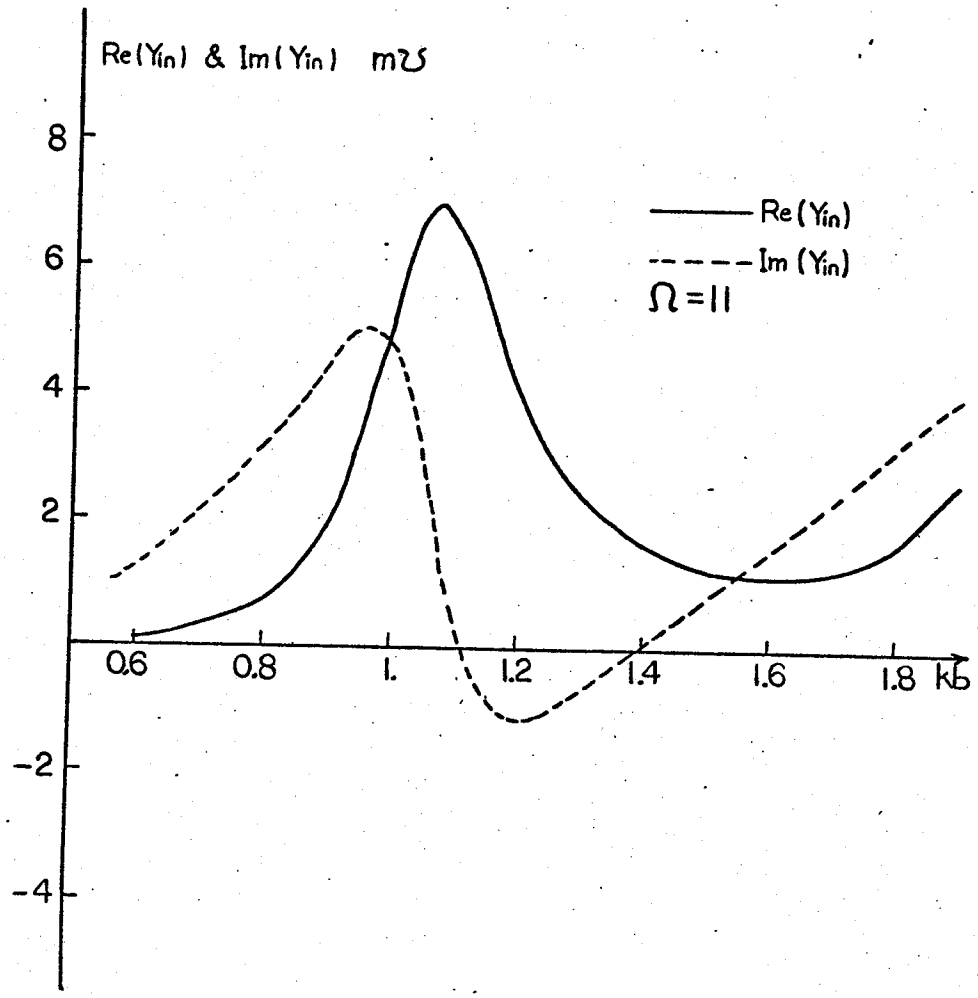

Figure 5.1 The conductance and the susceptance of a circular loop of radius b.

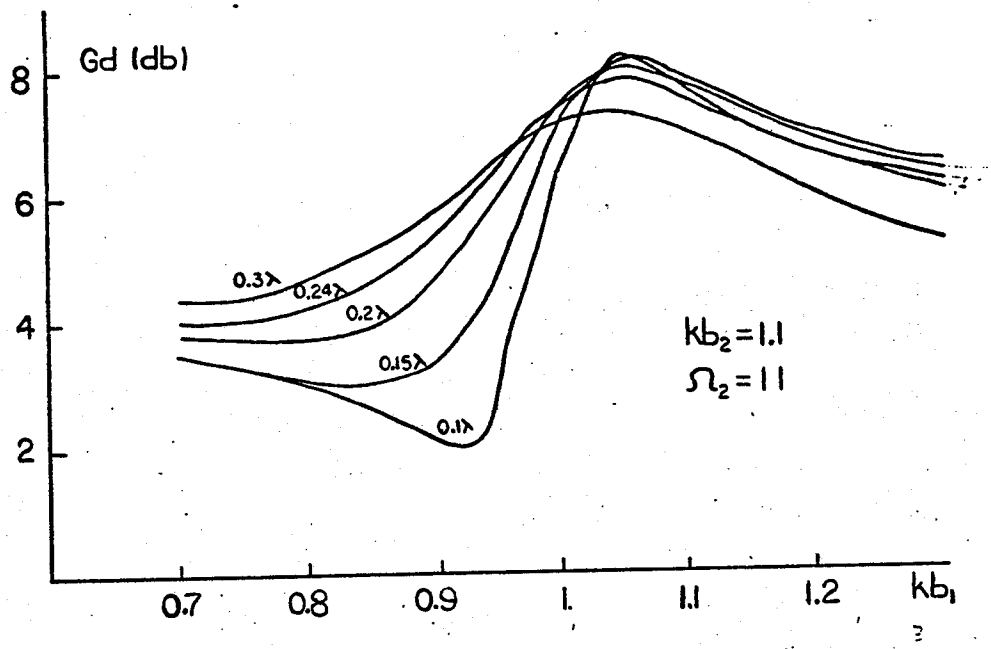

Figure 5.2 Directive gain of feeder-reflector combination in the positive z direction as a function of reflector size for various reflector spacing.

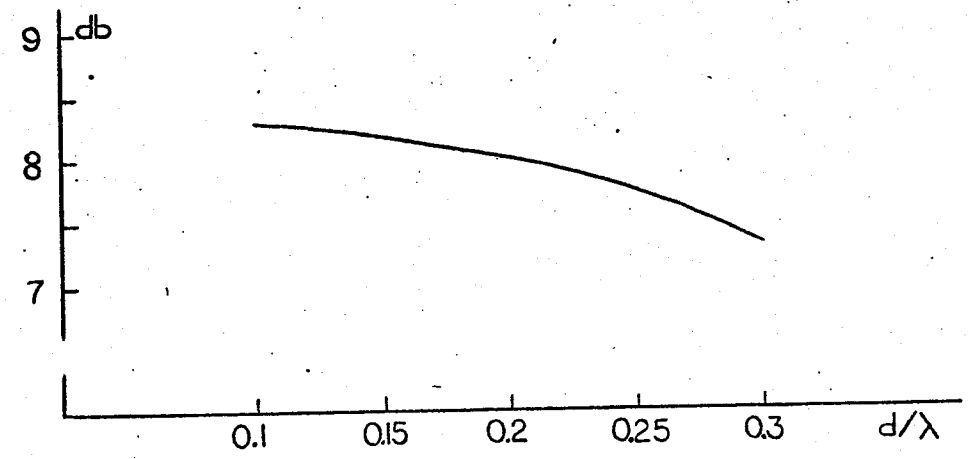

Figure 5.3 Maximum directive gain of feeder-reflector combination in the positive z direction as a function of reflector spacing.

Figure (5.2) shows the result of these computations for reflector spacings between 0.1λ and 0.3λ with $\Omega_2 = 11$. The maxima of these curves are for $kb_1 \simeq 1.05$. These maxima are plotted as a function of the reflector spacing in figure (5.3). This figure shows that the adjustment of the feeder-reflector combination for the maximum directive gain in +z direction is not too critical, although there is an optimum value for the spacing of 0.1λ and occurs for a reflector size of $kb = 1.05$.

5.4 Outline of Results

Before commencing the work, certain restrictions on the parameters were imposed.

i) In the previous chapter it was shown that for a useful radiation pattern the director sizes should be less than or equal to one wavelength. Therefore, the director sizes were limited to $kb = 0.7, 0.8, 0.9$ and 1.

ii) Five director spacings of 0.1λ, 0.15λ, 0.2λ, 0.25λ, and 0.3λ were chosen.

iii) A specific conductor diameter was selected, where the ratio of the driven element radius to the conductor radius, i.e., $\frac{b_2}{a}$, was equal to 38.94 or $\Omega_2 = 2 \ell n \, 2\pi \frac{b_2}{a} = 11$.

iv) The number of directors, which were placed in front of the feeder-reflector combination was varied from 1 to 10. Therefore, 200 different combinations were possible.

The numerical results are represented in the Tables (5.1) to (5.10). An examination of these tables shows that:

1. for the antennas given in the tables, the 3dB beamwidth in the E-plane is always greater than that in the H-plane,
2. for director spacings and sizes of 0.3λ and one wave length, respectively, the front to back ratio is relatively small and for more than two directors the antenna radiates mainly in the negative z direction,
3. for director sizes equal to 0.9λ the directive gain Gd has the largest value for any director spacings when the number of directors is more than two,
4. $kb = 0.9$ is the only director size for which Gd increases with increasing director spacings for any number of directors,
5. for director sizes equal to 0.7λ the value of Gd is almost invariant for director spacings $\frac{d_D}{\lambda} \geq 0.15$,
6. there are no side lobes in both the E and the H planes for directors $kb = 0.7$ and $\frac{d_D}{\lambda} \geq 0.25$,
7. the 3-dB beamwidth of the radiation patterns in both the E and H planes decreases with increasing director spacings no matter what the number of directors are, except when the director sizes are equal to one wave length,

8. the directive gain Gd increases with an increase in number of directors, except for the directos with kb = 1,
9. the average rise in Gd by adding a director to the array has the largest value when kb = 0.9 for the directors,
10. the maximum value of Gd in the tables is for director size and spacing equal to 0.9λ and 0.3λ, respectively, when the array has 10 directors,
11. the widest beamwidth was obtained with four directors when $d_D/\lambda = 0.25$ and kb = 1 ,
12. the level of first side lobe for director size equal to one wave length is much higher than that for the other director sizes especially for $d_D/\lambda \geq 0.2$, and
13. the level of first side lobe in the H-plane is usually lower than that in the E-plane.

It was seen in Chapter IV that the driven element, to a first approximation, has no effects on the forward radiation. Therefore, it is possible to obtain a resistive input impedance by variation of the size of the driven element, for which the data given in the tables for the radiation pattern and Gd will still be valid.

Also, it was shown in the previous chapter that the wire cross section has no significant effect on the directivity and the forward radiation. There was a change of only a few degrees in the position of nulls and less than 0.3 dB change

in the level of the first side lobes. Noting that this is for large variations of the wire cross section, (Ω_2 = 11 → 9), it may be said that, these tables could be used for other wire cross sections close to those assumed in the tables, except for the data on input admittance and front to back ratio.

Table 5.1 Computed characteristics of "three-element" circular loop Yagi arrays.

No. of elements	Director spacing	Director size	Input Admittance (U)	Gain Gd (db)	Front to back ratio (db)	3 db BW in H-plane	1st null in H-plane		1st side lobe in H-plane		3 db BW in E-plane	1st null in E-plane		1st side lobe in E-plane	
							Position (degree)	Level (db)	Position (degree)	Level (db)		Position (degree)	Level (db)	Position (degree)	Level (db)
3	0.1	1.0	0.700×10^{-3}, -0.800×10^{-2}	9.6	12.2	64.0	80.0°	-20.4	180°	-12.2	76.0°	95.0°	-22.6	180°	-12.2
	0.15		0.593×10^{-3}, -0.700×10^{-2}	10.0	12.5	60.0	70.0°	-22.0	115°	-12.6	68.5°	80.0°	-20.4	115°	-14.0
	0.2		0.547×10^{-3}, -0.628×10^{-2}	10.2	12.0	57.0	65.0°	-26.8	105°	-11.4	64.5°	70.0°	-22.3	105°	-11.5
	0.25		0.545×10^{-3}, -0.570×10^{-2}	10.1	9.3	55.5	65.0°	-31.0	102°	-10.4	61.5°	65.0°	-27.0	100°	- 9.8
	0.3		0.585×10^{-3}, 0.522×10^{-2}	9.9	7.1	56.0	61.0	-24.0	98°	- 9.3	60.0°	63.5°	-27.3	98°	- 8.4
3	0.1	0.9	0.340×10^{-2}, -0.580×10^{-2}	8.9	12.6	75.5	110.0°	-27.8	180°	-12.6	94.0°	115.0°	-27.0	180°	-12.6
	0.15		0.278×10^{-2}, -0.620×10^{-2}	9.2	15.3	72.5	105.0°	-27.8	180°	-15.3	88.5°	110.0°	-28.4	180°	-15.3
	0.2		0.208×10^{-2}, -0.616×10^{-2}	9.5	21.0	70.0	95.0°	-27.5	135°	-18.5	83.5	105.0°	-27.8	140°	-19.0
	0.25		0.159×10^{-2}, -0.586×10^{-2}	9.8	24.1	68.0	85.0°	-24.4	120°	-18.0	80.0	95.0°	-25.6	120°	-19.2
	0.3		0.130×10^{-2}, -0.550×10^{-2}	9.9	16.5	66.0	80.0°	-21.4	110°	-16.2	77.0	90.0°	-21.4	110°	-17.2
3	0.1	0.8	0.246×10^{-2}, -0.497×10^{-2}	8.6	11.6	77.5	120.0°	-25.4	180°	-11.6	98.0°	120.0°	-26.8	180°	-11.6
	0.15		0.245×10^{-2}, -0.514×10^{-2}	8.8	12.6	77.0	115.0°	-24.5	180°	-12.6	95.0°	120.0°	-27.9	180°	-12.6
	0.2		0.225×10^{-2}, -0.530×10^{-2}	9.0	14.2	75.0	115.0°	-23.2	180°	-14.2	91.5°	115.0°	-25.4	180°	-14.1
	0.25		0.198×10^{-2}, -0.533×10^{-2}	9.1	15.6	73.5	115.0°	-21.4	180°	-15.6	89.5°	115.0°	-23.8	180°	-15.6
	0.3		0.173×10^{-2}, -0.524×10^{-2}	9.2	15.3	72.5	140.0°	-22.5	180°	-15.3	86.5°	125.0°	-21.9	180°	-15.3
3	0.1	0.7	0.212×10^{-2}, -0.483×10^{-2}	8.5	11.0	78.5	122.5°	-25.8	180°	-11.0	100.0°	122.5°	-27.3	180°	-11.0
	0.15		0.215×10^{-2}, -0.488×10^{-2}	8.6	11.5	78.5	122.5°	-25.0	180°	-11.5	98.0°	120.0°	-26.7	180°	-11.5
	0.2		0.210×10^{-2}, -0.496×10^{-2}	8.7	12.2	78.0	122.5°	-24.0	180°	-12.2	96.0°	120.0°	-26.3	180°	-12.2
	0.25		0.199×10^{-2}, -0.500×10^{-2}	8.8	12.8	76.5	122.5°	-23.2	180°	-12.8	96.0°	120.0°	-25.3	180°	-12.8
	0.3		0.185×10^{-2}, -0.500×10^{-2}	8.8	12.9	76.0	127.5°	-23.0	180°	-12.9	92.5°	122.5°	-24.3	180°	-12.9

Table 5.2 Computed characteristics of "four-element" circular loop array.

No. of elements	Director spacing	Director size	Input Admittance (Y)	Gain Gd (db)	Front to back ratio (db)	3 db BW in H-plane	1st null in H-plane		1st side lobe in H-plane		3 db BW in E-plane	1st null in E-plane		1st side lobe in E-plane	
							Position (degree)	Level (db)	Position (degree)	Level (db)		Position (degree)	Level (db)	Position (degree)	Level (db)
4	0.1	1.0	0.345×10^{-2}, -0.588×10^{-2}	10.5	16.0	59.0	75°	-16.3	105°	-13.7	64.0°	70.0°	-15.9	105°	-11.8
	0.15		0.220×10^{-2}, -0.900×10^{-2}	10.5	11.0	55.5	70°	-13.0	85°	-12.6	60.0°	65.0°	-12.6	90°	-10.4
	0.2		0.514×10^{-3}, -0.730×10^{-2}	10.4	10.3	49.5	55°	-10.0	71°	- 9.4	53.0°	55.0°	-10.5	75°	- 9.0
	0.25		0.280×10^{-3}, -0.622×10^{-2}	10.0	7.5	43.0	44°	-11.8	70°	- 6.7	45.0°	46.0°	-12.0	70°	- 6.5
	0.3		0.287×10^{-3}, -0.546×10^{-2}	9.3	3.6	39.5	40°	-21.6	69°	- 5.4	41.0°	40.0°	-18.6	72°	- 4.9
4	0.1	0.9	0.212×10^{-2} -0.681×10^{-2}	9.7	21.3	68.5	85°	-27.4	135°	-17.2	81.0°	100.0°	-32.4	135°	-18.5
	0.15		0.152×10^{-2} -0.588×10^{-2}	10.1	20.5	64.5	80°	-34.8	115°	-16.0	74.0°	85.0°	-29.8	115°	-16.8
	0.2		0.160×10^{-2} -0.516×10^{-2}	10.3	13.0	62.5	75°	-24.8	105°	-14.4	70.5°	75.0°	-22.0	107°	-14.0
	0.25		0.209×10^{-2} -0.500×10^{-2}	10.4	11.8	61.5	70°	-24.5	100°	-13.8	68.0°	72.0°	-18.7	97°	-12.7
	0.3		0.209×10^{-2} -0.560×10^{-2}	10.7	15.7	59.0	66°	-21.4	91°	-14.1	65.5°	68.5°	-17.8	91°	-12.5
4	0.3	0.8	0.251×10^{-2} -0.273×10^{-2}	9.2	15.3	73.5	105°	-25.0	180°	-15.3	90.0°	115.0°	-25.4	180°	-15.3
	0.15		0.194×10^{-2} -0.560×10^{-2}	9.5	18.3	71.0	95°	-22.6	120°	-19.1	84.0°	105.0°	-22.2	125°	-20.7
	0.2		0.171×10^{-2} -0.519×10^{-2}	9.7	14.1	68.5	85°	-19.3	105°	-17.1	80.0°	95.0°	-17.7	105°	-17.5
	0.25		0.180×10^{-2} -0.490×10^{-2}	9.7	11.7	68.0	80°	-16.6	102°	-15.3	78.0°	130.0°	-27.9	180°	-11.7
	0.3		0.196×10^{-2} -0.493×10^{-2}	9.7	12.1	67.0	75°	-14.8	90°	-14.2	77.0°	125.0°	-31.4	180°	-12.1
4	0.1	0.7	0.228×10^{-2} $-0.516\ 10^{-2}$	8.8	12.9	76.5	116°	-23.7	180°	-12.9	94.5°	120.0°	-26.0	180°	-12.9
	0.15		0.205×10^{-2} -0.521×10^{-2}	9.1	14.4	74.5	120°	-21.4	180°	-14.2	90.0°	122.0°	-23.6	180°	-14.4
	0.2		0.182×10^{-2} -0.504×10^{-2}	9.2	13.2	73.0	135°	-23.1	180°	-13.2	87.0°	132.0°	-23.0	180°	-13.2
	0.25		0.180×10^{-2} -0.485×10^{-2}	9.2	11.5	72.5	137°	-25.6	180°	-11.6	85.5°	131.0°	-25.6	180°	-11.5
	0.3		0.188×10^{-2} -0.480×10^{-2}	9.1	11.2	72.0	130°	-29.0	180°	-11.2	84.5°	123.0°	-29.0	180°	-11.2

Table 5.3 Computed characteristics of "five-element" circular loop Yagi arrays

No. of elements	Director spacing	Director size	Input Admittance (Ω)	Gain Gd (db)	Front to back ratio (db)	3 db BW in H-plane	1st null in H-plane		1st side lobe in H-plane		3 db BW in E-plane	1st null in E-plane		1st side lobe in E-plane	
							Position (degree)	Level (db)	Position (degree)	Level (db)		Position (degree)	Level (db)	Position (degree)	Level (db)
5	0.1	1.0	0.139×10^{-2}, -0.926×10^{-2}	10.4	11.1	55.5°	130°	-22.8	180°	-11.1	60.0°	65°	-11.9	90	-10.2
	0.15		0.763×10^{-2}, -0.653×10^{-2}	10.6	13.7	49.0°	54°	- 8.8	65°	- 8.6	52.0°	52°	- 8.4	71	- 7.6
	0.2		0.328×10^{-2}, -0.820×10^{-2}	10.7	11.6	47.0°	95°	-41.2	122°	-14.0	49.5°	47°	- 7.1	62	- 6.6
	0.25		0.236×10^{-3}, -0.659×10^{-2}	7.7	6.6	42.0°	29°	- 4.1	47°	- 3.1	43.0°	30°	- 4.4	51	- 2.5
	0.3		0.204×10^{-3}, -0.557×10^{-2}	4.8	-1.3	—	—	—	—	—	—	—	—	—	—
5	0.1	0.9	0.153×10^{-2}, -0.604×10^{-2}	10.2	21.2	63.5°	80°	-32.0	112°	-15.5	72.5°	85°	-33.4	112	-16.3
	0.15		0.212×10^{-2}, -0.513×10^{-2}	10.6	12.5	50.0°	70°	-34.2	100°	-14.1	67.0°	70°	-24.6	100	-12.9
	0.2		0.232×10^{-2}, -0.587×10^{-2}	11.0	16.0	57.5°	65°	-34.0	90°	-14.4	63.0°	65°	- 7.8	90	-12.6
	0.25		0.150×10^{-2}, -0.558×10^{-2}	11.5	21.8	54.0°	60°	-28.0	82°	-14.9	59.0°	60°	-28.8	82	-12.4
	0.3		0.165×10^{-2}, -0.501×10^{-2}	11.5	12.3	52.0°	55°	-22.3	77°	-12.8	56.0°	53°	-19.2	77	-11.0
5	0.1	0.8	0.193×10^{-2}, -0.585×10^{-2}	9.7	20.8	70.0°	90°	-25.8	120°	-18.3	81.5°	100°	-23.1	125	-20.0
	0.15		0.176×10^{-2}, -0.515×10^{-2}	9.9	13.4	66.5°	80°	-20.7	105°	-15.9	76.0°	84°	-17.5	106	-15.7
	0.2		0.208×10^{-2}, -0.500×10^{-2}	10.0	12.5	64.5°	77°	-17.4	95°	-14.6	73.0°	73°	-14.2	92.5	-13.1
	0.25		0.194×10^{-2}, -0.522×10^{-2}	10.3	16.4	63.0°	70°	-15.9	85°	-14.1	70.5°	72°	-12.9	85	-12.1
	0.3		0.170×10^{-2}, -0.503×10^{-2}	10.4	14.0	61.5°	65°	-14.0	77°	-13.0	68.0°	66°	-11.6	82	-11.0
5	0.1	0.7	0.207×10^{-2}, -0.541×10^{-2}	9.2	15.6	73.0°	105°	-21.6	180°	-15.6	88.5°	115°	-23.2	180	-15.6
	0.15		0.180×10^{-2}, -0.507×10^{-2}	9.4	13.2	71.0°	90°	-17.9	105°	-17.5	83.5°	130°	-23.6	180	-15.2
	0.2		0.192×10^{-2}, -0.486×10^{-2}	9.4	11.6	70.0°	130°	-28.0	180°	-11.6	81.5°	130°	-28.0	180	-11.6
	0.25		0.194×10^{-2}, -0.493×10^{-2}	9.5	13.0	69.0°	120°	-30.7	180°	-13.0	80.0°	125°	-30.5	180	-13.0
	0.3		0.181×10^{-2}, -0.491×10^{-2}	9.5	13.0	68.0°	120°	-24.2	180°	-13.0	78.0°	120°	-26.4	180	-13.0

Table 5.4 Computed characteristics of "six-element" circular loop Yagi arrays.

No. of elements	Director spacing	Director size	Input Admittance (℧)	Gain Gd (db)	Front to back ratio (db)	3 db BW in H-plane	1st null in H-plane		1st side lobe in H-plane		3 db BW in E-plane	1st null in E-plane		1st side lobe in E-plane	
							Position (degree)	Level (db)	Position (degree)	Level (db)		Position (degree)	Level (db)	Position (degree)	Level (db)
6	0.1	1.0	0.994×10^{-3}, -0.712×10^{-2}	10.5	13.1	52.5°	115.0°	-28.3	180.0°	-13.1	55.0°	57.5°	- 8.5	70.0°	- 8.3
	0.15		0.128×10^{-2}, -0.873×10^{-2}	10.1	11.9	51.0°	90.0°	-27.1	120.0°	-12.5	54.0	95.0	-29.1	121.0	-12.3
	0.2		0.677×10^{-3}, -0.595×10^{-2}	9.1	13.2	49.5°	35.0°	- 3.6	40.0°	- 3.6	53.5	32.5	- 3.3	47.5	- 2.9
	0.25		0.285×10^{-3}, -0.696×10^{-2}	6.6	9.2	88.5°	60.0°	-22.4	82.5°	- 4.9	100.0	65.0	-17.9	82.5	- 5.3
	0.3		0.185×10^{-3}, -0.561×10^{-2}	- 7.9		—	—	—	—	—	—	—	—	—	—
6	0.1	0.9	0.198×10^{-2}, -0.534×10^{-2}	10.6	13.8	61.0°	70.0°	-33.9	102.5°	-10.9	72.5	72.5	-32.4	103.0	-13.2
	0.15		0.234×10^{-2}, -0.622×10^{-2}	11.2	16.8	56.5°	62.5°	-31.5	89.0°	-14.5	67.0	65.0	-33.0	90.0	-12.5
	0.2		0.156×10^{-2}, -0.538×10^{-2}	11.8	16.7	52.5°	56.0°	-34.4	77.5°	-13.5	56.0	57.5	-30.7	80.0	-11.8
	0.25		0.224×10^{-2}, -0.534×10^{-2}	12.0	13.5	50.0°	52.5°	-30.5	72.5°	-13.0	53.0	52.5	-24.0	72.5	10.9
	0.3		0.145×10^{-2}, -0.554×10^{-2}	12.5	25.8	48.0°	47.5°	-25.6	65.0°	-13.0	50.0	50.0	-22.1	67.5	-11.0
6	0.1	0.8	0.172×10^{-2}, -0.547×10^{-2}	10.0	15.9	66.5°	80.0°	-25.0	110.0°	-16.2	76.0	85.0	-20.3	107.5	-16.7
	0.15		0.218×10^{-2}, -0.511×10^{-2}	10.3	13.0	64.0°	71.0°	-20.0	95.0°	-14.7	71.0	73.0	-15.6	94.0	-13.1
	0.2		0.188×10^{-2}, -0.531×10^{-2}	10.7	18.0	60.5°	65.0°	-17.7	85.0°	-14.3	67.5	67.5	-14.1	85.0	-12.3
	0.25		0.184×10^{-2}, -0.495×10^{-2}	10.8	12.9	59.0°	60.0°	-14.9	75.0°	-13.0	65.0	62.5	-12.2	75.0	-10.8
	0.3		0.190×10^{-2}, -0.510×10^{-2}	10.8	15.6	58.0°	57.5°	-13.2	70.0°	-12.1	63.0	57.5	-10.8	70.0	- 9.9
6	0.1	0.7	0.183×10^{-2}, -0.533×10^{-2}	9.5	15.3	71.0°	90.0°	-20.0	110.0°	-16.8	85.0	135.0	-22.8	180.0	-15.3
	0.15		0.194×10^{-2}, -0.492×10^{-2}	9.6	12.0	69.0°	80.0°	-16.0	95.0°	-15.2	80.0	130.0	-28.7	180.0	-12.0
	0.2		0.195×10^{-2}, -0.502×10^{-2}	9.8	14.0	67.0°	75.0°	-13.8	82.5°	-13.8	77.0	122.5	-31.3	180.0	-14.0
	0.25		0.183×10^{-2}, -0.488×10^{-2}	9.8	12.5	66.0°	135.0°	-24.0	180.0°	-12.5	75.0	125.0	-23.5	180.0	-12.5
	0.3		0.189×10^{-2}, -0.487×10^{-2}	9.8	12.7	65.5°	130.0°	-29.8	180.0°	-12.7	73.0	127.5	-30.5	180.0	-12.7

Table 5.5 Computer characteristics of "seven-element" circular loop Yagi arrays.

No. of elements	Director spacing	Director size	Input Admittance (Ω)	Gain Gd (db)	Front to back ratio (db)	3 db BW in H-plane	1st null in H-plane		1st side lobe in H-plane		3 db BW in E-plane	1st null in E-plane		1st side lobe in E-plane	
							Position (degree)	Level (db)	Position (degree)	Level (db)		Position (degree)	Level (db)	Position (degree)	Level (db)
7	0.1	1.0	0.532×10^{-2}, -0.853×10^{-2}	10.6	16.6	50.0°	100.0°	-33.6	127.5°	-15.6	54°	50.0°	- 6.6	60.0°	- 6.5
	0.15		0.100×10^{-2}, -0.610×10^{-2}	9.1	17.5	62.5°	77.5°	-26.7	100.0°	-10.3	100°	80.0°	-20.4	100.0°	- 9.6
	0.2		0.460×10^{-3}, -0.711×10^{-2}	7.9	14.4	85.0°	63.0°	-15.9	82.5°	- 7.0	97°	65.0°	-13.9	82.5°	- 6.8
	0.25		0.594×10^{-3}, -0.758×10^{-2}	8.1	12.7	75.0°	52.5°	- 9.8	67.5°	- 7.0	81°	55.0°	-10.2	70.0°	- 5.8
	0.3		0.177×10^{-3}, -0.563×10^{-2}	- 3.3	- 9.1	—	—	—	—	—	—	—	—	—	—
7	0.1	0.9	0.293×10^{-2}, -0.583×10^{-2}	10.9	13.2	58.5°	67.5°	-27.7	95.0°	-14.3	64°	67.5°	-43.2	95.0°	-12.2
	0.15		0.157×10^{-2}, -0.568×10^{-2}	11.9	21.0	52.0°	58.0°	-26.0	77.5°	-13.0	55°	57.5°	-35.3	80.0°	-12.0
	0.2		0.242×10^{-2}, -0.559×10^{-2}	12.3	14.0	48.5°	52.5°	-30.1	70.0°	-13.2	51°	52.5°	-31.8	72.0°	-10.8
	0.25		0.149×10^{-2}, -0.536×10^{-2}	12.8	18.4	45.5°	47.5°	-33.8	65.0°	-12.7	48°	47.5°	-31.0	65.0°	-10.8
	0.3		0.206×10^{-2}, -0.545×10^{-2}	13.0	14.8	43.5°	45.0°	-26.9	60.0°	-12.3	46°	45.0°	-23.6	62.5°	-10.4
7	0.1	0.8	0.196×10^{-2}, -0.517×10^{-2}	10.3	13.0	64.0°	72.5°	-24.0	102.5°	-15.0	73°	77.5°	-18.4	100.0°	-14.1
	0.15		0.203×10^{-2}, -0.549×10^{-2}	10.8	18.6	60.0°	65.0°	-20.9	87.5°	-14.7	66°	67.5°	-16.0	87.5°	-12.6
	0.2		0.190×10^{-2}, -0.500×10^{-2}	11.0	13.2	57.0°	60.0°	-16.9	77.5°	-13.4	62°	60.0°	-15.8	77.5°	-11.1
	0.25		0.191×10^{-2}, -0.518×10^{-2}	11.2	17.4	55.0°	55.0°	-14.7	70.0°	-12.6	60°	55.0°	-12.1	70.0°	-10.2
	0.3		0.181×10^{-2}, -0.494×10^{-2}	11.2	13.2	52.0°	52.5°	-12.7	62.5°	-11.4	58°	52.5°	-10.7	65.0°	- 9.4
7	0.1	0.7	0.182×10^{-2}, -0.512×10^{-2}	9.7	13.1	69.5°	82.5°	-18.7	102.5°	-16.4	80°	132.5°	-25.8	180.0°	-13.1
	0.15		0.204×10^{-2}, -0.508×10^{-2}	10.0	14.0	66.0°	72.5°	-15.2	87.5°	-14.5	75°	125.0°	-32.5	180.0°	-14.0
	0.2		0.185×10^{-2}, -0.493×10^{-2}	10.1	13.0	64.0°	67.5°	-12.9	75.0°	-12.8	72°	117.5°	-23.2	180.0°	-15.0
	0.25		0.192×10^{-2}, -0.492×10^{-2}	10.1	13.4	63.0°	130.0°	-29.7	180.0°	-13.4	70°	127.5°	-31.2	180.0°	-13.4
	0.3		0.182×10^{-2}, -0.486×10^{-2}	10.1	12.6	62.0°	122.5°	-25.4	180.0°	-12.6	69°	120.0°	-27.7	180.0°	-12.6

Table 5.6 Computed characteristics of "eight-element" circular loop Yagi arrays.

No. of elements	Director spacing	Director size	Input Admittance (U)	Gain Gd (db)	Front to back ratio (db)	3 db BW in H-plane	1st null in H-plane		1st side lobe in H-plane		3 db BW in E-plane	1st null in E-plane		1st side lobe in E-plane	
							Position (degree)	Level (db)	Position (degree)	Level (db)		Position (degree)	Level (db)	Position (degree)	Level (db)
8	0.1	1.0	0.946×10^{-3}, -0.857×10^{-2}	9.7	13.3	54.0°	85.0°	-23.5	117.5°	-12.3	58.5	92.5°	-25.0	120.0°	-12.1
	0.15		0.891×10^{-2}, -0.826×10^{-2}	8.6	15.1	79.0°	67.5°	-12.8	85.0°	- 9.5	95.5	70.0°	-13.7	90.0°	- 8.2
	0.2		0.191×10^{-2}, -0.852×10^{-2}	8.5	15.0	78.5°	57.5°	-10.0	70.0°	- 8.4	85.5	57.5°	-10.0	72.5°	- 6.0
	0.25		0.324×10^{-3}, -0.707×10^{-2}	9.2	12.4	65.0°	47.5°	- 9.3	60.0°	- 7.2	69.0	47.5°	- 8.8	62.5°	- 5.2
	0.3		0.174×10^{-3}, -0.563×10^{-2}	0.6	- 5.4										
8	0.1	0.9	0.218×10^{-2}, -0.665×10^{-2}	11.4	18.0	55.0°	62.5°	-22.6	85.0°	-14.5	60.0	62.5°	-30.8	87.5°	-12.4
	0.15		0.236×10^{-2}, -0.523×10^{-2}	12.2	13.2	49.5°	52.5°	-25.2	72.5°	-13.1	52.0	52.5°	-30.5	75.0°	-10.8
	0.2		0.154×10^{-2}, -0.558×10^{-2}	12.9	23.4	45.5°	47.5°	-25.3	62.5°	-12.9	47.0	47.5°	-29.7	65.0°	-10.8
	0.25		0.217×10^{-2}, -0.563×10^{-2}	13.2	15.5	42.5°	42.5°	-33.8	57.5°	-12.4	44.5	42.5°	-33.3	60.0°	-10.3
	0.3		0.158×10^{-2}, -0.507×10^{-2}	13.5	14.2	40.5°	42.5°	-21.5	55.0°	-11.8	42.0	40.0°	-29.6	55.0°	-10.1
8	0.1	0.8	0.234×10^{-2}, -0.534×10^{-2}	10.5	13.5	62.0°	70.0°	-24.7	95.0°	-14.7	69.0	70.0°	-17.9	95.0°	-12.9
	0.15		0.180×10^{-2}, -0.523×10^{-2}	11.2	15.9	57.0°	60.0°	-20.8	80.0°	-14.1	62.0	60.0°	-16.4	80.0°	-11.9
	0.2		0.204×10^{-2}, -0.525×10^{-2}	11.5	16.7	54.0°	55.0°	-17.0	70.0°	-13.1	58.0	55.0°	-13.9	70.0°	-10.6
	0.25		0.187×10^{-2}, -0.497×10^{-2}	11.6	13.6	52.0°	50.0°	-14.3	62.5°	-12.0	55.0	50.0°	-12.1	65.0°	- 9.8
	0.3		0.178×10^{-2}, -0.510×10^{-2}	11.7	17.7	50.5°	47.5°	-12.6	57.5°	-11.1	53.5	47.5°	-10.7	60.0°	- 9.1
8	0.1	0.7	0.199×10^{-2}, -0.504×10^{-2}	9.9	12.4	67.5°	77.5°	-17.8	97.5°	-15.3	77.0	82.5°	-14.1	92.5°	-13.8
	0.15		0.189×10^{-2}, -0.510×10^{-2}	10.3	15.1	64.0°	67.5°	-14.8	82.5°	-13.9	71.0	70.0°	-11.7	80.0°	-11.4
	0.2		0.196×10^{-2}, -0.494×10^{-2}	10.3	13.2	61.5°	62.5°	-12.1	70.0°	-12.0	68.5	62.5°	- 9.6	70.0°	- 9.5
	0.25		0.185×10^{-2}, -0.489×10^{-2}	10.3	13.1	60.0°	122.5°	-25.6	180.0°	-13.1	66.0	120.0°	-28.0	180.0°	-13.1
	0.3		0.186×10^{-2}, -0.490×10^{-2}	10.3	13.9	59.5°	130.0°	-29.8	180.0°	-13.9	65.0	127.5°	-30.1	180.0°	-13.9

Tabel 5.7 Computed characteristics of "nine-element" circular loop Yagi arrays.

No. of elements	Director spacing	Director size	Input Admittance (U)	Gain Gd (db)	Front to back ratio (db)	3 db BW in H-plane	1st null in H-plane		1st side lobe in H-plane		3 db BW in E-plane	1st null in E-plane		1st side lobe in E-plane	
							Position (degree)	Level (db)	Position (degree)	Level (db)		Position (degree)	Level (db)	Position (degree)	Level (db)
9	0.1	1.0	$0.143x10^{-2}$, $-0.637x10^{-2}$	9.2	17.2	63.5°	80.0°	-20.8	102.5°	-11.4	95.0°	82.5°	-19.1	105.5°	-10.3
	0.15		$0.161x10^{-2}$, $-0.565x10^{-2}$	8.3	22.7	83.0°	60.0°	-12.4	76.5°	- 7.7	91.0°	60.0°	-11.1	77.5°	- 6.0
	0.2		$0.996x10^{-3}$, $-0.563x10^{-2}$	9.0	14.0	67.0°	47.5°	-10.2	62.5°	- 6.2	71.0°	47.5°	- 9.3	63.5°	- 4.9
	0.25		$0.766x10^{-3}$, $-0.545x10^{-2}$	9.9	9.9	50.5°	37.5°	- 9.2	51.5°	- 5.5	51.5°	37.5°	- 8.5	52.5°	- 4.4
	0.3		$0.175x10^{-3}$, $-0.564x10^{-2}$	0.4	- 5.8	—	—	—	—	—	—	—	—	—	—
9	0.1	0.9	$0.159x10^{-2}$, $-0.607x10^{-2}$	11.8	28.0	52.0°	57.5°	-20.5	77.5°	-13.8	55.0°	57.5°	-24.3	80.0°	-12.0
	0.15		$0.210x10^{-2}$, $-0.625x10^{-2}$	12.7	18.3	46.4°	50.0°	-20.9	68.0°	-13.2	48.5°	50.0°	-23.2	68.0°	-10.7
	0.2		$0.236x10^{-2}$, $-0.529x10^{-2}$	13.2	13.5	42.5°	42.5°	-24.4	59.0°	-12.1	44.0°	42.5°	-26.4	60.0°	-10.1
	0.25		$0.159x10^{-2}$, $-0.518x10^{-2}$	13.7	16.2	39.5°	40.0°	-27.7	54.0°	-11.7	40.5°	40.0°	-31.0	55.0°	-10.1
	0.3		$0.153x10^{-2}$, $-0.561x10^{-2}$	14.1	36.2	37.5°	37.5°	-31.7	50.0°	-11.7	38.5°	37.5°	-33.1	50.0°	-10.1
9	0.1	0.8	$0.220x10^{-2}$, $-0.574x10^{-2}$	10.9	17.9	58.5°	65.0°	-26.9	90.0°	-14.9	65.0°	67.5°	-18.6	90.0°	-12.7
	0.15		$0.210x10^{-2}$, $-0.511x10^{-2}$	11.5	13.6	54.5°	55.0°	-20.3	75.0°	-13.5	58.5°	57.5°	-16.1	75.0°	-11.0
	0.2		$0.181x10^{-2}$, $-0.511x10^{-2}$	11.9	15.9	51.5°	50.0°	-17.0	65.0°	-12.7	54.5°	50.0°	-14.2	65.0°	-10.2
	0.25		$0.189x10^{-2}$, $-0.517x10^{-2}$	12.0	18.4	49.0°	47.5°	-14.3	60.0°	-11.7	52.5°	47.5°	-12.4	60.0°	- 9.6
	0.3		$0.190x10^{-2}$, $-0.501x10^{-2}$	12.0	14.5	48.0°	45.0°	-12.2	55.0°	-10.6	50.0°	42.5°	-10.7	55.0°	- 8.8
9	0.1	0.7	$0.212x10^{-2}$, $-0.517x10^{-2}$	10.1	13.8	65.0°	72.5°	-17.6	92.5°	-14.9	73.5°	75.0°	-13.4	90.0°	-12.8
	0.15		$0.190x10^{-2}$, $-0.498x10^{-2}$	10.5	13.1	61.5°	62.5°	-14.1	75.0°	-13.1	66.5°	65.0°	-11.1	75.0°	-10.6
	0.2		$0.188x10^{-2}$, $-0.499x10^{-2}$	10.6	14.7	59.5°	57.5°	-11.7	65.0°	-11.5	64.5°	57.5°	- 9.3	65.0°	- 9.1
	0.25		$0.191x10^{-2}$, $-0.492x10^{-2}$	10.5	13.9	57.5°	132.5°	-28.9	180.0°	-13.9	63.0°	130.0°	-28.6	180.0°	-13.9
	0.3		$0.185x10^{-2}$, $-0.485x10^{-2}$	10.5	12.8	57.0°	122.5°	-26.5	180.0°	-12.8	62.0°	122.5°	-28.6	180.0°	-12.8

Table 5.8 Computed characteristics of "ten-element" circular loop Yagi arrays.

No. of elements	Director spacing	Director size	Input Admittance (℧)	Gain Gd (db)	Front to back ratio (db)	3 db BW in H-plane	1st null in H-plane		1st side lobe in H-plane		3 db BW in E-plane	1st null in E-plane		1st side lobe in E-plane	
							Position (degree)	Level (db)	Position (degree)	Level (db)		Position (degree)	Level (db)	Position (degree)	Level (db)
10	0.1	1.0	0.296×10^{-2}, -0.101×10^{-1}	8.9	20.0	75.0°	75.0°	-14.2	92.5°	-11.5	100.0°	75.0°	-16.0	95.0°	- 8.4
	0.15		0.715×10^{-3}, -0.784×10^{-2}	8.9	14.3	69.0°	52.5°	-8.3	62.5°	- 7.5	75.0°	52.5°	- 8.5	67.5°	- 6.2
	0.2		0.449×10^{-3}, -0.687×10^{-2}	9.7	12.0	51.5°	40.0°	-7.1	50.0°	- 5.8	54.0°	40.0°	- 7.1	52.5°	- 4.8
	0.25		0.327×10^{-3}, -0.611×10^{-2}	9.4	7.8	37.0°	27.5°	-6.4	42.5°	- 3.8	38.0°	30.0°	- 6.4	42.5°	- 3.1
	0.3		0.172×10^{-3}, -0.564×10^{-2}	- 1.5	- 6.7	—	—	—	—	—	—	—	—	—	—
10	0.1	0.9	0.195×10^{-2}, -0.538×10^{-2}	12.1	15.6	49.5°	52.5°	-20.0	73.5°	-13.1	52.0°	52.5°	-22.0	76.0°	-10.9
	0.15		0.160×10^{-2}, -0.552×10^{-2}	13.0	20.2	43.5°	45.0°	-19.5	61.5°	-12.3	45.0°	45.0°	-20.9	63.5°	-10.3
	0.2		0.161×10^{-2}, -0.578×10^{-2}	13.7	36.6	39.5°	40.0°	-20.9	55.0°	-12.0	41.0°	40.0°	-22.3	55.0°	-10.1
	0.25		0.196×10^{-2}, -0.579×10^{-2}	14.1	18.2	37.0°	37.5°	-24.2	50.0°	-11.6	38.0°	37.5°	-26.0	51.0°	- 9.9
	0.3		0.207×10^{-2} -0.532×10^{-2}	14.4	14.2	35.0°	35.0°	-28.7	47.5	-11.1	36.0°	35.0°	-29.9	47.5°	-9.6
10	0.1	0.8	0.185×10^{-2}, -0.565×10^{-2}	11.3	22.4	56.5°	60.0°	-27.5	82.5°	-14.7	61.5°	62.5°	-19.8	82.5°	-12.5
	0.15		0.208×10^{-2}, -0.544×10^{-2}	11.9	18.3	52.5°	52.5°	-21.1	70.0°	-13.4	55.0°	52.5°	-16.9	70.0°	-10.9
	0.2		0.206×10^{-2}, -0.511×10^{-2}	12.2	14.8	49.0°	47.5°	-16.9	62.5°	-12.3	52.0°	47.5°	-14.3	62.5°	-10.0
	0.25		0.189×10^{-2}, -0.499×10^{-2}	12.3	14.3	47.0°	42.5°	-14.1	55.0°	-11.3	49.0°	42.5°	-12.3	57.5°	- 9.4
	0.3		0.176×10^{-2}, -0.501×10^{-2}	12.4	15.7	45.0°	40.0°	-12.2	50.0°	-10.4	47.5°	40.0°	-11.0	52.5°	- 8.7
10	0.1	0.7	0.202×10^{-2}, -0.532×10^{-2}	10.4	16.4	63.0°	67.5°	-17.4	87.5°	-14.7	70.0°	70.0	-13.3	85.0°	-12.3
	0.15		0.201×10^{-2}, -0.503×10^{-2}	10.7	13.9	58.0°	60.0°	-13.7	72.5°	-12.7	65.0°	60.0	-10.8	72.5°	-10.1
	0.2		0.191×10^{-2}, -0.491×10^{-2}	10.8	13.2	57.0°	55.0°	-11.2	62.5°	-10.9	62.0°	52.5	- 9.1	62.5°	- 8.7
	0.25		0.186×10^{-2}, -0.489×10^{-2}	10.8	13.5	55.5°	125.0°	-28.1	180.0°	-13.4	60.0°	50.0	- 7.7	55.0°	- 7.6
	0.3		0.184×10^{-2}, -0.489×10^{-2}	10.7	14.1	54.0°	130.0°	-29.2	180.0°	-14.1	58.0°	127.5	-29.1	180.0°	-14.1

Table 5.9 Computed characteristics of "eleven-element" circular loop Yagi arrays.

No. of elements	Director spacing	Director size	Input Admittance (℧)	Gain Gd (db)	Front to back ratio (db)	3 db BW in H-plane	1st null in H-plane		1st side lobe in H-plane		3 db BW in E-plane	1st null in E-plane		1st side lobe in E-plane	
							Position (degree)	Level (db)	Position (degree)	Level (db)		Position (degree)	Level (db)	Position (degree)	Level (db)
11	0.1	1.0	0.856×10^{-3}, -0.792×10^{-2}	8.5	16.9	79.0°	64.0°	-11.7	81.0°	- 9.2	93.5°	67.5°	-12.1	86.0°	- 7.9
	0.15		0.294×10^{-2} -0.555×10^{-2}	9.8	14.4	61.5°	47.5°	- 8.6	59.0°	- 7.4	65.0°	47.5°	- 7.9	61.0°	- 5.4
	0.2		0.111×10^{-2}, -0.818×10^{-2}	10.2	10.9	47.0°	62.5°	-14.6	75.0°	-10.5	48.0°	35.0°	- 5.2	46.0°	- 4.4
	0.25		0.253×10^{-3}, -0.649×10^{-2}	7.3	6.8	80.0°	20.0°	- 2.5	32.5°	- 1.1	84.5°	21.0°	- 2.6	35.0°	- 0.6
	0.3		0.172×10^{-3} -0.564×10^{-2}	- 2.9	- 9.1	—	—	—	—	—	—	—	—	—	—
11	0.1	0.9	0.291×10^{-2}, -0.577×10^{-2}	12.3	13.5	47.5°	51.0°	-19.2	71.0°	-12.9	50.0°	51.0°	-20.9	72.5°	-10.4
	0.15		0.255×10^{-2}, -0.537×10^{-2}	13.2	13.6	41.0°	42.5°	-18.7	58.5°	-11.8	42.5°	42.5°	-19.3	59.0°	- 9.7
	0.2		0.213×10^{-2}, -0.510×10^{-2}	13.9	14.0	36.5°	37.5°	-20.0	51.5°	-11.2	38.0°	37.5°	-20.5	52.5°	- 9.5
	0.25		0.176×10^{-2} -0.506×10^{-2}	14.4	14.9	34.5°	35.0°	-22.0	47.5°	-10.9	35.0°	34.0°	-23.1	47.5°	- 9.5
	0.3		0.149×10^{-2}, -0.514×10^{-2}	14.8	16.4	32.5°	32.5°	-25.7	43.5°	-10.8	33.0°	32.0°	-27.9	45.0°	- 9.5
11	0.1	0.8	0.183×10^{-2}, -0.534×10^{-2}	11.6	16.2	55.0°	57.5°	-28.1	77.5°	-14.1	59.0°	57.5°	-20.1	79.0°	-11.9
	0.15		0.182×10^{-2}, -0.528×10^{-2}	12.3	18.4	49.5°	50.0°	-21.5	65.0°	-13.2	53.0°	50.0°	-17.6	67.5°	-10.8
	0.2		0.185×10^{-2}, -0.522×10^{-2}	12.6	19.8	46.5°	45.0°	-17.3	57.5°	-12.0	49.0°	45.0°	-14.9	59.0°	-10.0
	0.25		0.187×10^{-2}, -0.516×10^{-2}	12.7	19.2	45.0°	42.5°	-14.2	52.5°	-11.0	46.5°	41.0°	-12.8	53.5°	- 9.2
	0.3		0.186×10^{-2}, -0.509×10^{-2}	12.6	17.8	43.0°	38.5°	-12.2	48.0°	-10.2	45.5°	38.5°	-11.0	50.0°	- 8.6
11	0.1	0.7	0.188×10^{-2}, -0.526×10^{-2}	10.7	16.5	61.0°	65.0°	-17.2	82.5°	-14.4	67.0°	66.0°	-13.3	81.0°	-11.8
	0.15		0.193×10^{-2}, -0.511×10^{-2}	11.0	16.1	57.0°	56.0°	-13.4	67.5°	-12.4	62.0°	56.0°	-10.8	68.5°	- 9.8
	0.2		0.193×10^{-2}, -0.499×10^{-2}	11.0	15.0	55.0°	51.5°	-11.0	58.5°	-10.6	59.0°	50.0°	- 8.9	60.0°	- 8.5
	0.25		0.190×10^{-2}, -0.491×10^{-2}	10.9	14.2	53.5°	132.5°	-27.3	180.0°	-14.2	57.5°	46.5°	- 7.6	52.5°	- 7.4
	0.3		0.187×10^{-2}, -0.488×10^{-2}	10.8	13.6	52.0°	125.0°	-27.5	180.0°	-13.6	57.0°	122.5°	-30.2	180.0°	-13.6

Table 5.10 Computed characteristics of "twelve-element" circular loop Yagi arrays.

No. of elements	Director spacing	Director size	Input Admittance (℧)	Gain Gd (db)	Front to back ratio (db)	3 db BW in H-plane	1st null in H-plane		1st side lobe in H-plane		3 db BW in E-plane	1st null in E-plane		1st side lobe in E-plane	
							Position (degree)	Level (db)	Position (degree)	Level (db)		Position (degree)	Level (db)	Position (degree)	Level (db)
12	0.1	1.0	0.283×10^{-2}, -0.573×10^{-2}	8.7	26.4	80.5°	61.0°	-11.2	76.0°	- 8.9	88.0°	61.0°	-10.4	77.5°	- 6.5
	0.15		0.635×10^{-3}, -0.747×10^{-2}	9.9	12.5	51.0°	42.5°	- 6.2	46.5°	- 6.1	54.0°	41.0°	- 6.1	52.5°	- 5.0
	0.2		0.161×10^{-2}, -0.526×10^{-2}	10.2	12.7	40.5°	29.5°	- 4.5	38.5°	- 4.0	42.0°	28.5°	- 4.1	40.0°	- 3.1
	0.25		0.272×10^{-2}, -0.684×10^{-2}	6.3	8.4	71.0°	42.5°	- 9.1	53.5°	- 3.3	73.0°	44.0°	- 9.2	55.0°	- 3.0
	0.3		0.172×10^{-2}, -0.564×10^{-2}	- 2.7	- 8.9	—	—	—	—	—	—	—	—	—	—
12	0.1	0.9	0.225×10^{-2}, -0.667×10^{-2}	12.6	16.5	45.5°	50.0°	-17.1	66.0°	-13.0	47.0°	48.0°	-18.4	68.5°	-10.3
	0.15		0.191×10^{-2}, -0.623×10^{-2}	13.6	19.4	39.0°	40.0°	-16.8	54.0°	-11.7	40.0°	40.0°	-17.1	56.0°	- 9.6
	0.2		0.180×10^{-2}, -0.595×10^{-2}	14.3	21.3	35.0°	35.0°	-17.7	48.5°	-11.0	36.0°	35.0°	-18.2	50.0°	- 9.4
	0.25		0.172×10^{-2}, -0.578×10^{-2}	14.8	22.3	32.5°	32.5°	-20.1	45.0°	-10.7	33.0°	32.5°	-20.7	45.0°	- 9.4
	0.3		0.162×10^{-2}, -0.567×10^{-2}	15.2	23.0	30.5°	30.0°	-23.4	41.5°	-10.6	31.0°	30.0°	-24.4	42.5°	- 9.4
12	0.1	0.8	0.214×10^{-2}, -0.522×10^{-2}	11.8	14.0	52.5°	56.0°	-27.9	74.0°	-13.8	56.0°	56.0°	-20.5	76.0°	-11.2
	0.15		0.205×10^{-2}, -0.511×10^{-2}	12.5	14.4	47.0°	47.5°	-21.4	62.5°	-12.8	49.5°	47.5°	-17.8	63.5°	-10.3
	0.2		0.197×10^{-2}, -0.503×10^{-2}	12.8	14.6	44.5°	42.5°	-17.2	55.0°	-11.7	46.0°	42.5°	-15.1	56.0°	- 9.7
	0.25		0.190×10^{-2}, -0.500×10^{-2}	12.9	14.8	42.5°	40.0°	-14.2	50.0°	-10.8	44.0°	39.0°	-12.8	51.0°	- 9.0
	0.3		0.184×10^{-2}, -0.497×10^{-2}	12.9	14.8	41.0°	37.5°	-12.2	46.0°	-10.0	42.0°	36.5°	-11.0	47.5°	- 8.5
12	0.1	0.7	0.188×10^{-2}, -0.513×10^{-2}	10.8	14.3	59.0°	61.5°	-16.9	78.5°	-13.9	65.0°	62.5°	-13.0	77.5°	-11.3
	0.15		0.189×10^{-2}, -0.501×10^{-2}	11.2	14.4	55.0°	53.5°	-13.1	64.0°	-11.9	59.0°	54.0°	-10.7	65.0°	- 9.6
	0.2		0.188×10^{-2}, -0.494×10^{-2}	11.2	14.2	52.5°	48.5°	-10.7	56.0°	-10.2	56.0°	47.5°	- 8.9	57.0°	- 8.2
	0.25		0.186×10^{-2}, -0.489×10^{-2}	11.1	13.9	51.0°	46.0°	- 8.9	48.5°	- 8.7	54.5°	45.0°	- 7.5	51.0°	- 7.2
	0.3		0.184×10^{-2}, -0.487×10^{-2}	11.0	13.6	50.0°	130.0°	-28.9	180.0°	-13.6	53.5°	41.5°	- 6.5	46.0°	- 6.3

CHAPTER VI

CONCLUSION

The object of this thesis was to investigate the characteristics of circular loop arrays; such as the input admittance, the far radiation field, and the directive gains. A set of integral equations for the loop currents were obtained and were solved by expanding kernels and loop currents in Fourier series of azimuthal angle. The resonant property of loops was then used to retain only the resonant modes and if necessary their adjacent modes. It was shown that such an approximation adequately describes loop currents and reduces the require storage space and computational time considerably. Furthermore, when an array consisted of many unequal loops; and the active element was larger than the directors; it could support different resonant modes in different loops. These resonant modes had significant values only around their supporting loops and decreased rapidly in magnitudes for distant loops. As a result they could be computed to a reasonable accuracy by retaining only the adjacent loops and neglecting the remaining part of the array, an approach which effectively reduced the computational labour to a minimum.

The technique was then used to investigate the effects of circular loop yagi array parameters - such as the reflector size and spacing, the exciter size, the wire cross section, and the director size and spacing on the antenna characteristics.

It was found that varying the director size or spacing, while holding all other parameters fixed, has a significant effect in particular on the radiation field. Therefore, it was possible to obtain a desirable beamwidth by a suitable choice of the director size or spacing, or their combination. In particular, it was shown that for practically useful radiation patterns, the director circumferences have to be less than or equal to one wavelength, if the exciter size was about the wave length of the radiation frequency.

The reflector size and spacing was found to have negligible effects on the forward radiation, or on the directive gain Gd in the positive direction, but played a major role in controlling the input impedance of the array. Similarly, the size of the active loop or the wire cross section of the array elements had a negligible effect on the forward far field pattern or Gd, but affected the input impedance of the array. These parameters can be varied for obtaining desired input admittance without affecting the gain Gd or the forward radiation pattern.

Finally, extensive design data for circular loop Yagi array was obtained, which can be used for rapid design of such arrays. Generally speaking, an addition of a new director increases the directivity of the array, but the rate of the increase decreasesas array elements increase. For the arrays under investigation, the highest observed directivity was 15.2 db. This was obtained for a 10 director array with directos sizes and spacings of 0.9λ and 0.3λ, respectively.

REFERENCES

[1] S. Adachi and Y. Mushiake, "Theoretical formulation for circular loop antennas by integral equation method," Sci. Rep. Research Institutes of Tohoku University (RITU), B, 9, 1957, p. 9.

[2] S. Adachi and Y. Mushiaki, "Studies of large circular loop antennas," Sci. Rep. Research Institues of Tohoku University (RITU), B, 9, 2, 1957, pp. 79-103.

[3] J.E. Lindsay, Jr., "A parasitic end-fire array of circular loop elements," IEEE Trans. on Antennas and Propagation (Commun.), Vol. AP-15, Sept. 1967, pp. 697-698.

[4] E. Ledinegg, W. Papousek, and H.L. Brueckmann, "Low-frequency loop antenna arrays: ground reaction and mutual interaction," IEEE Trans. on Antennas and Propagation, Vol. AP-21, pp. 1-8, Jan. 1973.

[5] D Foster, "Loop antennas with uniform current," Proc. I.R.E. Vol. 32, pp. 603-607, Oct. 1944.

[6] G. Glinski, "Note on circular loop antennas with non-uniform current distribution," J. Applied Phys. Vol. 18, pp. 638-644, July 1947.

[7] T. Kashara, S. Adachi and Y. Mushiake, "Calculation of the impedances of impedance-terminated loop antennas by the emf method," Trans. IEEE, Japan, 52-B, pp. 73-80, March 1969.

[8] E. Hallen, "Theoretical investigations into transmitting and receiving qualities of antennas," Nova Acta Regiae Soc. Sci. Upsal. (Series IV), Vol. 2, pp. 1-44, 1938.

[9] J.E. Storer, "Impedance of thin-wire loop antennas," AIEE Trans. (Commun. Electron.), Vol. 75, pp. 606-619, Nov. 1956.

[10] T.T. Wu, "Theory of the thin circular loop antenna," J. Math. Phys., Vol. 3, pp. 1301-1304, Nov.-Dec. 1962.

[11] N. Inagaki, S. Ito and T. Sekiguchi, "A theory of a circular loop," J. Inst. Electron. Commun. Eng. in Japan, Vol. 53-B, pp. 135-142, Mar. 1970.

[12] R.W.P. King, C.W. Harrison, Jr., and D.J. Tingley, "The admittance of bare circular loop antennas in a dissipative medium," IEEE Trans. Antennas and Propatation, Vol. AP-12, pp. 434-438, July 1964.

[13] K. Iizuka, R.W.P. King, and C.W. Harrison, Jr., "Self and mutual admittances of two identical circular loop antennas in a conducting medium and in air," IEEE Trans. Antennas and Propagation, Vol. AP-14, pp. 440-450, July 1966.

[14] S. Ito, N. Inagaki and R. Sekiguchi, "An investigation of the array of circular-loop antenna," IEEE Trans., Antennas and Propagation, Vol. AP-19, pp. 469-476, July 1971.

[15] L.C. Shen and G.W. Raffoul, "Optimum design of Yagi array of loops," IEEE Trans. Antennas and Propagation, Vol. AP-22, pp. 829-830, Nov. 1974.

[16] F.M. Greene, "The near-zone magnetic field of a small circular-loop antenna," J. Res. Nat. Bur. Stand. Sect. C, Vol. 71C, pp. 319-326, Oct.-Dec. 1967.

[17] S. Ito, M. Kosugi, N. Inagaki and T. Sekiguchi, "Theory of a multi-element loop antenna," J. Int. Electron. Commun. Eng. in Japan, Vol. 54-B, No. 6, pp. 95-103, June 1971.

[18] N. Inagaki and R. Sekiguchi, "Integral equation and its solution for a cylindrical antenna having a finite gap at the driving point," J. Int. Electron. Commun. Eng. in Japan, Vol. 52-B, pp. 88-94, May 1969.

[19] N. Inagaki and R. Sekiguchi, "A note on the antenna integral equation," IEEE Trans. Antennas Propagat. (Commun.), Vol. AP-17, pp. 223-224, Mar. 1969.

[20] R.W.P. King and C.W. Harrison, Jr., Antennas and Waves, Cambridge, Mass.:M.I.T. Press, 1969.

[21] E.C. Jordan and K.G. Balmain, Electromagnetic Waves and Radiating Systems. Prentice-Hall, 2nd edition, pp. 354-355, 1968.

[22] F.J. Zuker, "The guiding and radiation of surface waves," Proc. Symp. on Modern Advances in Microwaves Techniques, Polytechnique Institute of Brooklyn, N.Y., 1954.

[23] R.A. Smith, "Aerials for metre and decimetre wavelengths," Cambridge University Press, Cambridge, England, pp. 150-151, 1950.

[24] H.W. Ehrenspeck and H. Poehler, "A new method for obtaining maximum gain from Yagi antennas," IRE Trans. Antennas Propagat., Vol. AP-7, pp. 379-386, Oct. 1959.

[25] G.A. Thiele, "Analysis of Yagi-Uda-type antennas," IEEE Trans. Antennas Propagat., Vol. AP-17, pp. 24-31, Jan. 1969.

APPENDIX A

Convergence of equation (2.20)

Equation (2.20) in Chapter II is

$$\frac{K_{ij}^{n}}{kb_i} = -j \sum_{m=o} \frac{(\frac{y}{2z})^{n+2m}}{m!(n+m)!} h_{n+2m}^{2}(z) \qquad (A.1)$$

where all parameters are the same as defined in Chapter II. When m increases the real part of the spherical Hankel function decreases and its imaginary part increases. Therefore, the real part of (A.1) remains as the dominant term. The progression of the real part of (A.1) was defined by

$$a_n^m = \frac{(-\frac{y}{2z})^{n+2m}}{m!(n+m)!} \eta_{n+2m}(z) \qquad (A.2)$$

where $\eta_{n+2m}(z)$ is the spherical Bessel function of second kind, of order n+2m. In the limit the ratio of the two adjacent terms a_n^{m+1} and a_n^m becomes

$$\frac{a_n^{m+1}}{a_n^m} \longrightarrow r = (\frac{2y}{z^2})^2 \qquad m \to \infty \qquad (A.3)$$

In the case of a practical array $d_{ij} \neq 0$, Z^2 is generally greater than 2y; therefore r is always less than one. The convergence of equation (A.1) becomes faster as r becomes smaller. That is, for a fixed b_i and b_j (radii of adjacent loops), equation (A.4) converges faster for larger spacing d_{ij}. Thus equation (A.1) can be approximated by a summation of a few terms. Some examples of the computed values

of a_n^m versus m for different values of kb_i and kb_j are given in this appendix, when n is taken as a parameter. Figure (A.1) is for $kb_i = kb_j = 1$, and $\frac{d}{\lambda} = 0.1$. It can be seen that when n increases, the number m at which the approximation (A.3) is valid also increases. In figure (A.2) the spacing is 0.2λ, and shows considerably faster convergence for a_n^m.

It is evident from this figure that the first few terms of the series in (A.1) represents a good approximation for the infinite series. Choosing only M terms of this series, the real part of (A.1) can be written as

$$\text{Re}\left(\frac{K_{ij}^n}{kb_i}\right) = \sum_{m=0}^{M} a_n^m + \sum_{m=M+1}^{\infty} a_n^m$$

where the second term on the right hand side represents the error in the approximation. Referring to equation (A.3) the error function can be written as

$$\sum_{n=M+1}^{\infty} a_n^m = a_n^{m+1}\,(1 + r + r^2 + \ldots)$$

which is a geometrical series with $r < 1$ and can be approximated by

$$\text{Error} = \frac{a_n^{m+1}}{1 - r} \qquad (A.4)$$

Figure (A.3) shows the numerical results of (A.1) for different values of spacing and the trunctation term M, up to $M = 10$

The error of this approximation for the case of $d/\lambda = 0.1$ is shown by the dashed line. For $d/\lambda = 0.2$ the error was so small that it could not be represented in the figure. This figure shows that both the magnitude of the summation and the resulting error decreases with increasing n. For $M = 15$ the respective values were also computed, but the numerical results for the summation were almost identical for those of the $M = 10$ case. The computed error however, was less, since the numerator of (A.4) decreases rapidly with increasing m as shown in figures (A.1) and (A.2). One therefore concludes that choosing $M = 10$ terms from the series is adequate in the above cases as long as n is less than 10.

The results for the case where $k\,b_1 = k\,b_2 = 1.5$ with $d/\lambda = 0.1$ were also investigated. It was found that the convergence of the series for this particular case was very slow. Figure (A.4) shows the behaviour of a_n^m with varying m for various values of n from 0 to 10. The magnitude of a_n^m again decreases with increasing m but the rate of decrease is very slow for large value of m. The results of the summation ($M = 15$) and the respective error are shown in figure (A.5).

The number of terms required to achieve a satisfactory estimate of the series for different value of kb_1, kb_2, and d/λ was found by the computer and are shown in the following table.

Table A.1 Required values of M for satisfactory convergence.

$kb_1 \simeq kb_2$	d/λ	number of terms M
$\simeq$ 1.0	0.1	10
$\simeq$ 1.3	0.1	10
$\simeq$ 1.5	0.1	15
$\simeq$ 1.8	0.2	10
$\simeq$ 2.0	0.2	10
$\simeq$ 2.5	0.3	10
$\simeq$ 3.0	0.3	10
$\simeq$ 4.0	0.3	12

It was shown in figures (A.1) and (A.2) that when d/λ increases the series converges faster. That is, the larger the z/y ratio the smaller the number of terms (M) required for a satisfactory result. Therefore, for given loop sizes the required values of M decrease, from those shown in the above table; as the spacing increases.

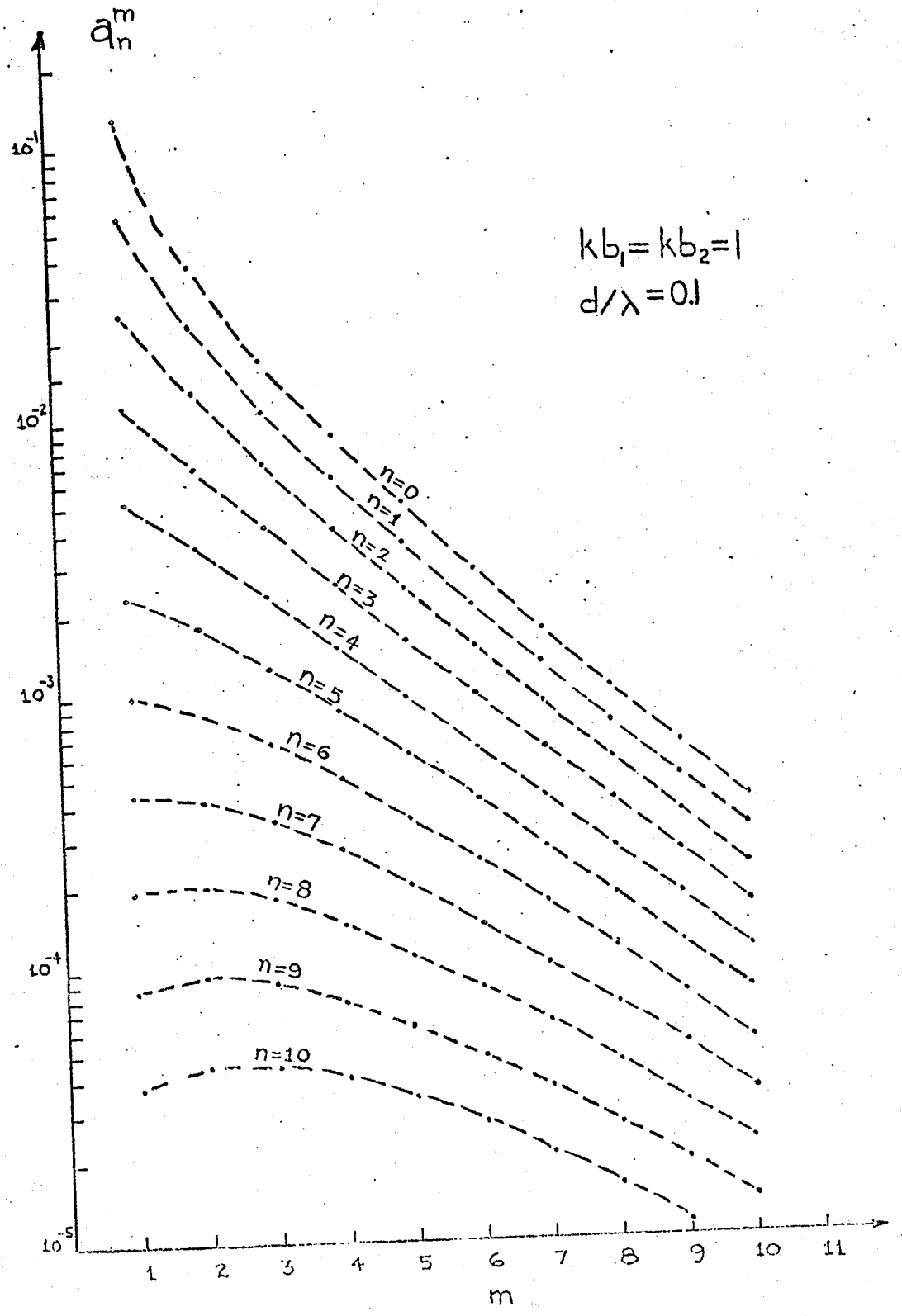

Figure A.1 Examples of computed values of a_n^m.

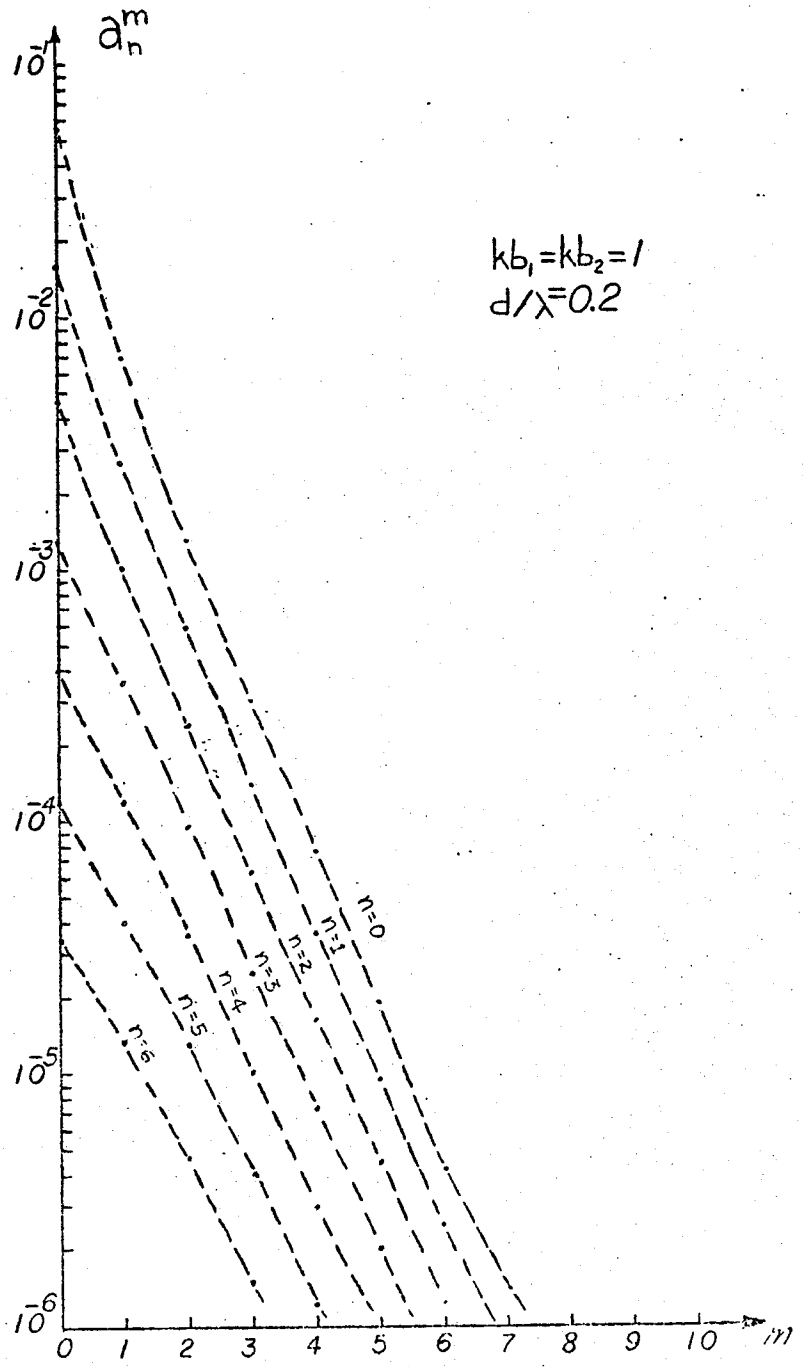

Figure A.2 Examples of computed values of a_n^m.

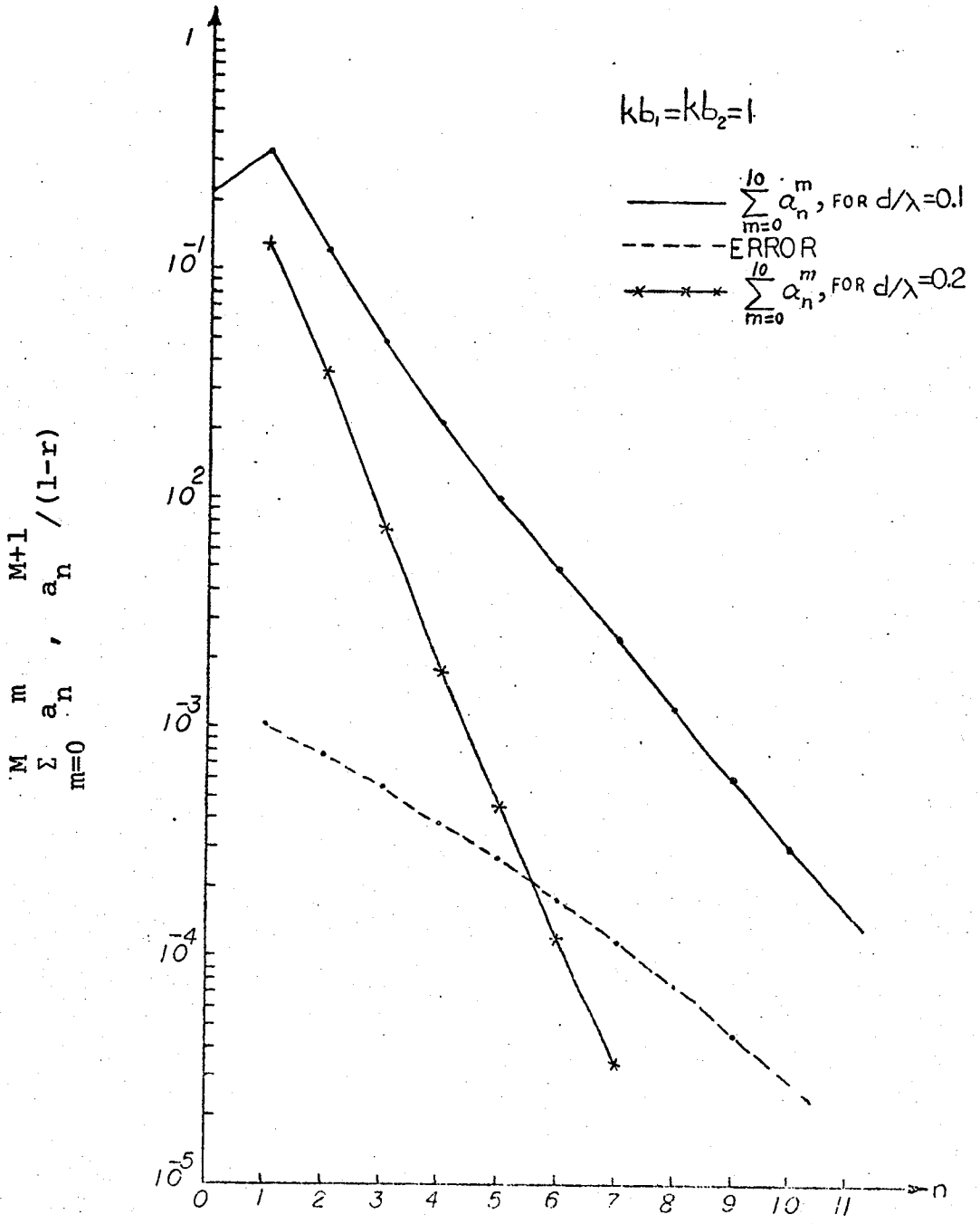

Figure A.3 Approximation $\sum_{m=0}^{M} a_n^m$ of $\mathrm{Re}(K_{ij})/kb_i$ and its error $a_n^{M+1}/(1-r)$.

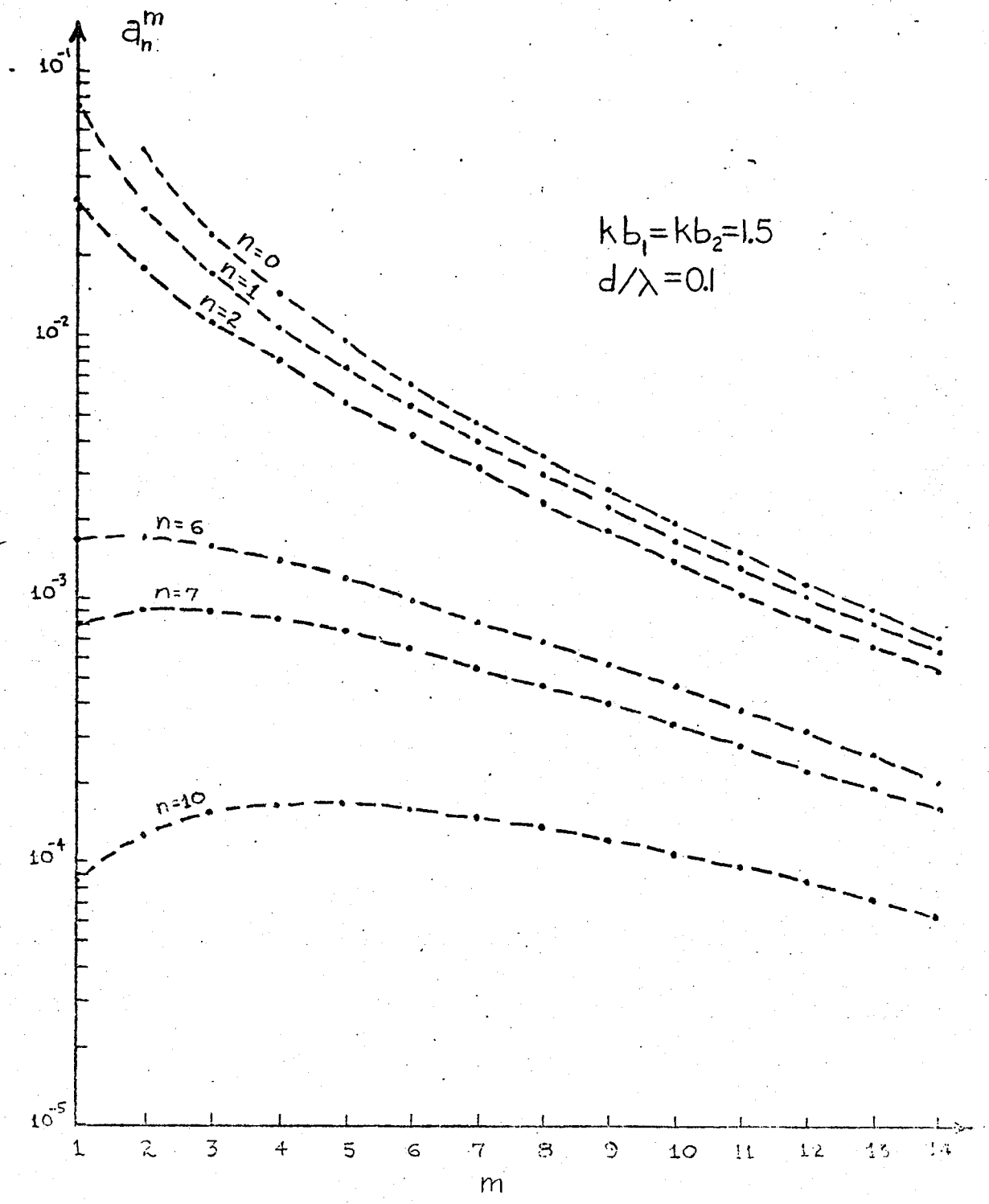

Figure A.4 Examples of computed values of a_n^m.

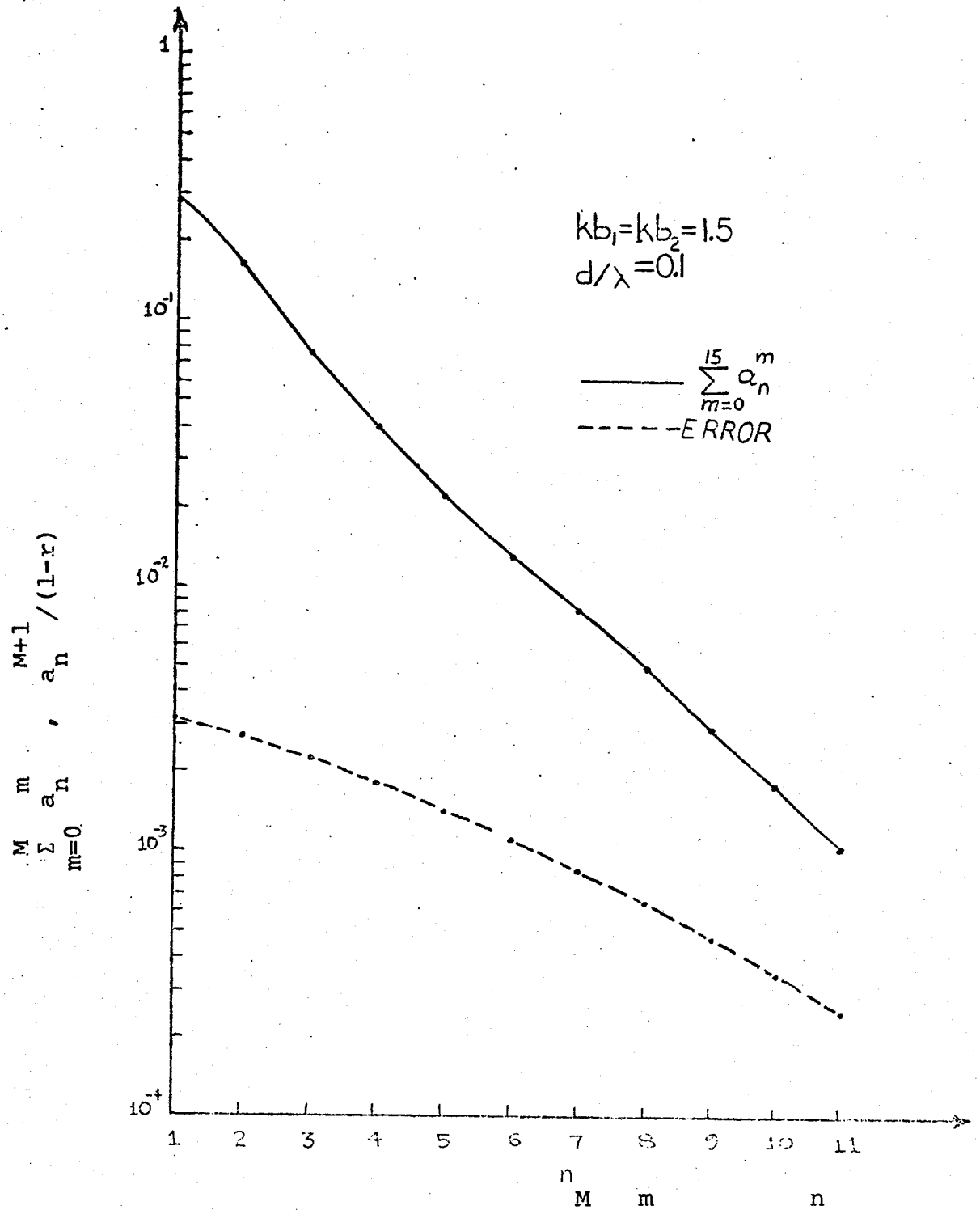

Figure A.5 Approximation $\sum_{m=0}^{M} a_n^m$ of $Re(k_{ij}^n)/kb_i$ and its error $a_n^{M+1}/(1-r)$.

APPENDIX B

Comparison Between Z_{ij}^{n} and Z_{ii}^{n}

It was stated in Chapter II that by increasing the parameter n, the nondiagonal elements Z_{ij}^{n} converges to zero very rapidly. Thus, the impedance matrix can be considered as a diagonal one when n is larger than a certain number m_o, which can be determined by the radii of the loops and their spacing. Here, some numerical results will be given for different b_i and b_j and their separation distance d_{ij}. Figure (B.1) shows the variation of $I_m(Z_{ij}^{n})$ with n for different values of spacing, when $k\,b_1 = k\,b_2 = 1$. Note that when $d/\lambda = 0.1$ and $\Omega = 11$ the ratio of $I_m(Z_{ii}^{10}/Z_{ij}^{10})$ is about 1000. Thus the matrix can be approximated by a diagonal one for n greater than 10. The value of n after which the matrix can be considered diagonal decreases with increasing spacing and increases with decreasing $\Omega = 2\,\ell n\, 2\pi\,\frac{b_i}{a}$.

Figure (B.2) represents the self and mutual impedances for $k\,b_1 = k\,b_2 = 2$ and the separation distances 0.2λ and 0.3λ. From this figure it is evident that taking 10 and 6 matrix inversion are adequate for 0.2λ and 0.3λ spacings, respectively.

From these figures it can be concluded that the value of m_o, after which the matrix may be safely approximated by a diagonal one, increases with decreasing separation between the loops or increasing the size of the loops.

The self and mutual impedances of the loops for different sizes and spacings were computed and for each case the optimum value of m_o was obtained. The results are shown in Table (B.1).

Table B.1 Required values of m_o after which Z^n_{ij} can be assumed diagonal.

$k\,b_1 \simeq k\,b_2$	d/λ	m_o
1.0	0.1	10
1.0	0.2	6
1.0	0.3	4
1.5	0.2	7
1.5	0.3	5
2.0	0.2	10
2.0	0.3	6
4.0	0.3	10

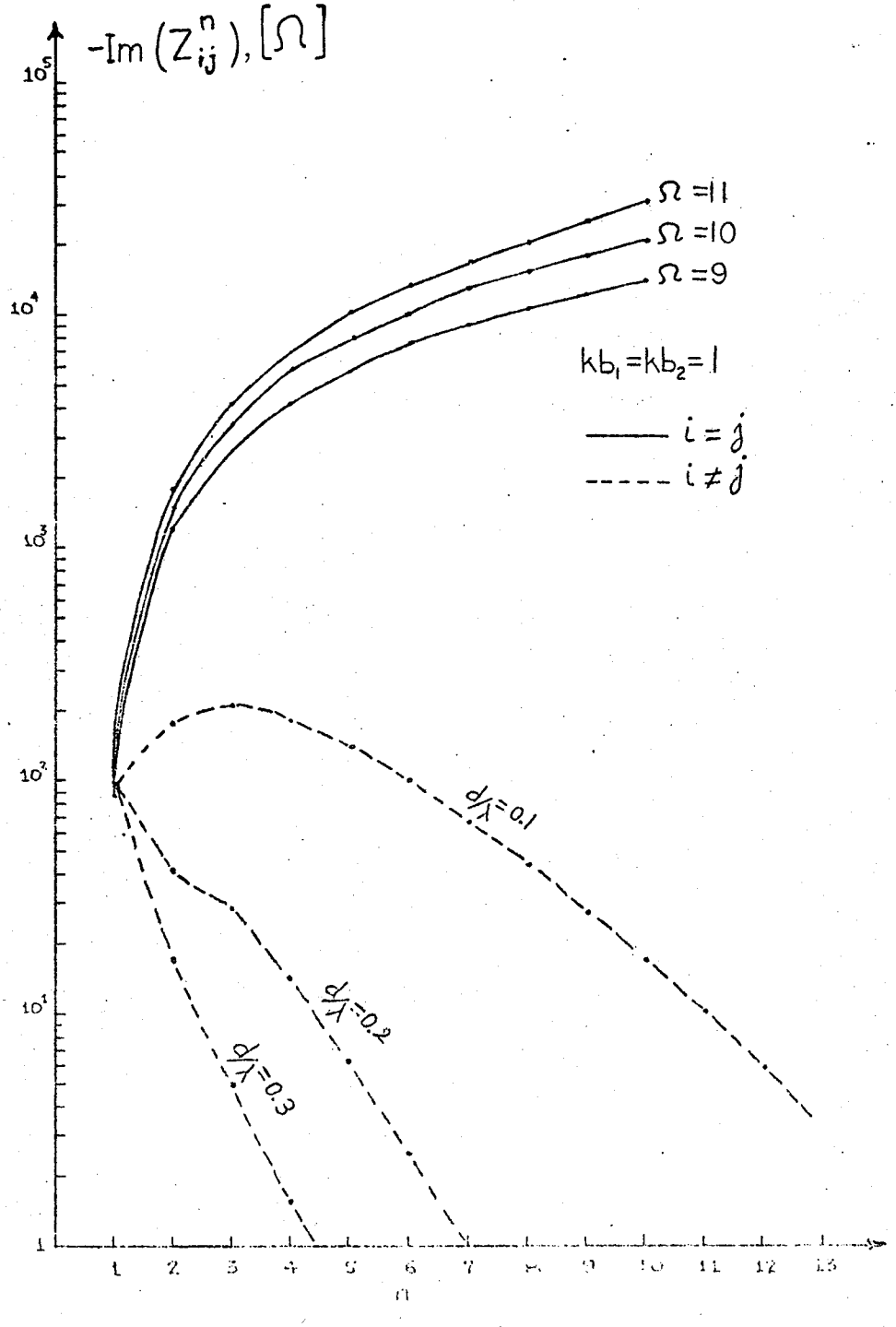

Figure B.1 Comparison between the imaginary parts of generalized self and mutual impedance.

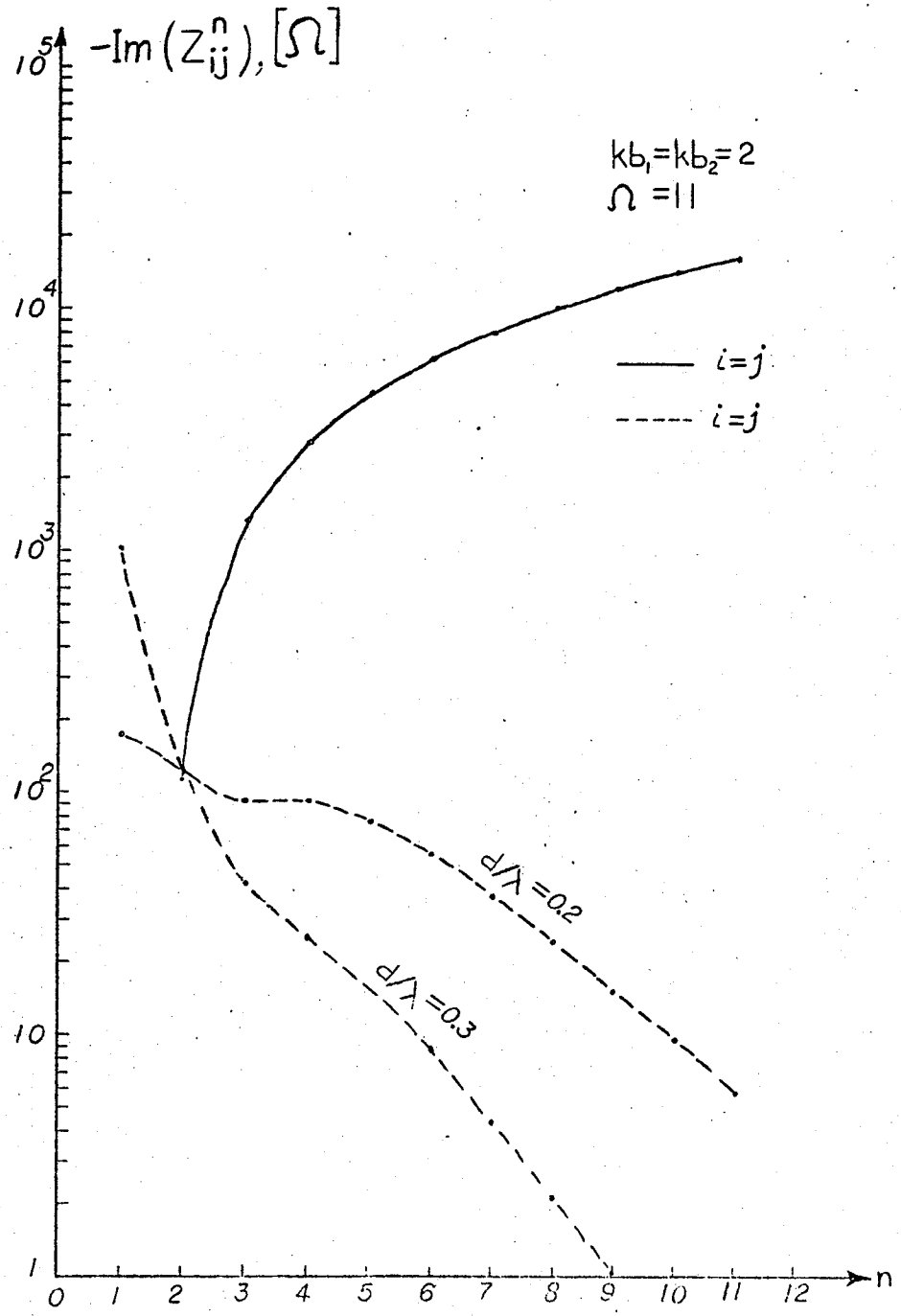

Figure B.2 Comparison between the imaginary parts of generalized self and mutual impedance.